

# Lithologies and Chronologic Opportunities of Materials to be Returned from the Artemis Exploration Zone

Ruby V Patterson<sup>1</sup>, Thomas John Lapen<sup>1</sup>, David A Kring<sup>2</sup>, Myriam Lemelin<sup>3</sup>, and McKayla L Meier<sup>4</sup>

<sup>1</sup>University of Houston

<sup>2</sup>Lunar and Planetary Institute

<sup>3</sup>Université de Sherbrooke

<sup>4</sup>University of Idaho

January 16, 2024

## Abstract

The Artemis exploration zone is a geologically-complex region likely hosting some of the oldest and as-yet-unstudied materials on the Moon. We review six potential Artemis landing sites (001, 004, 007, 011, 102, and 105) within candidate Artemis III landing regions ‘Connecting Ridge,’ ‘Peak Near Shackleton,’ ‘Leibnitz Beta Plateau,’ ‘de Gerlache Rim,’ and ‘de Gerlache Rim 2.’ Kaguya Spectral Profiler mineral data were used to determine average lithological composition at each landing site. Potentially accessible geologic materials, their ages and significance, and appropriate application of radiometric chronometers are discussed in reference to return samples from each potential landing site. Chronologic analyses of return samples from the Artemis exploration zone will enable the anchoring of the lunar impact flux curve, determine the absolute timing of pivotal events in lunar geologic history, and reveal geological diversity of the differentiated lunar body.

1 **Lithologies and Chronologic Opportunities of Materials to be Returned from the**  
2 **Artemis Exploration Zone**

3

4 **Ruby V. Patterson<sup>1</sup>, Thomas J. Lapen<sup>1</sup>, David A. Kring<sup>2</sup>, Myriam Lemelin<sup>3</sup>, and McKayla**  
5 **L. Meier<sup>4</sup>**

6 <sup>1</sup>University of Houston.<sup>2</sup>Lunar and Planetary Institute.<sup>3</sup>Université de Sherbrooke.<sup>4</sup>University of  
7 Florida.

8 Corresponding author: Ruby Patterson (rubypatterson1@gmail.com)

9 \*Alternate affiliation: Jacobs at NASA Johnson Space Center, 2101 NASA Parkway, Building 31,  
10 Room 156, Houston, TX, 77058; ruby.v.patterson@nasa.gov.

11 **Key Points:**

- 12 • The Artemis lunar missions will explore a feldspathic impact terrain and return samples  
13 from unexplored terrain.
- 14 • Likely lithologies, ages, and chronometers are discussed for six potential landing sites.
- 15 • Artemis return samples from will be unique from Apollo samples and have the possibility  
16 of determining absolute ages of significant events in lunar history.  
17

## 18 **Abstract**

19 The Artemis exploration zone is a geologically-complex region likely hosting some of the oldest  
20 and as-yet-unstudied materials on the Moon. We review six potential Artemis landing sites (001,  
21 004, 007, 011, 102, and 105) within candidate Artemis III landing regions ‘Connecting Ridge,’  
22 ‘Peak Near Shackleton,’ ‘Leibnitz Beta Plateau,’ ‘de Gerlache Rim,’ and ‘de Gerlache Rim 2.’  
23 Kaguya Spectral Profiler mineral data were used to determine average lithological composition at  
24 each landing site. Potentially accessible geologic materials, their ages and significance, and  
25 appropriate application of radiometric chronometers are discussed in reference to return samples  
26 from each potential landing site. Chronologic analyses of return samples from the Artemis  
27 exploration zone will enable the anchoring of the lunar impact flux curve, determine the absolute  
28 timing of pivotal events in lunar geologic history, and reveal geological diversity of the  
29 differentiated lunar body.

30

## 31 **Plain Language Summary**

32 Artemis astronauts will bring new samples from the Moon back to Earth. We discuss the  
33 geology of some landing sites the astronauts might visit, what types of rocks they may encounter,  
34 and how to examine them using geochronology. The application of geochronology to Moon rocks  
35 is essential to know the absolute timing of major events in lunar and early Solar system history.

## 36 **1 Introduction**

37 The Artemis exploration zone (AEZ) includes terrain dominated by photogeologically-mapped  
38 and stratigraphically-determined Nectarian and pre-Nectarian age surfaces. These surfaces have  
39 materials that can help answer important questions regarding impact chronology, history of major  
40 lunar events such as formation and differentiation, and an opportunity to sample deeply excavated  
41 materials. To answer these questions, detailed petrologic analyses coupled with chronologic  
42 analyses of specimens collected from the AEZ are required.

43

44 Examination of impact-cratered surfaces can determine fluxes in impact events in lunar history  
45 (Neukum et al., 1975; Boyce et al., 1977; Kring, 2008; Mazrouei et al., 2019; Lagain et al., 2022;  
46 Fairweather et al., 2022). Establishing the ages of specific impact craters and basins is important  
47 because these ages can anchor a crater chronology of the lunar surface (Arvidson et al., 1979;  
48 Neukum, 1984; Neukum et al., 2001; Che et al., 2021; Yue et al., 2022) and better define the  
49 bombardment history of the inner solar system (Kring et al., 2005; Kring, 2006, 2007, 2008, 2009).  
50 The returned lunar samples by the Apollo program were subjected to radioisotope dating, but many  
51 of the sampling sites might be part of the perturbed megaregolith formed by ejecta of large impact  
52 basins (Howard et al., 1974; Moore et al., 1974; Head et al., 1993; Haskin, 1998; Haskin et al.,  
53 1998; Petro and Pieters, 2008) and many studied specimens cannot be reliably attributed to a  
54 specific impact event (Korotev et al., 2002). The Imbrium basin is dated at roughly ~3.5 Ga  
55 (Deutsch and Stöffler, 1987; Spudis et al., 1988; Merle et al., 2014; Zhang et al., 2015), but ages  
56 of other significant lunar basins, such as the Orientale Basin, have yet to be firmly established  
57 (Stöffler et al., 2006; Meyer et al., 2016; Wu et al., 2019). The mapped ages of features in Figure  
58 1 are in flux based on crater-counting ages determined from orbit (Tye et al., 2015; Deutsch et al.,  
59 2020). While Spudis et al. (2008) mapped Shackleton crater with a 3.6 Ga age, Zuber et al. (2012),  
60 Tye et al. (2015), and Kring et al. (2021) reported Imbrian ages of ~3.69 Ga, 3.51 +0.05/-0.08 Ga,

61 and  $3.43 \pm 0.04/-0.05$  Ga, respectively. Moreover, while Spudis et al. (2008) mapped Shoemaker  
62 and Faustini craters with Nectarian ages, Tye et al. (2015) report pre-Nectarian ages, similar to  
63 those at Haworth. The variable age estimates illustrate the need for sample return and radiometric  
64 analyses in Earth-based laboratories. The age of the South Pole-Aitkin (SPA) basin, thought to be  
65 the oldest and largest basin on the Moon and, thus, a key anchor point in defining the lunar  
66 chronology, is still not precisely known (Wilhelms et al., 1987; Hiesinger et al., 2012). The South  
67 Pole-Aitken Terrane has not yet been directly sampled but it is the focus for the crewed Artemis  
68 missions (Jolliff et al., 2000) (Figure 1).

69

70 Sampling impact-generated pre-Nectarian- and Nectarian-age materials in the Artemis  
 71 exploration zone also provides a way to test the crater counting calibration curve and refine the  
 72 impact flux during the first billion years of Earth-Moon history; i.e., testing the lunar cataclysm

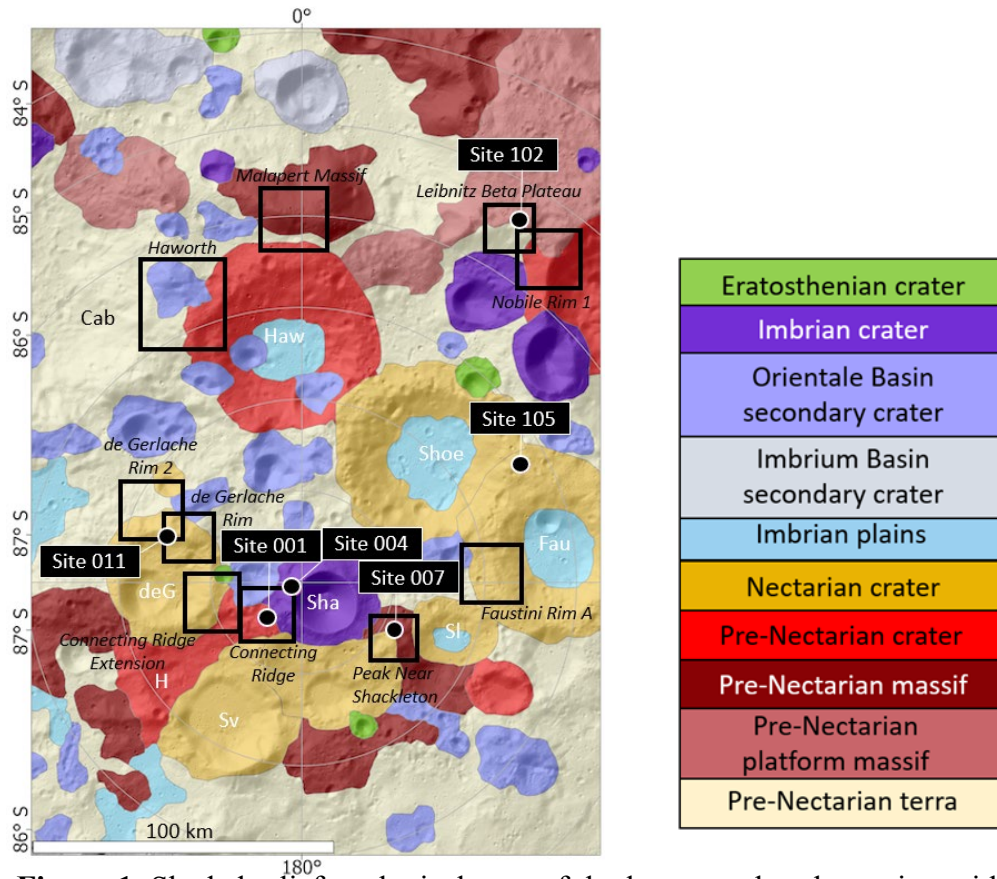


**Figure 1.** Shaded relief geological map of the lunar south polar region with the locations of several potential Artemis landing sites (001, 004, 007, 011, 102, and 105). Base map by Allender et al. (2019) in the LPI Lunar South Pole Atlas using geology of Spudis et al. (2008) and Lunar Orbiter Laser Altimeter data. The mapped ages of features are in flux based on crater-counting ages determined from orbit. For example, while Spudis et al. (2008) mapped Shackleton crater with a 3.6 Ga age, Zuber et al. (2012), Tye et al. (2015), and Kring et al. (2021) reported Imbrian ages of  $\sim 3.69$  Ga,  $3.51 \pm 0.05/-0.08$  Ga, and  $3.43 \pm 0.04/-0.05$  Ga, respectively. Moreover, while Spudis et al. (2008) mapped Shoemaker and Faustini craters with Nectarian ages, Tye et al. (2015) report pre-Nectarian ages, similar those that of Haworth. Those disparate ages illustrate the need for sample return and radiometric analyses in Earth-based laboratories. Cab- Cabeus; Haw- Haworth; Shoe- Shoemaker; Fau- Faustini; deG- de Gerlache; Sha- Shackleton; Sl- Slater; H- Henson; Sv- Sverdrup.

73 hypothesis, which is the highest priority science objective as defined by the National Research  
 74 Council (NRC) (2007). In addition, the region may contain debris from the SPA basin. Recovering  
 75 debris with an SPA impact-reset age will provide an opportunity to address the second highest  
 76 priority science objective (NRC, 2007): to provide an anchor to the basin-forming epoch on the  
 77 Moon. Currently, ages for SPA range from 4.39 Ga to 4.25 Ga (Hiesinger et al., 2012; Morbidelli  
 78 et al., 2012). Collectively, those data will refine the crater calibration curve, which can then be  
 79 applied to surfaces around the entire Moon and other planetary surfaces in the Solar system. The

80 pre-Nectarian and Nectarian impact events in the Artemis exploration zone excavated and  
81 produced breccias composed, in part, of unusually old highland terrain crust. Samples of that  
82 material could provide additional opportunities to constrain the timing of the giant Moon-forming  
83 impact, lunar differentiation, crustal formation, and subsequent magmatism, which are tied to  
84 several other important scientific objectives (NRC, 2007; Artemis III Science Definition Team  
85 Report).

86  
87 The impact cratering process is critical for excavating materials from depth and allows access  
88 to materials that may otherwise be deeply buried. Exhumed lithologies also provide information  
89 on the local stratigraphy (Pieters et al., 1994; Kring, 2009; Kenkmann and Artemieva, 2021), for  
90 example, at Shackleton crater (Gawronska et al., 2020). Because SPA is the largest and oldest  
91 impact basin on the Moon (Wilhelms et al., 1987), it may contain rare upper mantle materials at  
92 the surface in select locations (Moriarty et al., 2021). Thus, a cross-section of lunar crust up to 10's  
93 of kilometers deep may be developed if the return sample collection strategy includes samples  
94 collected from varied crater features (e.g., modification zones, central uplifts, etc.) and impact  
95 breccias (Kring, 2009). Impact crater ejecta may also allow for the determination of the average  
96 composition of impacted crust from the sampling of homogenized subsurface lithologies in the  
97 form of impact melt materials (Kring, 2009). The environmental consequences (e.g., dust lofting,  
98 ejecta blanketing, flood basalts, rockfall; mountain-forming, etc.) of these impacts may also be  
99 inferred through orbital, field, and sample observation of impact craters (Mukhametshin et al.,  
100 2018; Michaut and Pinel, 2018; Xie et al., 2020; Bickel et al., 2020). The delivery and abundance  
101 of elements through impacts may also be determined and used to piece together a history of the  
102 chemical evolution of the lunar interior and crust (Bottke et al., 2010; Barnes et al., 2016; Joy et  
103 al., 2016, 2020; Zhu et al., 2019). Finally, investigations and sampling of heavily impact-cratered  
104 terrain may also provide access to impact melt samples from other craters (Kring et al., 2005;  
105 Kring, 2007, 2009).

106  
107 This study reviews six potential Artemis landing sites (001, 004, 007, 011, 102, and 105) within  
108 candidate Artemis III landing regions 'Connecting Ridge,' 'Peak Near Shackleton,' 'Leibnitz Beta  
109 Plateau,' 'de Gerlache Rim,' and 'de Gerlache Rim 2' (NASA, 2020b, 2022). The numbered  
110 potential landing sites correspond to the illumination sites identified in previous work (Bussey et  
111 al., 2010; Mazarico et al., 2011; Speyerer and Robinson, 2013). Kaguya Spectral Profiler mineral  
112 count data were used to determine average lithological composition at each landing site. Potential  
113 accessible geologic materials, their ages and significance, and appropriate application of  
114 radiometric chronometers are discussed in reference to return samples from each potential landing  
115 site. Chronologic analyses of return samples from the Artemis exploration zone will enable the  
116 anchoring of the lunar impact flux curve, determine the absolute timing of pivotal events in lunar  
117 geologic history, and reveal geological diversity of the differentiated lunar body.

## 118 **1.1 Input Data**

119 Kayuga Spectral Profiler (SP) is a visible to near infrared spectrometer with a ~500 m spatial  
120 footprint acquiring data via three spectral bands (one visible, two near infrared) between 500 and  
121 2600 nm (Haruyama et al., 2008). However, topography in the polar regions causes different  
122 surfaces to receive widely uneven solar illumination, from no direct incident sunlight in  
123 topographic depressions (such as permanently shaded regions) to abundant sunlight on steep Sun-  
124 facing slopes, which makes spectral interpretation challenging. Lemelin et al. (2022) converted

125 the SP radiance data (level 2B1) measured in each SP orbit into bidirectional reflectance using the  
 126 photometric function of Yokota et al. (2011), which allowed the conversion of radiance data into  
 127 reflectance data at a standard viewing geometry of 30° incidence angle and 0° emission angle.  
 128 However, as the photometric function of Yokota et al. (2011) assumes a flat sphere, reflectance  
 129 measurements higher or lower than expected occur on sloped surfaces. The Lunar Orbiter Laser  
 130 Altimeter (LOLA) onboard LRO acquires reflectance data at 1064 nm and is unaffected by slope  
 131 effects as it sends its own illumination. Lemelin et al. (2022) thus scaled the gridded SP reflectance  
 132 data to the gridded and calibrated LOLA data at their common wavelength of 1064 nm. They could  
 133 then calculate FeO abundances using reflectance data at 750 and 950 nm, and use Hapke radiative  
 134 model (e.g., Hapke, 1981, 2001) to estimate the abundance of olivine, low-calcium pyroxene  
 135 (LCP), high-calcium pyroxene (HCP), and plagioclase on continuum removed spectra, using FeO  
 136

	Potential Landing Site					
	001	004	007	011	102	105
<b>Copernican</b> < 0.80 Ga						
<b>Eratosthenian</b> 0.8 to 3.20 Ga						
<b>Upper Imbrian</b> 3.20 to 3.80 Ga	Shackleton	Shackleton				
<b>Lower Imbrian</b> 3.80 to 3.85 Ga	Shackleton Spudis, Marvin, Orientale (Secondary)	Shackleton Spudis + Orientale (Secondary)		Orientale (Secondary)		Malinkin + Orientale (Secondary)
<b>Nectarian</b> 3.85 to 3.92 Ga	de Gerlache, Unnamed?			de Gerlache		Shoemaker + Faustini
<b>pre-Nectarian</b> > 3.92 Ga	Henson, Sverdrup, Marvin	Sverdrup	Slater Massif Terra	Terra	Nobile Platform Massif Terra	Terra

**Figure 2.** Summary of age units at each potential landing site in accordance with Figure 1. Upper and lower age limits of each time period are from Stöffler et al. (2006). Although not visible at the scale mapped in Figure 1, all sites will contain small Copernican-age craters.

137  
 138 as a constraint. We used these gridded mineral maps and the gridded abundance of FeO to study  
 139 the probable geology of the Artemis region.

## 140 1.2 Potential Landing Sites

141 The Artemis III mission will not be supported with a rover, so crew will be limited to walking  
 142 extravehicular activities (EVAs) within 2 km distance of the Human Landing System (HLS)  
 143 (Coan, 2020; Kring et al., 2023). An unpressurized Lunar Terrain Vehicle (LTV) will be deployed

144 for later missions (NASA, 2021, 2023) and should provide an exploration range up to 10 km radial  
145 distance from a lander. For the purposes of our study, we utilize that 10 km radial distance around  
146 potential Artemis landing sites to evaluate the types of samples available for collection and return  
147 to Earth.

#### 148 1.2.1 Site 001 (‘Connecting Ridge’ region)

149 Potential Artemis landing site 001 (NASA, 2020a) (Site “SP-1” at (-89.45, 222.69) in Mazarico  
150 et al. (2011); “Point B” at (89.44°S, 141.8°W) in Bussey et al. (2010)) is within the Artemis III  
151 candidate landing region called “Connecting Ridge” and located on a massif ridge connecting  
152 Shackleton and Henson craters (Figure 1a). This ridge itself is roughly pre-Nectarian in age  
153 (Stöffler et al., 2006) but is cross-cut by Shackleton crater and secondary crater ejecta believed to  
154 be of significantly younger Imbrian age (3.51 to  $3.69 \pm 0.4$  Ga) (Spudis et al., 2008; Zuber et al.,  
155 2012). The ridge will be covered with Shackleton ejecta, potentially including fragments of the  
156 original highland crust, components from the lunar magma ocean and later intrusive rocks,  
157 cryptomare from SPA, plus impact melts from Shackleton, SPA, and other pre-Nectarian impacts  
158 (Kring, 2019; Halim et al., 2021; Kring et al., 2022). Anticipated dominant lithologies are  
159 anorthosite below the Shackleton crater rim down to ~900 m, regolith, and breccia (Gawronska et  
160 al., 2020). Lowest FeO values within the Artemis exploration region determined by Kaguya SP  
161 (~5 to 7 wt. %) are found in the 89° to 90°S region near Shackleton crater (applies to Site 004 as  
162 well) (Lemelin et al., 2022).

#### 163 1.2.2 Site 004 (along margin of ‘Connecting Ridge’ region)

164 Potential Artemis landing site 004 (NASA, 2020a) ( Site “SP-4” at (-89.78, 204.27) in  
165 Mazarico et al. (2011); “Point A” at (89.68°S, 166.0°W) in Bussey et al. (2010)) is along the  
166 margin of Artemis III candidate landing region called “Connecting Ridge” on a portion of  
167 Shackleton crater (ridge is pre-Nectarian age, 4.52 to 3.92 Ga, (Stöffler et al., 2006); crater is  
168 Imbrian age;  $3.6 \pm 0.4$  Ga (Spudis et al., 2008; Zuber et al., 2012; Tye et al., 2015; Halim et al.,  
169 2021)) rim and is nearly coincident with the geographic south pole of the Moon (Figure 1).  
170 Imbrium secondary crater materials and pre-Nectarian ejecta from Henson crater are accessible  
171 within a 10 km radial distance (Figure 2). This site contains multiple rock exposures (Gawronska  
172 et al., 2020). Anticipated lithologies include pure anorthosite exposures (Yamamoto et al., 2012;  
173 Lemelin et al., 2017). Sites 001 and 004 provide a unique opportunity to sample rays from Tycho  
174 crater that reach directly between the two sites (Lemelin et al., 2022). Both sites provide an  
175 opportunity to sample pre-Nectarian crater, Imbrian crater, and Imbrian secondary crater materials.

#### 176 1.2.3 Site 007 (‘Peak near Shackleton’ region)

177 Potential Artemis landing site 007 (NASA, 2020a) (Site “SP-7” at (-88.81, 123.64) in Mazarico  
178 et al. (2011); “Point D” at (88.79°S, 124.5°E) in Bussey et al. (2010)) is within the Artemis III  
179 candidate landing region “Peak near Shackleton” located on a massif ridge between Shackleton  
180 and Slater craters (Figure 1a). Within a 10 km radial distance, Site 007 would enable the sampling  
181 of materials from the pre-Nectarian massif, Nectarian crater, and Imbrian crater (Figure 2). This  
182 site may provide the possibility to observe layered strata from Shackleton and compare ejecta and  
183 stratigraphy with Slater crater. Layered terrain is 10 to 50 m thick in Shackleton (Halim et al.,  
184 2021). The lateral extent of these layers is difficult to observe due to poor illumination conditions,  
185 but they may be ejecta produced from older impacts (i.e., Haworth, Shoemaker, Faustini).

186 Interestingly, numerical modeling efforts have determined the top bed in this stratigraphic  
187 sequence may contain over ~150 m of Shackleton ejecta (Halim et al., 2021). Kumari et al. (2022)  
188 identified 3,204 resolvable boulders (ranging from 0.7 to 14 m diameter) within a 10 km radius of  
189 site 007.

#### 190 1.2.4 Site 011 (‘de Gerlache Rim 1’ and ‘de Gerlache Rim 2’ regions)

191 Potential Artemis landing site 011 (NASA, 2020a) (Site “SP-11” at (-88.67, 291.90) in  
192 Mazarico et al. (2011); “Point C” at (88.71°S, 68.7°W) in Bussey et al. (2010)) is within the  
193 Artemis III candidate landing region “de Gerlache Rim”. De Gerlache Rim 1 is approximately  
194 centered on the crater rim, while de Gerlache Rim 2 is mostly north of the crater rim (Figure 1).  
195 Based on absolute crater counting models, de Gerlache is believed to be Nectarian in age (Tye et  
196 al., 2015; Deutsch et al., 2020) and, just beyond de Gerlache Rim 1, its rim is cross-cut by an  
197 Eratosthenian-age Marvin crater. The de Gerlache impact appears to be younger than the pre-  
198 Nectarian ‘Connecting Ridge’ massif (Spudis et al., 2008) and, thus, may have covered the massif  
199 with ejecta prior to the Shackleton impact. Pre-Nectarian terra, Nectarian crater, and Imbrian  
200 secondary crater materials are present within a 10 km radial distance from Site 011 (Figure 2).  
201 This site may allow for volatile sampling within secondary craters and comparison to Apollo  
202 permanently shadowed region (PSR) crater samples (Li and Milliken, 2017; Kereszturi et al.,  
203 2022). The de Gerlache ejecta within the region may provide samples of anorthositic crustal  
204 lithologies and SPA ejecta. Within a 10 km radial distance around site 011, over 3,774 boulders  
205 from 0.7 to 26 m in diameter have been identified (Kumari et al., 2022).

#### 206 1.2.5 Site 102 (‘Leibnitz Beta Plateau’ region)

207 Potential Artemis landing site 102 (NASA, 2020a) (Site “SP-20” at (-85.43, 31.73) in Mazarico  
208 et al. (2011)) is within the Artemis III candidate landing region called “Leibnitz Beta Plateau”  
209 located atop informally-named Mons Leibnitz Beta, which is now called Mons Mouton (Figure 1).  
210 The Leibnitz Mountains lie on the topographically-high ring outlining the SPA basin (Garrick-  
211 Bethell and Zuber, 2009). This plateau is bounded by a nearly vertical cliff facing south-poleward.  
212 The cliff may provide a unique opportunity to access a roughly 8-km-thick cross-section of lunar  
213 crust. Massifs like Mons Mouton may also provide an opportunity to identify additional lithologies  
214 produced by early lunar magmatic processes. This site may allow for sampling from adjacent pre-  
215 Nectarian and Nectarian aged impacts Haworth ( $4.18 \pm 0.02$  Ga), Shoemaker ( $4.15 \pm 0.02$  Ga),  
216 and Faustini ( $4.10 \pm 0.03$  Ga) craters (Figure 2; Tye et al., 2015). NASA’s VIPER rover is set to

217 land and traverse near this site to search for and sample volatiles up to approximately 1 meter deep  
218 within the regolith (Shirley and Balaban, 2022).

### 219 1.2.6 Site 105

220 Potential Artemis landing site 105 (NASA, 2020a) ((-87.18, 62.84) in Patterson et al. (2022)  
221 is located between pre-Nectarian aged Shoemaker ( $4.15 \pm 0.02$  Ga) and Faustini ( $4.10 \pm 0.03$  Ga)  
222 craters (Tye et al., 2015) (Figures 1, 2). Site 105 is downslope from Site 102. This region contains  
223 many large blocks and boulders (1.5 to 9 m diameter) (Patterson et al., 2022) and the floors of  
224 Shoemaker and Faustini likely have icy volatile deposits (Tye et al., 2015; Patterson et al., 2022;  
225 Brown et al., 2022), and the ridge bisecting Faustini and Shoemaker crater rims has ejecta deposits  
226 likely to be up to Nectarian in age (Tai Udovicic et al., 2022). This site contains the lowest FeO  
227 values (~5-7 wt. %) of all of the 84° to 90° S region (Figure 1a; Lemelin et al., 2022).

**Table 1.** Commonly applied radiogenic isotope systems and the methods by which they may be analyzed.

Isotope System	Analytical Technique				
	Bulk sample or glass	Mineral/bulk rock isochron	Single mineral	In-situ (Laser ablation/secondary ion)	Wet chemistry
$^{40}\text{K} \rightarrow ^{40}\text{Ar}$ ( $^{40}\text{Ar} - ^{39}\text{Ar}$ )	X		X	X	
$^{87}\text{Rb} \rightarrow ^{87}\text{Sr}$		X		X	X
$^{147}\text{Sm} \rightarrow ^{143}\text{Nd}$		X			
$^{146*}\text{Sm} \rightarrow ^{142}\text{Nd}$		X			
$^{176}\text{Lu} \rightarrow ^{176}\text{Hf}$		X	X	X	X
$^{187}\text{Re} \rightarrow ^{187}\text{Os}$		X			
$^{232}\text{Th} \rightarrow ^{208}\text{Pb}$		X	X	X	X
$^{235}\text{U} \rightarrow ^{207}\text{Pb}$		X	X	X	X
$^{238}\text{U} \rightarrow ^{206}\text{Pb}$		X	X	X	X

## 228 2 Isotope Chronology

229 The timing of major events, including the timing of lunar differentiation, duration of igneous  
230 activity, and impact history, can be constrained with isotope chronology of lunar materials (e.g.,  
231 Nyquist and Shih, 1992). Foundational chronologic analyses of Apollo 11 samples are  
232 summarized in the Proceedings of the Apollo 11 Lunar Science Conference (1970) and “The Moon  
233 Issue” of the journal *Science* (Abelson, 1970, and articles in the issue) and laid the groundwork  
234 for all future studies of lunar return samples. The commonly applied isotope systems are  
235 summarized in Table 1 and described below. Each radiometric system is best suited to a particular  
236 subset of geologic events and temperatures. For example, some approaches are best suited to date  
237 high-temperature igneous crystallization, whereas other systems best reflect cooling below 300 to  
238 500 °C. Furthermore, the radiometric systems may require specific minerals and/or chemical  
239 compositions. Thus, some chronologic approaches may be more suitable to different lunar  
240 lithologies than others, simply by the nature of the texture and/or mineralogy of the sample. The

241 ages of secondary processes, such as impact metamorphism, may also be determined, depending  
 242 on the material and degree of metamorphism/melting.

## 243 2.1 U-Th-Pb

244 The  $^{238}\text{U}$ - $^{206}\text{Pb}$ ,  $^{235}\text{U}$ - $^{207}\text{Pb}$ , and  $^{232}\text{Th}$ - $^{208}\text{Pb}$  isotope systems are some of the most versatile  
 245 isotope systems that can be applied to a wide variety of lunar lithologies. These systems were  
 246 developed prior to the Apollo 11 mission and were applied to the first returned specimens (e.g.,  
 247 Silver, 1970; Tatsumoto and Rosholt, 1970). Because  $^{238}\text{U}$ - $^{206}\text{Pb}$  and  $^{235}\text{U}$ - $^{207}\text{Pb}$  reflect two isotope  
 248 systems in the U-Pb system, ages can be determined using multiple approaches including standard  
 249 U-Pb isochrons, inverse Pb-Pb isochrons, and U-Pb concordia diagrams (e.g., Wetherill and Tera-  
 250 Wasserburg diagrams). The  $^{238}\text{U}$ ,  $^{235}\text{U}$ , and  $^{232}\text{Th}$  half-lives are 4.468, 0.704, and 14.01 Ga,  
 251 respectively (Steiger and Jäger, 1977). Despite recent studies that refine the decay constants (e.g.,  
 252 Amelin and Zaitsev, 2002; Schoene et al., 2006), the IUGS-IUPAC recommends the decay  
 253 constants of Jaffey et al. (1971) for  $^{238}\text{U}$  and  $^{235}\text{U}$  (Villa et al., 2022). Uranium and Th-rich and  
 254 high U/Pb and/or Th/Pb ratio trace phases such as zircon, baddeleyite, zirconolite, tranquillityite,  
 255 apatite, merrillite, and monazite are documented in many lunar lithologies and have the potential  
 256 for precise chronology (e.g., Lovering et al., 1974; Rasmussen et al., 2008; Barboni et al., 2017;  
 257 Shaulis et al., 2017). Even in materials without these trace phases, many lunar rocks and/or their  
 258 sources have relatively high  $^{238}\text{U}/^{204}\text{Pb}$  ratios (denoted as  $\mu$ ) of about 360 to over 2600 for lunar  
 259 basaltic rocks (e.g., Snape et al., 2018) whereas the  $\mu$ -value of the terrestrial mantle is about 8  
 260 (e.g., Ballhaus et al., 2013).

261  
 262 Since most lunar rocks have experienced secondary processes such as thermal and/or impact  
 263 metamorphism, some mineral hosts are more resilient to disturbances of the U-Th-Pb systems than  
 264 others. For example, zircon has the potential to preserve the U-Th-Pb systematics of crystallization  
 265 from a melt and will retain those characteristics even through metamorphic events that would  
 266 disturb U-Th-Pb in other materials (Cherniak and Watson, 2001). Zircon is considered one of the  
 267 most robust time capsules nature has to offer. Uranium and Pb in baddeleyite also has the potential  
 268 to record igneous events despite the host rock being subjected to high-grade metamorphic  
 269 conditions (Niihara et al., 2009). Microstructural analyses of trace phases such as baddeleyite can  
 270 reveal relict polymorphs that provide additional context for age data (White et al., 2020). Other U  
 271 and/or Th-rich mineral hosts such as apatite, however, are less resistant to disturbances than zircon  
 272 for any given temperature-time (T-t) history (Chew et al., 2021) and can record the timing of  
 273 metamorphic events (Nemchin et al., 2009).

274  
 275 Analytical approaches for U-Th-Pb analyses include in-situ (minimally destructive) or wet  
 276 chemical (fully destructive). In-situ analyses usually involve either a laser or secondary ion source  
 277 that samples the material of interest at spatial resolutions between 5 and 100  $\mu\text{m}$ . The advantages  
 278 of in-situ approaches are that analyses often have petrological context through microstructural  
 279 and/or mineral textural data. Age data can be collected from very small specimens (Che et al.,  
 280 2021) and clasts (Snape et al., 2018). One disadvantage of in-situ analyses is that the measurement  
 281 precision is often significantly less than that of wet chemical approaches such as isotope-dilution  
 282 thermal ionization mass spectrometry (ID TIMS; see Schoene (2014) for a full treatment of the  
 283 methods). In lithologies that do not typically contain U and Th-rich trace phases, measurement of  
 284 the  $^{207}\text{Pb}/^{206}\text{Pb}$  and  $^{204}\text{Pb}/^{206}\text{Pb}$  ratios of other phases such as pyroxene can yield precise ages. For  
 285 example, Borg et al. (2011) measured an age of  $4359.2 \pm 2.4$  Ma for sequentially-dissolved

286 pyroxene in ferroan anorthosite 60025. Overall, with modern analytical techniques, the ages of  
 287 most lunar lithologies can be precisely determined with the U-Th-Pb systems.

## 288 2.2 Rb-Sr

289 The Rb-Sr isotope system has been applied to Apollo lunar materials since they were collected  
 290 (Gopalan et al., 1970; Hurley and Pinson, Jr., 1970; Papanastassiou et al., 1970) and has the  
 291 potential for precise chronology (Rankenburg et al., 2007) and chemical/isotopic tracing (Borg et  
 292 al., 2022). The IUGS-IUPAC-recommended decay constant for  $^{87}\text{Rb}$  is  $(1.3972 \pm 0.0045) \times 10^{-11}\text{a}^{-1}$   
 293 (Villa et al., 2015). Great care must be taken in comparing data because many studies used  
 294 and/or still use the value of  $1.42 \times 10^{-11}\text{a}^{-1}$  reported in Steiger and Jäger (1977) and other studies  
 295 may adopt the new decay constants. In any case, most published age data can be recalculated to  
 296 the same or updated decay constant.

297  
 298 Strontium isotopic and  $^{87}\text{Rb}/^{86}\text{Sr}$  ratios of rock, glass, and/or mineral materials are typically  
 299 measured with wet chemical approaches (destructive analyses) where the materials are digested  
 300 and Rb and Sr are chemically purified and analyzed (Charlier et al., 2006). Common lunar rock-  
 301 forming minerals such as pyroxene, plagioclase, K-feldspar, and olivine have highly variable  
 302 Rb/Sr ratios making them amenable for dating using the isochron approach. Very recent  
 303 advancements in mass spectrometry have enabled in-situ analysis of  $^{87}\text{Sr}/^{86}\text{Sr}$  and  $^{87}\text{Rb}/^{86}\text{Sr}$  by  
 304 laser ablation plasma-source mass spectrometry (Dauphas et al., 2022) opening a vast new area for  
 305 investigation with a minimally-destructive, high-spatial resolution ( $\sim 100\ \mu\text{m}$ ) technique.

306  
 307 In addition to chronology, the Rb-Sr system can be used as an isotope tracer. For example,  
 308 Borg et al. (2022) model the Rb-Sr isotope systematics of the Earth, Moon, and Theia (the proto-  
 309 Earth impactor) to constrain the timing of volatile addition and the timing of the Moon-forming  
 310 event. The Rb-Sr isotope system can also be used to trace potential mixing relationships and the  
 311 sources of lunar igneous rocks (Hui et al., 2013), and potentially define model age constraints in  
 312 materials that cannot otherwise be dated (McLeod et al., 2016).

## 313 2.3 Sm-Nd

314 Similar to U-Pb, Sm-Nd consists of two isotope systems ( $^{146}\text{Sm}-^{142}\text{Nd}$  and  $^{147}\text{Sm}-^{143}\text{Nd}$ ) in one  
 315 element system, except  $^{146}\text{Sm}$  is now extinct. The Sm-Nd system has been applied to most lunar  
 316 lithologies for chronology and tracers of magma sources (Nyquist et al., 1995; Brandon et al.,  
 317 2009; Carlson et al., 2014; Borg et al., 2015; Johnston et al., 2022). The IUGS-IUPAC  
 318 recommended half-lives of  $^{146}\text{Sm}$  and  $^{147}\text{Sm}$  are 0.068 – 0.103 and  $106.25 \pm 0.38\ \text{Ga}$ , respectively  
 319 (Villa et al., 2020). Given the uncertainty of the  $^{146}\text{Sm}$  decay rate, recent papers (McLeod et al.,  
 320 2014) use both half-life values of 0.068 and 0.103 Ga in their model calculations.

321  
 322 High-precision analyses of Sm-Nd requires wet chemical approaches and relatively large  
 323 samples with minimum mass requirements of 0.05 to 1 g, depending on Sm and Nd concentrations,  
 324 mineralogy, and grain size. Most lunar rocks and minerals have overall low concentrations of Sm  
 325 and Nd (ppb to ppm concentrations) and limited natural variations in Sm/Nd ratios due to their  
 326 similar geochemical characteristics in most materials. The range in  $^{147}\text{Sm}/^{144}\text{Nd}$  ratios in most  
 327 lunar minerals (feldspar, pyroxene, olivine, phosphate) is limited between about 0.14 to 0.30,  
 328 unlike Rb-Sr, U-Th-Pb, and Lu-Hf where the range in parent/daughter ratios can be orders of  
 329 magnitude greater. Despite the limited range in Sm/Nd ratios and resulting limited variations in

330 radiogenic Nd isotopic compositions, advancements in mass spectrometry allow very high  
 331 precision (few ppm) measurements of  $^{143}\text{Nd}/^{144}\text{Nd}$  and  $^{142}\text{Nd}/^{144}\text{Nd}$  ratios (Rankenburg et al., 2006;  
 332 Boyet and Carlson, 2007). These high-precision measurements are also required to accurately  
 333 measure and ultimately correct neutron capture effects from cosmic ray exposure that can alter the  
 334 Sm and Nd isotopic compositions (Nyquist et al., 1995; Brandon et al., 2009).

335  
 336 Measured Sm and Nd isotopic compositions corrected for neutron capture effects have yielded  
 337 many robust ages of lunar materials (Carlson et al., 2014; Borg and Carlson, 2023). As opposed  
 338 to the other isotope systems listed in Table 1, Sm and Nd are geochemically similar lanthanide  
 339 elements that are relatively immobile during periods of shock metamorphism. Other elements,  
 340 such as the alkalis (Rb), can be more easily mobilized than Sm-Nd. This is evident in some studies  
 341 that compare Sm-Nd and Rb-Sr measured on the same sample aliquots where there can be greater  
 342 scatter about a Rb-Sr isochron than for a Sm-Nd isochron (Edmunson et al., 2009). In addition to  
 343 standard isochron chronology, coupled  $^{146-147}\text{Sm}-^{142-143}\text{Nd}$  isotope systematics can be used to  
 344 assess the mantle closure ages (i.e., the duration of lunar magma ocean crystallization) for the  
 345 sources of lunar basalts (Boyet and Carlson, 2007; Brandon et al., 2009; McLeod et al., 2014).  
 346 Finally, the nature and compositions of lunar mantle source compositions and potential mixtures  
 347 can be assessed with the Sm-Nd system (Borg et al., 2009; Srivastava et al., 2022).

#### 348 2.4 Lu-Hf

349 The Lu-Hf isotope system was first applied to lunar materials by Patchett and Tatsumoto  
 350 (1981) and Unruh et al. (1984). Few subsequent papers presented Lu-Hf data (Beard et al., 1998)  
 351 until the application of plasma-source mass spectrometry; now the Lu-Hf isotope system is  
 352 routinely applied to lunar materials (Taylor et al., 2009; Sprung et al., 2013; Gaffney and Borg,  
 353 2014; Carlson et al., 2014; Melanie Barboni et al., 2017). The  $^{176}\text{Lu}$  half-life used by the isotope  
 354 geochemistry community changed from the value of 35.82 Ga (Patchett and Tatsumoto, 1980) to  
 355 a value of about 37.12 Ga (Scherer et al., 2001; Söderlund et al., 2004), so care must be taken  
 356 when comparing Lu-Hf isotope data and models in the literature. Hult et al. (2014) summarize  
 357 many  $^{176}\text{Lu}$  half-life measurements and propose a value of  $37.22 \pm 0.29$  Ga.

358  
 359 The Lu-Hf isotope system is enhanced by the different geochemical behavior of Lu and Hf and  
 360 resultant large range in  $^{176}\text{Lu}/^{177}\text{Hf}$  ratios in many lunar materials. For example, most zircon has  
 361 1-3 wt% Hf and Lu in ppm concentrations resulting in  $^{176}\text{Lu}/^{177}\text{Hf}$  ratios typically  $< 0.002$ .  
 362 Combined with its robust retention of U-Th-Pb isotopes for precise chronology, zircon is also a  
 363 powerful Lu-Hf isotope tracer requiring minimal age corrections (Taylor et al., 2009; Barboni et  
 364 al., 2017). Phosphate minerals have the potential for  $^{176}\text{Lu}/^{177}\text{Hf}$  ratios of over 100 (Amelin, 2005).  
 365 Overall, in addition to zircon, many oxide minerals can have very low  $^{176}\text{Lu}/^{177}\text{Hf}$  ratios of  $< 0.01$ ,  
 366 whereas phosphates and garnet have the potential for  $^{176}\text{Lu}/^{177}\text{Hf}$  ratios greater than 1.0. Therefore,  
 367 Lu-Hf mineral isochron chronology has the potential for relatively large spreads in Lu/Hf ratios  
 368 even in lithologies with a simple mineralogy (e.g., Lapen et al., 2010).

369  
 370 Modern analytical methods for Lu-Hf chronology and/or isotope tracer studies include both  
 371 in-situ laser ablation mass spectrometry and wet chemical approaches applied to bulk rock and/or  
 372 mineral separates. Because Hf concentrations are in the ppb to ppm range for most rock-forming  
 373 minerals, wet chemical approaches are required for analysis with minimum sample sizes typically  
 374 of 0.05 to 0.10 g. Hafnium-rich minerals such as zircon and baddeleyite can be analyzed for Lu-

375 Hf isotopes by in-situ approaches (Ibanez-Mejia et al., 2014). All Lu-Hf isotope data of lunar  
 376 materials should be assessed for neutron capture effects and corrected (Sprung et al., 2013; Gaffney  
 377 and Borg, 2014; Barboni et al., 2017).

### 378 2.5 Ar-Ar

379 Turner (1970) presented some of the first applications of the  $^{40}\text{Ar}/^{39}\text{Ar}$  method to Apollo 11  
 380 samples. Since then,  $^{40}\text{Ar}/^{39}\text{Ar}$  data have been essential for unraveling the timing of primary and  
 381 secondary lunar events such as protolith formation and impact metamorphism, respectively.  
 382 Depending on the material and its temperature-time history, the  $^{40}\text{Ar}/^{39}\text{Ar}$  method has the potential  
 383 to provide precise dates of a wide-range of lunar materials (Turner et al., 1973; Turner and  
 384 Cadogan, 1975; Dalrymple and Ryder, 1991, 1993, 1996; Jourdan, 2012; Fernandes et al., 2013).  
 385 Impact events that produced melt can be precisely dated and help build impact flux estimates  
 386 (Dalrymple and Ryder, 1993, 1996; Culler et al., 2000; Cohen et al., 2000; Kring and Cohen, 2002;  
 387 Norman et al., 2006; Mercer et al., 2015, 2019; Zellner and Delano, 2015). The timing of lunar  
 388 volcanism, often expressed as fine-grained and/or amorphous materials (e.g., lunar orange glass  
 389 beads in 74220 soil), can be precisely dated (Huneke, 1978; Spangler et al., 1984; Zellner et al.,  
 390 2009) whereas other isotope systems that rely on mineral-liquid fractionation processes would not  
 391 typically yield precise age determinations of these bulk materials.

392  
 393 Potassium-40 has a branched decay to  $^{40}\text{Ca}$  (89.32%) and  $^{40}\text{Ar}$  (10.68%) with a total decay  
 394 constant of about  $5.53 \times 10^{-10} \text{ yr}^{-1}$  (Renne et al., 2011). Associated  $^{40}\text{K}$ - $^{40}\text{Ca}$  chronology of felsic  
 395 lunar materials (Shih et al., 1993) is possible for specialized applications. Analytical details of the  
 396  $^{40}\text{Ar}$ - $^{39}\text{Ar}$  method are complex (McDougall et al., 1999; Cohen et al., 2000, 2005; Swindle et al.,  
 397 2009; Weirich et al., 2010; Wittmann et al., 2011; Mercer and Hodges, 2016; Niihara et al., 2019;  
 398 Schaen et al., 2020; Beard et al., 2022). Recent advancements in in-situ analytical approaches  
 399 (Mercer et al., 2015) make it easier for analyses of critical petrographic contexts.

400  
 401 Argon-Ar thermochronology is especially useful for understanding the potentially complex  
 402 temperature-time (T-t) history of lunar materials. For short T-t histories relative to the diffusivity  
 403 of Ar in a particular material, Ar-Ar data may have remained a closed system since the last Ar-  
 404 degassing event such as melting (Cohen et al., 2000). For T-t histories that are long and/or extreme  
 405 enough to facilitate Ar loss, the timing of these Ar-loss events may be recorded in the measured  
 406 Ar isotope data (Niihara et al., 2019; Schaen et al., 2020). Overall, Ar-Ar approaches, both in-situ  
 407 and conventional, are a critical tool for unraveling primary and secondary processes operative on  
 408 the Moon.

409

## 410 3 Lunar Lithologies

411 The Artemis exploration zone is a feldspathic highland terrain that was originally anorthositic  
 412 crust, covered and/or mixed with more mafic lithologies excavated by the SPA and other basin-  
 413 forming events producing a mixed - nominally noritic - composition (Pieters et al., 2001; Hawke,  
 414 2003; Spudis et al., 2008; Lin et al., 2020; Huang et al., 2020; Krasilnikov et al., 2023). Major  
 415 minerals in the surface regolith are plagioclase, pyroxene, and olivine, in that order. Reflectance  
 416 spectra suggest the region has an average anorthite abundance of ~80 to 90 wt% and ~5 to 10 wt  
 417 % Fe) (Lemelin et al., 2022).

418

419

420

421

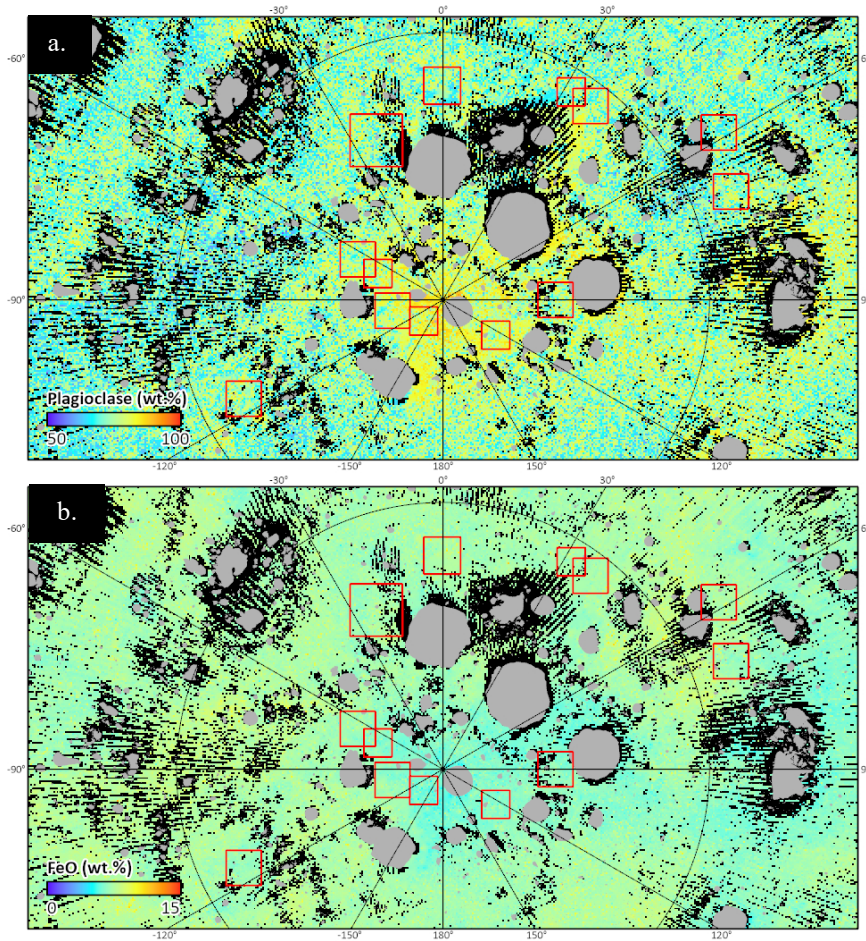


**Figure 3.** Colorized counts of Kaguya SP mineral data used to determine average lithological composition at each of the candidate landing regions (red squares). Gray areas represent permanently shadowed regions, which were masked during analyses. Black areas are areas with no mineral count data available. **(a)** Colorized counts of plagioclase from 50 to 100 wt. %. **(b)** Colorized counts of iron from 0 to 15 wt. %.

**Table 2.** Artemis zonal statistics of mineralogy at each landing site within an exploration zone of 10 radial kilometers. The values below contain minerals modeled from Spectral Profiler data with all PSRs masked from Lemelin et al. (2022). The four sites closest to the south pole (001, 004, 007, and 011) have similar mineralogy. The mineral error is on the order of  $\pm 8$  wt. % and FeO about 2 wt. %. SD = standard deviation.

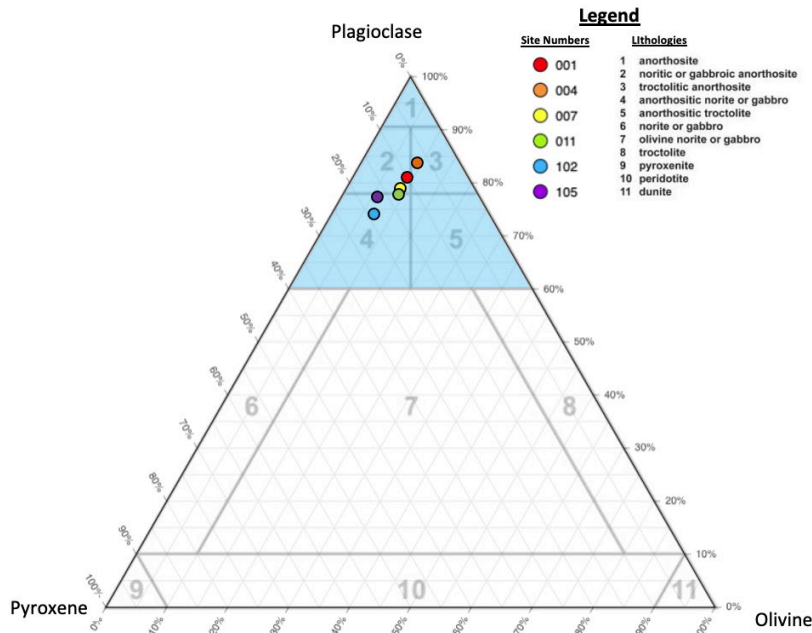
Site #	Lat.	Long.	FeO		Plagioclase		Low-Ca Pyroxene		High-Ca Pyroxene		Olivine	
			Mean	1 SD	Mean	1 SD	Mean	1 SD	Mean	1 SD	Mean	1 SD
001	-89.45	-137.31	6.2	0.4	81	5	10	6	0	2	9	6
004	-89.78	-155.73	6.1	0.4	83	4	8	5	0	1	9	6
007	-88.81	123.64	6.5	0.4	79	5	12	6	0	1	9	6
011	-88.67	-68.1	6.7	0.4	78	5	13	7	0	2	9	6
102	-85.55	37.57	7.2	0.3	74	5	19	7	0	1	7	5
105	-88.8	123.95	6.4	0.3	78	5	16	8	0	0	6	5

422

423 The basin-forming event that created SPA would have been an exceptionally violent impact  
 424 (Potter et al., 2012) that excavated material from depth where mafic to ultramafic materials likely  
 425 existed (Kring, 2005; Hurwitz and Kring, 2014), produced melt, fallback ejecta, and brecciated  
 426 basin floor materials (Petro and Pieters, 2008; Moriarty et al., 2021). This, coupled with billions  
 427 of years of subsequent impacts results in a complicated and varied lithological suite of outcrops  
 428 and potential return sample targets. The lithologies discussed here are those which were defined  
 429 by Stöffler et al. (1980) (Figure 4, Table 3). They may exist as homogenous hand samples (e.g., ~  
 430 5 to 20 cm) or even at the outcrop scale, although there is a strong likelihood of polymict breccias  
 431 housing a multitude of lithologies, much like NWA 5000 and various Apollo samples (Duncan et  
 432 al., 1975; Grieve et al., 1975; Stöffler et al., 1985; Nagurney et al., 2016; Marks et al., 2019; Cao  
 433 et al., 2021). Some lithologies, such as dunite (Shearer et al., 2015), are exceedingly rare within  
 434 the Apollo collection and exist as chips and fragments within brecciated samples. Because it  
 435 crystallizes at depth, dunite solely relies on impact excavation processes or incorporation into  
 436 magmas as xenoliths to be exposed on the lunar surface. The spatial resolution of this study (>500  
 437 m) preclude identification of litho-fragments within an individual sample, driving the need for  
 438 polymict breccia return samples.

439  
 440 We understand lunar rocks exist within a continuum of lithologies, however they are discussed  
 441 below in accordance with the classification schema outlined in Figure 4. With the exception of  
 442 impact melts or fine-grained basaltic clasts, we predict most lithologies in the Artemis exploration  
 443 zone to be relatively coarse-grained (~1 to 3 mm grain size; Joy et al., 2008).

444



445

446

447 **Figure 4.** Average landing site lithological composition displayed relative to plagioclase,  
 448 pyroxene, and olivine. Blue shaded region represents the zone of statistical uncertainty from our  
 449 analysis. Modified after Stöffler et al. (1980).

450

451 **Table 3.** List of lunar lithologies that might be included in the regolith within each site. (List of  
 452 lithologies from Hiesinger (2006)). Gray-filled boxes: within the standard deviation range of

453 average composition calculated from this study (PSRs not masked); X: presence of lithology  
 454 recognized; Y= existence of lithology likely, but below detection limit of current instrumentation;  
 455 Z: lithology possibly present as clasts. References: [1] Gawronska et al. (2020); [2] Lemelin et al.  
 456 (2022); [3] Yamamoto et al. (2012); [4] Uemoto et al. (2010); [5] Halim et al. (2021); [6] Ohtake  
 457 et al. (2009); [7] Borst et al. (2012); [8] Kraettli et al. (2022); [9] Gagnepain-Beyneix et al. (2006);  
 458 [10] Kring (2019); [11] Kring et al. (2022).  
 459

Lithology	Sites					
	001	004	007	011	102	105
Purest Anorthosite (PAN) <sup>[1-4]</sup>	Y	X	Y	Y	X	X
Anorthosite <sup>[1-3,5,6]</sup>	X	X	X	X	X	X
Noritic or Gabbroic Anorthosite <sup>[2]</sup>	X	X	X	X	X	X
Troctolitic Anorthosite <sup>[2]</sup>	X	X	X	X	X	X
Anorthositic Norite or Gabbro <sup>[2]</sup>	X	X	X	X	X	X
Anorthositic Troctolite <sup>[2]</sup>	X	X	X	X	X	X
Norite or Gabbro <sup>[2]</sup>	X	X	X	X	X	X
Olivine Norite or Gabbro <sup>[2]</sup>	X	X	X	X	X	X
Troctolite <sup>[7]</sup>	Y	Y	Y	Y	Y	Y
Pyroxenite <sup>[8,9]</sup>	Z	Z	Z	Z	Z	Z
Peridotite <sup>[7]</sup>	Z	Z	Z	Z	Z	Z
Dunite <sup>[7]</sup>	Z	Z	Z	Z	Z	Z
Basaltic material <sup>[7,10]</sup>	Z	Z	Z	Z	Z	Z

Impact Melt <sup>[10,11]</sup>	Z	Z	Z	Z	Z	Z
Impact Breccia <sup>[1,11]</sup>	Z	Z	Z	Z	Z	Z

460

## 461 3.1 Anorthositic Lithologies

462 Anorthositic lithologies include anorthosite (and ‘purest anorthosite’) and noritic, gabbroic,  
 463 and troctolitic anorthosite. These lithologies are all characterized by having high proportions of  
 464 plagioclase with low, but variable proportions of pyroxene and olivine. Anorthitic plagioclase  
 465 tends to have relatively low concentrations of REE, K, Rb, and U, making direct chronometric  
 466 analyses difficult. The complex thermal and impact histories for many lunar anorthositic rocks  
 467 (see Shearer et al., 2006, and references therein) further compromises the accuracy and precision  
 468 of chronologic measurements. Despite these challenges, chronology of anorthositic rocks by U-  
 469 Pb of mafic phases, mineral and bulk-rock Sm-Nd, and Ar-Ar have been successfully  
 470 accomplished (e.g., Norman et al., 2003; Borg et al., 2011; Marks et al., 2019). Given the overall  
 471 low concentrations in alkali elements, Rb/Sr ratios are low, making Rb-Sr analyses of anorthositic  
 472 rocks useful as a petrogenetic tracer and for calculating model ages (e.g., Borg et al., 2022).

## 473 3.1.1 Anorthosite

474 Anorthosites are coarse-grained igneous rocks that may record early lunar differentiation  
 475 processes. Anorthositic lithologies are common on the Moon because they may have formed from  
 476 early differentiation and crust-forming processes (Anderson et al., 1970; Wood et al., 1970; Wood,  
 477 1970; Ohtake et al., 2009). They are mineralogically defined as > 90 % by volume of plagioclase  
 478 (Figure 4), suggesting they are cumulates produced from an ancient melt (Lucey et al., 2006).  
 479 Mafic minerals in some lunar anorthosites have relatively low Mg/(Mg+Fe) ratios (Lucey et al.,  
 480 2006), and plagioclase within them is typically An<sub>96</sub> which may reflect the Moon’s depletion in  
 481 sodium and other volatile elements (Borg et al., 2022).

## 482 3.1.2 Purest Anorthosite

483 A particularly pure anorthosite exists in the south polar region and is composed of >97 wt. %  
 484 anorthite with <2 wt. % pyroxene (Ohtake et al., 2009). Because it is almost pure anorthite, this  
 485 variant is known as ‘purest anorthosite’ (PAN) (Ohtake et al., 2009). Outcrops that correspond to  
 486 PAN spectra are recognized at the geographic south pole and extend into the massif bridging  
 487 Shackleton to de Gerlache crater (toward the west) and Slater crater (toward the east) (Gawronska  
 488 et al., 2020). The physical extent of the PAN unit is debated because no significant samples of  
 489 PAN were identified within the Apollo collection (Lemelin et al., 2015). Exposures of anorthosites  
 490 (90 to 100 wt. % plagioclase) are somewhat rare in the Artemis region, with a few concentrated  
 491 around Shackleton crater and on or near the ridge between Shackleton and Henson craters (~88.5  
 492 °S, 128 °W, near Site 004) (Lemelin et al., 2022). In this region, PAN could be intact and  
 493 crystalline, or potentially comprise portion of megabreccia with blocks 100 m in size (Gawronska  
 494 et al., 2020).

495 Small clasts of PAN might exist within lunar meteorites (Nagaoka et al., 2014), but PAN is not  
 496 known to exist within the Apollo collection. Some attribute the remote detection of PAN to an  
 497 erroneous calibration of spectral data (Warren and Korotev, 2022). The closest representative

498 sample is 97.6% An (mode) ferroan anorthosite 15415 ('Genesis Rock') (Steele and Smith, 1971;  
 499 Wilshire et al., 1972; Turner, 1972), which formed after the Moon's crust solidified and, therefore,  
 500 not representative of the LMO flotation crust remnants present in the south polar region (Ohtake  
 501 et al., 2009). For direct testing of the earliest flotation crust products of lunar crust formation, PAN  
 502 samples should be collected from the SPA, the oldest impact structure on the Moon.

503  
 504 PAN is mineralogically-pure in a scale detectable by remote sensing (Ohtake et al., 2009;  
 505 Cheek et al., 2013; Donaldson Hanna et al., 2014; Lemelin et al., 2019). A potential opportunity  
 506 to study the petrogeneses PAN materials could greatly improve the understanding of early lunar  
 507 differentiation processes (Yamamoto et al., 2012; Gawronska et al., 2020; Kring et al., 2022).  
 508 Return samples of PAN composition would help determine the spatial extent and composition of  
 509 the primary feldspathic crust, improve our inventory of the variety of age, distribution, and origin  
 510 of lunar rock types, aid in determining the composition of the lower crust and bulk Moon, and  
 511 clarify the local and regional complexity of the current lunar crust (NRC Concepts 3a, 3b, 3c, 3d).  
 512 Study of PAN return samples would aid understanding of how massifs were generated from the  
 513 SPA basin-forming impact (Kring et al., 2020), and the successive geologic evolution of the region  
 514 (NRC Concepts 1b, 1c). PAN samples may also provide an anchor to the early Earth-Moon impact  
 515 flux curve by determining the age of the oldest lunar basin (SPA) (Kring, 2007; Mazrouei et al.,  
 516 2019), establish a precise chronology of lunar geologic events (Marks et al., 2019), help determine  
 517 the thickness of the lunar crust (Spudis and Davis, 1986), aid characterization of lunar crust  
 518 variability on regional and global scales (NRC Concepts 1b, 1c, 2a). If anorthosite were to be  
 519 collected in-situ from strata exposed on the massif cliff (pole-ward) side of Site 102, this would  
 520 directly enable the investigation of the structure and composition of the lunar crust (Spudis and  
 521 Davis, 1986; Kring et al., 2020) (NRC Concepts 2a, 2d). It would also reveal more about the multi-  
 522 ring impact basin structure of SPA, quantify the effects of planetary characteristics (composition,  
 523 density, impact velocities) on crater formation and morphology, and allow the extent of lateral and  
 524 vertical mixing of local and ejecta material to be measured (NRC Concepts 6b, 6c, 6d).

### 525 3.1.3 Noritic, Gabbroic, or Troctolitic Anorthosite

526 Noritic/gabbroic anorthosites belong to the ferroan anorthosite (FAN) suite of lunar rocks and  
 527 have been confirmed to exist within the SPA farside Highlands by analyses of the Chang'E-5  
 528 return sample CE5C0800YJYX132GP (Wang, 2022). Noritic/gabbroic anorthosite or troctolitic  
 529 anorthosite (77.5 to 90 wt. % plagioclase, Figure 4) are the second most abundant lithologies in  
 530 the south polar region (Lemelin et al., 2022). The parent melts of noritic/gabbroic anorthosites are  
 531 believed to be produced during the lunar magma ocean (LMO) overturn by the decompression  
 532 melting of upwelling Mg cumulates and coincident mixing with incompatible element enriched  
 533 materials (e.g., potassium, rare earth elements, and phosphorous-rich; KREEP) (Hess and  
 534 Parmentier, 1995; Elkins-Tanton et al., 2002, 2011). However, Apollo FANs are not representative  
 535 of all lunar highland-type crust (Gross et al., 2014, 2020; Xu et al., 2020), so further study of  
 536 noritic/gabbroic anorthosites returned by Artemis astronauts would provide information about the  
 537 early evolution of the Moon as relevant to the LMO hypothesis.

538  
 539 Troctolitic anorthosite is an anorthosite with a minor olivine component (Figure 4) and the  
 540  $Mg\# = 87 \pm 5$  (Lucey et al., 2006). Troctolitic anorthosite is a member of the magnesian suite (Mg-  
 541 suite) of lunar lithologies and does not belong to the ferroan anorthosite (FAN) group of lunar  
 542 lithologies (Lucey et al., 2006). It is representative of the average lithological composition of Site

543 004 (Lemelin et al., 2022). The collection of noritic or gabbroic anorthosite samples from the lunar  
 544 surface would enable a more in-depth understanding of lunar crust formation and differentiation  
 545 through the study of coexisting pyroxene and plagioclase, which is rare in other early LMO  
 546 cumulates (Elardo et al., 2011). A better understanding of LMO crystallization trends from a more  
 547 complete suite of materials that record this process will better inform thermal models of the Moon  
 548 and the thermal state of the interior during early crustal formation periods (Shearer and Papike,  
 549 2005; Elardo et al., 2011) (NRC Concepts 2a, 2d) (NRC, 2007).

550

551 Noritic/gabbroic return samples would improve our understanding of the extent and  
 552 composition of the primary feldspathic crust and other products of planetary differentiation, in turn  
 553 quantifying the local and regional complexity of the current lunar crust (NRC Concepts 3a, 3c,  
 554 3d). This can be most accurately accomplished by collecting samples with known impact crater  
 555 sources (i.e., in ejecta blankets with a clear crater source or in-situ from strata within crater walls).  
 556 Certain samples may also enable clarification of the lateral rock type variability on regional and  
 557 global scales.

558

559 Geochronological analyses of noritic/gabbroic anorthosites would improve the established  
 560 global lunar time scale and timing of large impact basin formation (Wood et al., 1970; Hawke,  
 561 2003) (NRC Concepts 1b, 1c). Noritic/gabbroic samples will add to our efforts to inventory the  
 562 diversity of lunar crustal rocks with respect to composition, age, distribution, and origin (NRC  
 563 Concepts 3b, 3c). For example, should troctolitic anorthosite be collected from Shackleton ejecta,  
 564 it would improve the understanding of early mafic cumulate products from the Lunar Magma  
 565 Ocean (LMO), in particular the precipitation and equilibration of olivine within the lunar crust  
 566 (Elkins-Tanton et al., 2011; Elardo et al., 2011) (NRC Concepts 3a, 3b, 3c, 3d). Direct sampling  
 567 of troctolitic anorthosite could show how it was generated and preserved relative to the SPA basin-  
 568 forming impact (Miljković et al., 2021) (NRC Concepts 1b, 1c, 2a, 3a, 3b, 3c, 3d), and the later  
 569 geologic evolution of the region (NRC Concepts 1b, 1c) (NRC, 2007).

## 570 3.2 Mafic Lithologies

571 Lunar mafic lithologies include troctolite, norite, and gabbro, including anorthositic and  
 572 olivine-bearing norite and gabbro. Many of these lithologies, especially coarse-grained varieties,  
 573 contain a mineralogic diversity that allows for most chronologic systems in Table 1 to be applied.  
 574 Methods involving Rb-Sr, Sm-Nd, and Lu-Hf isochron approaches have been applied (e.g., Borg  
 575 and Carlson, 2023, and references therein). In many cases, important U-rich accessory phases such  
 576 as zircon, baddeleyite, and phosphate group minerals are present, allowing for in-situ chronology  
 577 by laser ablation and ion probe (e.g., Shaulis et al, 2017; Merle et al., 2020).

### 578 3.2.1 Anorthositic Norite, Gabbro, or Troctolite

579 The regolith of the south polar region is dominated by anorthositic noritic/gabbroic and  
 580 anorthositic troctolitic mineral spectra (Lemelin et al., 2022). Of that regolith, anorthositic  
 581 norite/gabbro and anorthositic troctolite (60 to 77.5 wt. % plagioclase with varying proportions of  
 582 clino- to orthopyroxene, Figure 4) were identified at sites 011, 102, and 105 (Lemelin et al., 2022).  
 583 Anorthositic troctolite is an igneous rock with more plagioclase component than traditional  
 584 troctolite (Figure 4) It is still unknown if anorthositic troctolites from the AEZ will be coarse- or

585 fine-grained. Anorthositic troctolites from SPA may signify lithologies formed very early on in  
586 lunar history (Lucey et al., 2006).

587

588 If anorthositic norite/gabbro or anorthositic troctolite were to be collected from the Artemis  
589 region, those samples may illuminate how differentiation occurred after the overturn of the LMO  
590 including a better characterization of the thermal state of the interior (Elkins-Tanton et al., 2011;  
591 Elardo et al., 2011) (NRC Concepts 2a, 2b, 2d). These differentiation products are valuable tools  
592 to understand more details of the extent and composition of varied lithologies, and to quantify our  
593 inventory of the nuanced complexities therein (i.e., variety, age, distribution, origin) (NRC  
594 Concepts 3a, 3b, 3d) (NRC, 2007). Anorthositic norite/gabbros may also aid in the understanding  
595 of the bombardment history of the inner solar system recorded within the uniquely preserved lunar  
596 crust in samples with impact-reset ages (Kring, 2019). This would allow for the anchoring of the  
597 impact flux curve, determining the cadence of the creation of lunar basins (Kring, 2007), and  
598 establishing a precise absolute chronology of the geologic evolution of the lunar south pole region  
599 (NRC Concepts 1a, 1b, 1c).

### 600 3.2.2 Gabbro and Norite

601 Gabbro is a general term for a coarse-grained (typically plutonic) mafic igneous rock composed  
602 of plagioclase, Ca-rich clinopyroxene (augite), and <5 wt% of each of olivine and orthopyroxene  
603 (Figure 4). Norite is an orthopyroxene-bearing gabbro, with < 5 wt. % clinopyroxene or olivine  
604 (Figure 4). Lunar norites are distinguished from lithologies termed ‘gabbro-norites’ by the absence  
605 of a discrete high-Ca pyroxene phase and presence of a wider variety of trace phases (Papike et  
606 al., 2006). Because Shackleton crater is on the edge of the SPA basin, target material of Shackleton  
607 may be ancient noritic crust which may be exposed within crater walls (Gawronska et al., 2020).  
608 Gabbro/norite lithologies in SPA are believed to originate from upper mantle ejecta and contain a  
609 high abundance of Th- and K-bearing materials (Moriarty et al., 2021).

610

611 Gabbros and other mafic lunar lithologies can be used to define magmatic periods and chemical  
612 characteristics of mantle components contributing to the sources of the magmas (Papike et al.,  
613 2006). Gabbroic/noritic cumulates may not have participated in the gravitational overturn during  
614 the time of SPA formation (Moriarty et al., 2021), so return samples of this type would reveal  
615 critical information about magmatic differentiation events in early lunar history (NRC Concepts  
616 2a, 2b, 2d, 3a, 3b, 3d).

617

618 If gabbro or norite were to be collected from the Artemis region, it would aid in understanding  
619 the diversity of lunar crustal rocks through the comparison with Apollo samples of similar  
620 composition (NRC Concepts 3a, 3b, 3c, 3d, 6c, 6d). The large-scale lateral and vertical distribution  
621 of gabbro/norite lithologies could be better determined through in-situ observations of strata in  
622 crater walls and determination of source magmas via geochemical study (Shaulis et al., 2017).  
623 Defining isochron ages from analyses of these pyroxene-rich lithologies would aid in the  
624 understanding of the bombardment history of the inner solar system recorded within the lunar crust  
625 (Shih et al., 1993; Norman et al., 2003; Carlson et al., 2014; Zhang et al., 2021) (NRC Concepts  
626 1a, 1b, 1c, 3a, 3b, 3c, 3d). Gabbro/norite analyses could also show how magmatic events, including  
627 differentiation, transpired after the LMO overturn (NRC Concepts 2a, 2b, 2d, 3a, 3b, 3d) (NRC,  
628 2007).

### 629 3.2.3 Olivine Norite or Gabbro

630 Olivine norite or gabbro are composed of 10 to 50 wt. % plagioclase with varying proportions  
631 of olivine and pyroxene (Figure 4). This lithology is included in the Mg-suite of lunar rocks, which  
632 is representative of the crustal growth and basaltic magmatism period in lunar history (Shearer and  
633 Papike, 2005). The Chinese lunar farside mission Chang'E-4 identified a rock of olivine norite  
634 composition that is believed to have crystallized from the SPA impact pool using a visible and  
635 near-infrared spectrometer aboard the Yutu-2 rover (Lin et al., 2020). Although olivine  
636 norite/gabbro is not a dominant lithology within a 10-km radial exploration zone from any of the  
637 six potential crewed Artemis landing sites, fragments of it could be entrained in breccias. The  
638 Yutu-2 rover discovery of an olivine norite greatly increases the likelihood of finding others like  
639 it within SPA on the lunar nearside. Compositions consistent with olivine norite have been  
640 recognized but those compositions can also represent clast contamination in breccia (Lemelin et  
641 al., 2019). Olivine norite has also been recognized to exist as the most abundant host lithology of  
642 olivine on the edges of the innermost ring material of several basins (e.g., Moscoviense, Humorum,  
643 Imbrium, and Serentitatis), although may represent 'contamination' from basaltic materials  
644 (Yamamoto et al., 2010; Lemelin et al., 2019).

645  
646 If olivine norite/gabbro were to be collected from the Artemis region, it would shed light on  
647 impact kinematics and 'contamination' effects within impact structures (Lemelin et al., 2019),  
648 reveal a more detailed record of the bombardment history of the inner solar system recorded within  
649 the lunar crust (NRC Concepts 1a, 1b, 1c, 3a, 3b, 3c, 3d), and add valuable information to the  
650 diversity of lunar crustal rocks in an impact terrane (NRC Concepts 3a, 3b, 3c, 3d, 6c, 6d) (NRC,  
651 2007). The higher proportions of olivine within an olivine norite or gabbro would allow for more  
652 opportunities to investigate early differentiation processes within the lunar crust.

### 653 3.2.4 Troctolite

654 Troctolite is composed of plagioclase and olivine, with < 5 wt. % of pyroxene (Stöffler et al.,  
655 1980; Prissel and Prissel, 2021). Troctolites are included in the "Mg-suite" of nonmare lunar rocks  
656 and analyzed specimens contain a whole rock composition of  $Mg \# = 87 \pm 5$ . Troctolites are the  
657 most abundant Mg-suite sample type in the Apollo collection (Shearer et al., 2015), but the spatial  
658 distribution on a global scale is not well understood.

659  
660 Troctolites may represent the start of mantle materials in a subsurface depth profile (Hess,  
661 1994). An olivine-bearing lithology, possibly troctolite, is abundant in the peak-ring of the  
662 Shrodingier basin near the Artemis exploration zone. The original spectroscopy was published by  
663 Kramer et al. (2013). An LRO picture showing many kilometers of rock exposure in the peak ring  
664 was published by Kring et al. (2017). Hydrocode calculations indicate the olivine-bearing lithology  
665 was uplifted from depths of 20 to 30 km (Kring et al., 2016). Previous study of phosphorous  
666 diffusion patterns within olivine grains within lunar troctolite 76535 revealed a two-stage cooling  
667 model (initial rapid cooling at high temperatures, then slow cooling at lower temperatures) (Nelson  
668 et al., 2021). Therefore, continued study of lunar troctolites in impact ejecta or fragments of  
669 troctolites harvested from polymict breccias would lead to greater understanding of the thermal  
670 history of the Moon. However, if troctolite were to be collected from in-situ outcrops within crater  
671 walls, it would provide the most detailed context of the specific landing site's history through the  
672 observation of geologic relationships and large-scale textures. Because the global distribution of

673 Mg-suite lithologies is still unknown, the sampling of troctolite (or another in-situ mafic lithology)  
 674 could bring more understanding to their spatial extent and source regions (Shearer et al., 2015).

675  
 676 If troctolite were to be collected from impact ejecta or otherwise, it would allow for the creation  
 677 of a more detailed absolute chronology of serial magmatism, crust/mantle formation and evolution,  
 678 and impact and degassing events (McCallum et al., 2006; Elardo et al., 2012; Shearer et al., 2015;  
 679 McCubbin and Barnes, 2020) (NRC Concepts 1a, 1b, 1c, 1e). Troctolite samples would improve  
 680 the understanding of the structure and composition of the lunar interior, including a potentially  
 681 stratified upper mantle (Moriarty et al., 2021) (NRC Concepts 2a, 2b, 2d), and elucidate the nature  
 682 of the lower crust-mantle boundary (NRC Concepts 3a, 3b, 3c, 3d) (NRC, 2007).

### 683 3.3 Ultramafic Lithologies

684 Lunar ultramafic lithologies include pyroxenite, peridotite, and dunite. These lithologies are  
 685 typically incompatible trace-element (ITE) depleted, thus rock and mineral compositions can be  
 686 low in REE, U, K, and Rb. Depending on the mineralogy and ITE compositions, Rb-Sr, Sm-Nd,  
 687 and Lu-Hf have been applied to certain martian and terrestrial ultramafic specimens (e.g., Lapen et  
 688 al. 2005; 2010). Currently, lunar ultramafic rock specimens are extremely rare but are extremely  
 689 important for unraveling the timing of early lunar differentiation.

#### 690 3.3.1 Pyroxenites

691 Pyroxenite is a cumulate, igneous rock comprised of >90 wt. % pyroxene (Figure 4). It is  
 692 believed to be representative of lunar upper mantle layers crystallized directly from the LMO, and  
 693 thus difficult to observe in-situ due to a mostly subsurface existence (Gagnepain-Beyneix et al.,  
 694 2006; Kraettli et al., 2022). Despite the presence of deep craters within SPA, pyroxenite is not  
 695 currently known to be present at outcrop-scale within the Artemis region, which may be a relic of  
 696 the generally coarse spatial resolution of spectral data. Pyroxenite may, however, have been  
 697 excavated from depth and exist at the surface as lithic fragments within brecciated hand samples  
 698 within the Artemis region.

699  
 700 If pyroxenite were to be collected from impact ejecta, it would improve the understanding of  
 701 the structure and composition of the lunar interior (NRC Concepts 2a, 2b, 2d), elucidate the nature  
 702 of the lower crust-mantle boundary (NRC Concepts 3a, 3b, 3c, 3d), and reveal a more detailed  
 703 absolute chronology of impact events that led to the formation of SPA (NRC Concepts 1a, 1b, 1c,  
 704 1e) (NRC, 2007).

#### 705 3.3.2 Peridotite

706 Peridotite is an olivine-rich (Figure 4) cumulate igneous rock that is not yet known to exist  
 707 within the SPA region, however olivine-rich exposures have been identified throughout SPA  
 708 (Pieters et al., 2001; Yamamoto et al., 2010, 2012). Although it is not yet known to exist in sizable  
 709 deposits identifiable by current detection limitations, the possibility of a peridotite fragment  
 710 existing in a brecciated sample remains.

711  
 712 If peridotite were to be collected from impact ejecta, it would improve the understanding of  
 713 the composition of the lunar mantle and therefore, increase knowledge of structure and  
 714 differentiation in the lunar interior (NRC Concepts 2a, 2b, 2d), allow interpretation of the nature

715 of the lower crust-mantle boundary (NRC Concepts 3a, 3b, 3c, 3d), and reveal a more detailed  
716 absolute chronology of impact events, specifically the formation kinematics of the SPA basin  
717 (NRC Concepts 1a, 1b, 1c, 1e) (NRC, 2007).

### 718 3.3.3 Dunite

719 Dunite is composed of 90 to 100 vol. % olivine (Figure 4). Olivine exposures have been  
720 detected within walls, ejecta, and peaks of craters within the SPA basin (Yamamoto et al., 2010).  
721 It is unclear whether the exposures were excavated upper mantle (dunite) material or Mg-rich  
722 plutonic material (troctolite) in the Moon's lower crust (Yamamoto et al., 2010). Deep-seated  
723 olivine-rich layers would be hidden by a differentiated impact melt sheet (Grieve et al., 1991;  
724 Nakamura et al., 2009; Hurwitz and Kring, 2014), but later impacts could have excavated and  
725 exposed the olivine. This olivine-rich lithology is best observed at young, fresh craters in the  
726 concentric regions around large basins (Yamamoto et al., 2010). It is possible the SPA impact may  
727 have excavated into the mantle (Lucey et al., 1998), although it would have reprocessed the  
728 material in some manner (e.g., giant, differentiated impact melt sheet (Hurwitz and Kring, 2014).  
729

730 Very little ultramafic material exists within the Apollo collection. The only sample large  
731 enough to make the parent rock known (dunite fragments 72415-72418) has been extensively  
732 crushed and shows a complex history of shock, deformation, and recrystallization (Albee et al.,  
733 1974; Dymek et al., 1975; Lally et al., 1976; Papike et al., 2006). Dunite is representative of lunar  
734 mantle materials. The collection and return of in-situ lunar dunite to Earth would be a significant  
735 finding, as none of this yet exists in the lunar collections and is only hypothesized to exist in select  
736 areas within SPA. If dunite were to be collected from outcrop, it would improve the understanding  
737 of the structure and composition of the lunar interior (NRC Concepts 2a, 2b, 2c, 2d), however this  
738 scenario is unlikely because dunite exists at depth and would not easily be exhumed. If dunite is  
739 present within the Artemis exploration zone, it most likely exists as fragments and chips within  
740 ejecta blankets produced via impact cratering processes significant enough to reach the lunar  
741 mantle depths (Vaughan and Head, 2014; Moriarty and Pieters, 2018).  
742

743 Any lunar dunite would be a unique and rare addition to the lunar collection and could increase  
744 our knowledge of the diversity of lunar crustal rocks (NRC Concepts 3a, 3b, 3c, 3d). Because it  
745 would have been excavated from depth via large impactor, it could a) act as a 'probe' to examine  
746 mantle lithologies and petrologic evolution of the lunar interior, and b) highlight information about  
747 the bombardment history of the inner solar system (NRC Concepts 1a, 1b, 1c, 1e) (NRC, 2007).

### 748 3.4 Basaltic Materials

749 Basaltic materials are fine-grained mafic rocks that display a wide range in compositions  
750 similar to the suite of mafic plutonic rocks described earlier. Understanding the ages of these  
751 materials constrains the volcanic history of the Moon. Some basaltic materials have U-rich  
752 accessory phases that can be dated in-situ or can be dated by the Pb isotope systematics of other  
753 igneous phases (e.g., Curran et al., 2019; Li et al., 2021). In many cases, and where the rock has  
754 a relatively simple thermal history, Ar-Ar chronology has the potential for precise determinations  
755 of eruption ages.  
756

757 Photogeologic studies and return samples confirmed the lunar mare areas are formed by large  
758 volumes of flood basaltic lava, like the Columbia River Basalts on Earth (Wilson and Head, 1981).

759 Although no traditional mare materials are confirmed to exist at the surface in SPA, it likely resides  
760 in considerable quantities at depth in this region and is known as cryptomare. Cryptomare is  
761 basaltic in composition and represents some of the earliest volcanism on the Moon that has been  
762 buried by the later emplacement of crater ejecta material and basin-forming events (Head and  
763 Wilson, 1992). Cryptomare within SPA is estimated to cover a minimum area of  $2.5 \times 10^5 \text{ km}^2$ , be  
764 at least 400 m thick, volumetrically encompass  $>1.0 \times 10^5 \text{ km}^3$ , and be 3.63 to 4.1 Ga (Shearer et  
765 al., 2006). Cryptomare is observed within SPA through examination of dark-haloed craters  
766 (Schultz and Spudis, 1983) which enable the darker albedo cryptomare to be studied against the  
767 lighter albedo regolith materials. In-situ cryptomare exposures may not be present or accessible at  
768 any of the six potential landing regions but may still be present within the Artemis exploration  
769 zone as hashed fragments within crater ejecta. Impact melt ponds also exist on the margins of  
770 craters and are composed of basaltic ‘mare’ material, though they are not the classical mare  
771 deposits we were familiarized with from the Apollo landing sites.

772

773 If basaltic materials were to be collected in-situ from ‘cryptomaria’ strata within crater walls,  
774 application of geochronology methods would primarily reveal vital information about early lunar  
775 volcanism including the lunar volcanic flux, mantle sources, and compositional variability of  
776 basalts (NRC Concepts 5a, 5b, 5d). Impact melt ponds may also be sampled in-situ from the outer  
777 margins of craters within the Artemis region but would be more telling of the bombardment history  
778 of a region than a distinct new type of volcanism generated from depth (NRC Concepts 1a, 1b, 1c,  
779 1e). Collecting ‘mare’ type materials from impact ejecta would also prove useful toward  
780 establishing absolute chronology (NRC Concept 1c), broaden our understanding of the diversity  
781 of lunar crustal rocks (NRC Concept 3a, 3b, 3d), and reveal limited information on lunar volcanism  
782 (NRC Concept 5a, 5b, 5d) (NRC, 2007).

### 783 3.5 Impact Melts

784 Impact melt is created by intense shock pressures and temperatures that result in instantaneous  
785 melting and rapid quenching of a rock during impact. The original rock bulk chemistry is  
786 preserved, but the mineralogy and petrography is destroyed to varying degrees (Kettrup et al.,  
787 2003). Chronology of these materials typically rely on systems that are susceptible to thermal  
788 disturbances and systems (e.g., Ar-Ar) that can be applied to melts (Turner, 1972; Turner et al.,  
789 1973; Dalrymple and Ryder, 1993, 1996; Zellner and Delano, 2015; Norman et al., 2019) .  
790 Distinctions between impact melt, impact glasses, and volcanic glasses are important. Impact  
791 glasses are similar to volcanic glasses but are instead associated with shock and metamorphosed  
792 lithic fragments. Impact melt fragments are found in breccia deposits within and outside impact  
793 craters (‘suevite’), and as spherules in distal ejecta (‘tektites’) (Dressler and Reimold, 2001).  
794 Impact melt rocks differ from impact glasses in that they occur as massive bodies of rock  
795 crystallized from melt bodies, commonly in the form of sheet-like masses, in the interior of some  
796 impact craters.

797

798 Most impact-melt rocks contain lithic and mineral clasts from the target (Dressler and  
799 Reimold, 2001 and references therein; Stahle, 1972), which show clear shock and thermal effects  
800 (Bischoff and Stöffler, 1984). Complete homogenization of a target rock is only achieved in  
801 impacts by vaporization and whole-rock melting. The shock pressures required to produce whole-  
802 rock melting of gabbro is  $>75\text{-}80 \text{ GPa}$ , dunite is  $>60\text{-}70 \text{ GPa}$ , and most relevant to SPA, anorthosite  
803 is  $>45\text{-}50 \text{ GPa}$  (Müller and Hornemann, 1969; Stöffler and Hornemann, 1972; Stöffler, 1974;

804 Reimold and Stöffler, 1978; Schaal et al., 1979; Ostertag, 1983; Bischoff and Stöffler, 1992).  
805 Material identified as impact melt composes 30-50% of all hand-specimen-sized rocks returned  
806 from highland landing sites and ~50% of all lunar soil materials, including non-mare collections  
807 (Ryder, 1981). Impact-melt rocks from the parent crater are the most reliable for dating the time  
808 of impact (Staudacher et al., 1982; Stephan and Jessberger, 1992; Deutsch and Scharer, 1994) and  
809 should be the first choice for any dating effort.

810

811 The SPA impact likely formed from a 170 km diameter impactor with an energy of  
812  $\sim 4 \times 10^{26}$  J, replacing the basin center with a melt pool of mantle-dominated composition (Potter  
813 et al., 2012). This large melt pond would have cooled slow enough to differentiate within itself,  
814 creating a differentiated melt sheet within SPA, and therefore the Artemis region (Hurwitz and  
815 Kring, 2014). Sampling of different locations (e.g., quenched margins vs. strongly differentiated  
816 center) of the SPA impact melt sheet would reveal a more detail about the impact, its age, and  
817 thermal history of the Moon.

818

819 Sampling of varied locations of a differentiated melt sheet within SPA would uniquely enable  
820 fundamental information about impact processes including melt sheet differentiation (Hurwitz and  
821 Kring, 2014) (NRC Concepts 6a, 6b, 6c, and 6d), make a distinct and diverse addition to our current  
822 sample collection of lunar crustal rocks (NRC Concepts 3a, 3b, 3d), aid in untangling the  
823 bombardment history of the inner solar system (Kettrup et al., 2003; Lin et al., 2020) (NRC  
824 Concepts 1a, 1b, 1c), and better constrain the thickness and variability of the lunar crust within  
825 SPA (Wieczorek and Zuber, 2001; Besserer et al., 2014) (NRC Concepts 2a, 2b). Impact melt  
826 fragments collected from ejecta would reveal impact event timing in the Artemis region, although  
827 in some cases it may be difficult to identify the source crater of the melt.

### 828 3.6 Impact Breccias

829 Impact breccias can contain a wide assortment of lithologies, a range in textures, materials with  
830 wide ranges in thermal histories, and contain clasts from various locations/levels in the Moon.  
831 Because of this variability, thus the chronologic opportunities can be rock/clast specific. Due to  
832 the classification of SPA as an impact terrain, a significant fraction of the surface lithologies  
833 available to Artemis astronauts and robotic assets will be breccias. Impact breccias are composed  
834 of older rocks that have been broken or melted by meteoroid impact (Stöffler et al., 1979). The  
835 components of breccias may be mineral and lithic fragments, crystallized impact melt, or glassy  
836 impact melt. Despite their randomized nature of rock and mineral components generated by  
837 impacts, they are lithified by the heat and shock associated with the impact. Most of the rock  
838 fragments in breccias of the distal part of the continuous ejecta deposits are from the local bedrock  
839 (Deutsch and Stöffler, 1987; Stöffler and Ryder, 2001).

840

841 A melt rock with clasts of unmelted (potentially shock-metamorphosed) targeted material is  
842 an 'impact melt breccia.' These melt bodies may intrude into fractures on the crater floor as veins  
843 and dikes that have been resampled by later impact events (Dressler and Reimold, 2001).  
844 Conversely, breccias composed of exclusively clastic components are 'fragmental' or 'lithic', and  
845 allow for the possibility to identify the nature of their dominant source rock types (Dressler and  
846 Reimold, 2001). The lithology, texture, and clast-types within breccias can be so widely varied  
847 that they, as a group, host the potential to address a majority of the NRC (2007) concepts. For  
848 example, a single polymict impact breccia could contain fragments from units with the ability

849 reveal the age of the SPA basin (NRC Concepts 1b, 1c), record a history of the ancient thermal  
850 state of the lunar interior (NRC Concept 2d), contain a wide diversity of lithologies (e.g., polymict  
851 breccias) (NRC Concepts 3a, 3b, 3c, 3d), host a cryptomare clast (NRC Concepts 5a, 5b, 5d), host  
852 a clast from a specific impact-associated unit such as a differentiated melt sheet (NRC Concepts  
853 6a, 6b, 6c), and exist as a mixture of units from depth and local ejecta and regolith materials (NRC  
854 Concepts 6d, 7a, 7c, 7d). Breccias are common to find in impact terrains but vary greatly in their  
855 contents. Each brecciated sample will require a highly individualized approach to the analyses and  
856 assessment of applicable NRC Concepts (2007).

857

### 858 3.7 Regolith Breccias and Soils

859 The lunar regolith was created by large impacts which reduced the grain size of the underlying  
860 bedrock (Horz et al., 1991; McKay et al., 1991). This regolith layer records the Moon's impact  
861 history and the nature and timing of material delivered to the Moon's surface (e.g., Lucey et al.,  
862 2006). Due to the high velocity of impact (e.g., Le Feuvre and Wieczorek, 2011) and resultant  
863 melting and/or vaporization, a projectile imparts its geochemical signature into impact melt  
864 deposits it creates (Morgan et al., 1972a, b; Ganapathy et al., 1974; Higuchi and Morgan, 1975;  
865 Gros et al., 1976; James, 1996, 2002; Norman et al., 2002; Puchtel et al., 2008). However, some  
866 impactors completely or partially survive the lunar impact process intact, as evidenced by  
867 unmelted fragments of meteorites that have been found in lunar rocks and soils (e.g., McSween Jr,  
868 1976; Jolliff et al., 1993; Zolensky et al., 1996; Rubin, 1997; Zolensky, 1997; Day et al., 2006).  
869 When paired with a time of impact, these partially unmelted samples help to provide better  
870 geochemical and chronological constraints for models of Solar system dynamics and causes of  
871 impact spikes to the Earth-Moon system (Turner et al., 1973; Tera et al., 1974; Dalrymple and  
872 Ryder, 1993, 1996; Cohen et al., 2000; Kring and Cohen, 2002; Kring et al., 2005; Norman et al.,  
873 2006; Čuk et al., 2010). Geochemical and chronological evidence from lunar samples informs our  
874 understanding of the Earth-Moon system, and the wider inner Solar system. Ages of lunar regolith  
875 breccias and soils can be estimated from the trapped  $^{40}\text{Ar}/^{36}\text{Ar}$  ratio of a sample. The abundances  
876 of trapped  $^{40}\text{Ar}$  within a regolith sample is normalized to  $^{36}\text{Ar}$  as an indicator of the point in time  
877 of the last exposure to solar wind (i.e., the space environment), before closure of the system  
878 through burial by an ejecta blanket or a basalt flow. Variations of trapped Ar with time has been  
879 used to estimate the ages of lunar regolith samples (Eugster et al., 1980, 1983, 2001; McKay et al.,  
880 1986; Eugster and Polnau, 1997). A model age representing breccia closure represents the last time  
881 grain-size components of the breccia were exposed to solar wind and may be used to calculate the  
882 formation time of the breccia (Joy et al., 2011, after Eugster et al., 2001). The technique was used  
883 to determine the ages of 191 lunar regolith samples from Apollo, Luna, and meteorite collections  
884 (Fagan et al., 2014).

885

886 In addition to what was stated in the impact breccia section, regolith breccias and lunar soils  
887 have the potential to address physical properties of the extremely cold (and possible volatile-rich)  
888 polar regolith (NRC Concept 4d), measure the extent of lateral and vertical mixing of local and  
889 ejecta material (NRC Concept 6d), and utilize the Moon as a natural laboratory for regolith  
890 processes and weathering on anhydrous airless bodies (NRC Concepts 7a, 7b, 7c, 7d).

## 891 4 Chronologic Applications: Limitations and Opportunities

892 In the previous sections, the Artemis exploration zone lithologies are described and the science  
893 potential for these returned materials is discussed. Applications of chronologic approaches to these  
894 lithologies and some specific and unresolved major questions are informed by previous  
895 chronologic studies (Nyquist and Shih, 1992; Nyquist et al., 2001; Carlson et al., 2014; Borg et  
896 al., 2015; Barboni et al., 2017; Papike et al., 2018; Borg and Carlson, 2023). A primary question  
897 is: what is the age of the Moon? This seemingly simple question has been exceedingly difficult to  
898 answer.

899

### 900 4.1 Age of the Moon and timing of the LMO

901

902 In the context of a Moon-forming impact model of Lock et al. (2018), the violence of this event  
903 served to destroy most, if not all evidence of the impactor and proto-Earth. The Moon would have  
904 formed from a terrestrial synestia and undergone a magma ocean phase (Elkins-Tanton et al., 2011;  
905 Elardo et al., 2011). During the lunar magma ocean (LMO) crystallization phase, metal-silicate  
906 differentiation would take place. The timing of lunar core formation is robustly constrained to have  
907 occurred after 4.51 to 4.50 Ga based on the short-lived  $^{182}\text{Hf}$ - $^{182}\text{W}$  isotope system (Touboul et al.,  
908 2007; Kruijjer and Kleine, 2017). Thus, the Moon formed *after* 4.51 – 4.50 Ga. Constraints on the  
909 first silicate minerals to form in the crust and mantle during the magma ocean crystallization phase  
910 is where significant debate exists. Prominent, accessible lithologies that should reflect LMO  
911 fractionation products are anorthositic flotation cumulate rocks that form after about 75% of the  
912 LMO crystallized (Rapp and Draper, 2018). As discussed in Borg and Carlson (2023), numerous  
913 attempts to date lunar anorthosites have yielded many different results. They discuss many issues  
914 that could result in ‘excess’ scatter about an isochron (meaning that the scatter is greater than  
915 predicted from analytical uncertainties alone) and initial isotopic compositions that suggest open-  
916 system behavior or variable effects of secondary processes. Thus, Borg and Carlson (2023) suggest  
917 that the most reliable ages are those that are supported by independent confirmation with another  
918 isotopic system and from these criteria conclude that anorthosites related to LMO crystallization  
919 are likely no older than about 4.36 Ga. There are, however, other studies that show relatively robust  
920 isochrons indicative of older ages but lack independent confirmation. These include a Sm-Nd  
921 mineral and whole rock isochron age of  $4.463 \pm 0.040$  Ga in Descartes breccia 67215 (Norman et  
922 al., 2003), an Sm-Nd isochron age of  $4.436 \pm 0.034$  for an anorthositic clast in Y-86032 (Nyquist  
923 et al., 2006). The oldest reliable age determined directly from a ferroan anorthosite constrains how  
924 late the Moon-forming event was. The potential for additional anorthositic materials from the  
925 Artemis explorations areas, especially the potential PAN lithologies, may provide materials that  
926 could help better constrain the timing of LMO crystallization and the age of lunar formation,  
927 overall. Other constraints on the age of the Moon come from Lu-Hf model ages of lunar zircon  
928 (Barboni et al., 2017). These data provide strong evidence that the Moon-forming event occurred  
929 at about 4.50-4.51 Ga and highlight an ‘old versus young’ Moon formation debate. Collection of  
930 any materials containing zircon (e.g., gabbroic clasts) in the exploration zone can further test the  
931 Lu-Hf constraints on lunar formation.

932

933 In addition to the sample return of materials that may help directly date the Moon-forming  
934 event through an expanded sample suite, new analytical opportunities are evolving. These include  
935 advances in in-situ Rb-Sr isotopic analyses (Dauphas et al., 2022; Zhang, 2022). Because  
936 anorthositic lithologies are susceptible to disturbance and have experienced protracted thermal

937 histories that may have resulted in isotopic disequilibrium (Borg and Carlson, 2023), in-situ  
 938 approaches have the potential for identifying sample areas (e.g., in a thick or thin section) that are  
 939 disturbed and those that are more pristine. This information will be invaluable for identifying lunar  
 940 materials that best preserve their primary or protolith components and target those areas for dating.  
 941 Robust ages, as defined by Borg and Carlson (2023), determined directly from LMO products will  
 942 have major implications for lunar age models and the timing and duration of the LMO.

943  
 944 Another way to date the LMO is to assess the formation timing of lunar mantle sources. A  
 945 robust method to determine when the lunar mantle ceased evolving through LMO crystallization  
 946 processes is to investigate the  $^{146}\text{Sm}$ - $^{142}\text{Nd}$  and  $^{147}\text{Sm}$ - $^{143}\text{Nd}$  isotopic compositions of lunar  
 947 materials (Nyquist et al., 1995; Boyet and Carlson, 2007; Borg et al., 2019). These studies show  
 948 that the lunar mantle closed to fractionation at about 4.33 Ga, but these data do not constrain when  
 949 LMO crystallization began. Thus, additional constraints on the timing of LMO crystallization can  
 950 be made if additional LMO products were collected and returned, such as those that may have been  
 951 excavated from depth during the SPA impact (Potter et al., 2012; Hurwitz and Kring, 2014;  
 952 Garrick-Bethell et al., 2020; Lin et al., 2020; Moriarty et al., 2021).

#### 953 954 4.2 Timing of Lunar Magmatism

955  
 956 Lunar magmatism has been ongoing until at least  $2.030 \pm 0.003$  Ga (Li et al., 2021). Models  
 957 that explain the evolution of lunar magmatism through time are underpinned by robust chronology.  
 958 While anorthositic rocks are often associated with LMO processes, lunar magmatism is often  
 959 associated with materials that are more basaltic in composition. Because these materials (which  
 960 include mare basalt, cryptomare, and most Mg-suite rocks) have more diverse mineralogies than  
 961 anorthositic rocks, the chronologic opportunities are far greater and essentially encapsulate all of  
 962 the systems and approaches listed in Table 1. Of critical note, trace U-rich phases such as zircon  
 963 and baddeleyite have the potential for precise U-Pb ages, even in thermally and chemically  
 964 disturbed specimens. In thermally undisturbed specimens and/or fine-grained or amorphous  
 965 specimens, precise Ar-Ar chronology can yield precise magmatic age determinations (e.g.,  
 966 Jourdan, 2012 and references therein). Precise mineral isochrons have been successfully applied  
 967 to numerous basaltic lunar compositions coarse enough for mineral separations (Nyquist and Shih,  
 968 1992; Rankenburg et al., 2007; Carlson et al., 2014). Given that most of the compositional mapping  
 969 noted in section 2 indicates anorthositic compositions, mafic clasts could be present that are below  
 970 the spatial resolution of spectral mapping. Thus, mafic lithologies have relatively high probabilities  
 971 of success for chronology and these data can better inform models for the magmatic evolution of  
 972 the Moon and help develop thermal models that explain at least  $\sim 2.5$  billion years of lunar  
 973 magmatic activity.

#### 974 975 4.3 Impact Processes and the Age of SPA

976  
 977 The Artemis exploration zones are located within the SPA basin and within heavily impacted  
 978 terrain. It is expected that most materials collected from these regions will have been affected to  
 979 some degree by impact processes. Figure 2 summarizes some of the predicted geology and unit  
 980 ages that might be encountered in the exploration zones. Critical to assessing the source(s) of  
 981 ejecta and their impact ages, dating impact metamorphism and/or impact melting is required.  
 982 Standard approaches involve Ar-Ar analyses of impact glass or material that experienced  
 significant Ar-loss during impact metamorphism. Materials that crystallized from an impact melt

983 can have U-rich phases that can be dated by in-situ U-Pb analyses or can be dated by mineral  
984 isochron approaches. In most cases, specimens that developed through impact processes can be  
985 dated in a variety of ways depending on the severity of impact metamorphism/melting; often, both  
986 the age of the protolith and the age of thermal metamorphism can be established (Burgess et al.,  
987 2007; Fernandes et al., 2013; Shaulis et al., 2017; Černok et al., 2021). The opportunity that impact  
988 materials would be collected from mapped terrains, connections between ejecta and impact basin  
989 can be strengthened. For impact chronology, the limit on science return is not the analytical  
990 techniques, it's the nature and types of samples collected from the surface and how they relate to  
991 the surface geology.

## 992 **5 Sampling Strategy**

993 The lithologies detected in the Artemis region by numerous previous studies (Yamamoto et  
994 al., 2012; Lemelin et al., 2017, 2022) were identified at relatively coarse spatial resolutions (1  
995 km/pixel; 500 m/pixel). It should be noted that two upcoming instruments with improved spatial  
996 resolution (Imaging Infrared Spectrometer aboard Chandrayaan-2; High-Resolution Volatiles and  
997 Minerals Moon Mapper aboard Lunar Trailblazer) will launch prior to crewed Artemis activities.  
998 Both instruments will produce data at a spatial resolution of 70 to 80 m/pixel, which will  
999 dramatically increase the mineralogical detail available to identify less abundant lithologies (i.e.,  
1000 PAN, olivine-rich units, mafic lithologies, etc.).

1001  
1002 The Apollo astronauts were instructed to collect the greatest diversity of samples with the  
1003 coarsest grain sizes to allow for easier mineral separation in laboratory analyses on Earth (Phinney,  
1004 2015). This practice does not need to hold true for the Artemis astronauts. There is benefit in  
1005 collecting the greatest diversity of samples possible with respect to grain size and composition. To  
1006 broaden the potential science impact from returned samples, the Artemis astronauts should focus  
1007 on material diversity and areas that may contain deeply excavated materials, among other activities  
1008 and sampling related to the broader mission goals.

## 1009 **6 Concluding Remarks**

1010 The Artemis exploration zone contains several regions that may be explored by future crewed  
1011 and uncrewed surface missions. Lithologies in this region were created from igneous and impact  
1012 processes that have persisted over billions of years. Some brecciated samples may contain clasts  
1013 petrogenetically unrelated to one another, which could be an efficient strategy to study a greater  
1014 variety of lunar lithologies without venturing over large spatial regions on the surface. The  
1015 potential for such breadth of lithological variety in an as-yet-unexplored region of the Moon will  
1016 provide chronologic opportunities for untangling the mysterious history of lunar evolution.  
1017 Chronologic opportunities that exist from analyses of returned samples include U-Th-P, Rb-Sr,  
1018 Sm-Nd, Lu-Hf, and Ar-Ar.

1019 These data will address issues such as the age of the Moon, timing of crucial events in lunar  
1020 history, allow for recalibration of melt extraction model ages, crystallization ages of lithologies,  
1021 and impact flux during the early Solar system. It is evident samples returned from the Artemis  
1022 exploration zone will provide incredible insight into the history of the Moon and early Solar  
1023 system. There is no 'silver bullet' analytical approach for all sample types. It will take a highly

1024 coordinated effort between lithologies, chronometers, instruments, and institutions to fully  
1025 understand what can be learned from these precious samples.

## 1026 **Acknowledgments**

- 1027 • The author acknowledges the Center for Lunar Science and Exploration for providing  
1028 funding to support the completion of this manuscript.
- 1029 • Since beginning this manuscript, the first author has become employed by Jacobs at  
1030 NASA Johnson Space Center in addition to her doctoral studies at University of  
1031 Houston.

## 1032 **Open Research**

1033 The reflectance and compositional mosaics used in this study are derived from Lemelin et al.  
1034 (2022) and can be found in Zenodo:[10.5281/zenodo.5847000](https://zenodo.org/record/5847000).

## 1035 **References**

- 1036 Abelson P. H. (1970) The Moon Issue. *Science* **167**, 447–447.
- 1037 Albee A. L., Chodos A. A., Dymek R. F., Gancarz A. J., Goldman D. S., Papanastassiou D. A.  
1038 and Wasserburg G. J. (1974) Dunite From the Lunar Highlands: Petrography,  
1039 Deformational History, Rb-Sr Age. In *Lunar and Planetary Science Conference* p. 3.
- 1040 Amelin Y. (2005) Meteorite Phosphates Show Constant <sup>176</sup>Lu Decay Rate Since 4557 Million  
1041 Years Ago. *Science* **310**, 839–841.
- 1042 Amelin Y. and Zaitsev A. N. (2002) Precise geochronology of phoscorites and carbonatites:: The  
1043 critical role of U-series disequilibrium in age interpretations. *Geochimica et*  
1044 *Cosmochimica Acta* **66**, 2399–2419.
- 1045 Anderson A. T., Crewe A. V., Goldsmith J. R., Moore P. B., Newton J. C., Olsen E. J., Smith J.  
1046 V. and Wyllie P. J. (1970) Petrologic History of Moon Suggested by Petrography,  
1047 Mineralogy, and Crystallography. *Science* **167**, 587–590.
- 1048 Arvidson R. E., Boyce J., Chapman C., Cintala M., Fulchignoni M., Moore H., Neukum G.,  
1049 Schultz P. H., Soderblom L., Strom R., Woronow A. and Young R. (1979) Standard  
1050 techniques for presentation and analysis of crater size-frequency data. *Icarus* **37**, 467–  
1051 474.
- 1052 Ballhaus C., Laurenz V., Münker C., Fonseca R. O. C., Albarède F., Rohrbach A., Lagos M.,  
1053 Schmidt M. W., Jochum K.-P., Stoll B., Weis U. and Helmy H. M. (2013) The U/Pb ratio  
1054 of the Earth’s mantle—A signature of late volatile addition. *Earth and Planetary Science*  
1055 *Letters* **362**, 237–245.
- 1056 Barboni Melanie, Boehnke P., Keller B., Kohl I. E., Schoene B., Young E. D. and McKeegan K.  
1057 D. (2017) Early formation of the Moon 4.51 billion years ago. *Sci. Adv.* **3**, e1602365.

- 1058 Barboni M, Boehnke P., Keller C., Kohl I., Schoene B., Young E. and McKeegan K. (2017) The  
 1059 Age of the Moon. In id. 1900. Lunar and Planetary Science XLVIII. Lunar and Planetary  
 1060 Institute, The Woodlands, Texas.
- 1061 Barnes J. J., Kring D. A., Tartèse R., Franchi I. A., Anand M. and Russell S. S. (2016) An  
 1062 asteroidal origin for water in the Moon. *Nat Commun* **7**, 11684.
- 1063 Beard B. L., Taylor L. A., Scherer E. E., Johnson C. M. and Snyder G. A. (1998) The Source  
 1064 Region and Melting Mineralogy of High-Titanium and Low-Titanium Lunar Basalts  
 1065 Deduced from Lu-Hf Isotope Data. *Geochimica et Cosmochimica Acta* **62**, 525–544.
- 1066 Beard S. P., Swindle T. D., Lapen T. J. and Kring D. A. (2022) Ar-Ar and U-Pb ages of  
 1067 Chelyabinsk and a re-evaluation of its impact chronology. *Meteorit & Planetary Scien*  
 1068 **57**, 2276–2288.
- 1069 Besserer J., Nimmo F., Wiczorek M. A., Weber R. C., Kiefer W. S., McGovern P. J., Andrews-  
 1070 Hanna J. C., Smith D. E. and Zuber M. T. (2014) GRAIL gravity constraints on the  
 1071 vertical and lateral density structure of the lunar crust. *Geophys. Res. Lett.* **41**, 5771–  
 1072 5777.
- 1073 Bickel V., Aaron J., Manconi A., Loew S. and Mall U. (2020) Impacts drive lunar rockfalls over  
 1074 billions of years. *Nature Communications* **11**.
- 1075 Bischoff A. and Stöffler D. (1984) Chemical and structural changes induced by thermal  
 1076 annealing of shocked feldspar inclusions in impact melt rocks from Lappajärvi Crater,  
 1077 Finland. *J. Geophys. Res.* **89**, B645.
- 1078 Bischoff A. and Stöffler D. (1992) Shock metamorphism as a fundamental process in the  
 1079 evolution of planetary bodies: Information from meteorites. *European Journal of*  
 1080 *Mineralogy* **4**, 707–755.
- 1081 Borg L., Connelly J., Boyet M. and Carlson R. (2011) The Age of Lunar Ferroan Anorthosite  
 1082 60025 with Implications for the Interpretation of Lunar Chronology and the Magma  
 1083 Ocean Model. In id. 1171. Lunar and Planetary Science XLII. Lunar and Planetary  
 1084 Institute, The Woodlands, Texas.
- 1085 Borg L. E., Brennecka G. A. and Kruijer T. S. (2022) The origin of volatile elements in the  
 1086 Earth–Moon system. *Proc. Natl. Acad. Sci. U.S.A.* **119**, e2115726119.
- 1087 Borg L. E. and Carlson R. W. (2023) The Evolving Chronology of Moon Formation. *Annu. Rev.*  
 1088 *Earth Planet. Sci.* **51**, annurev-earth-031621-060538.
- 1089 Borg L. E., Gaffney A. M., Kruijer T. S., Marks N. A., Sio C. K. and Wimpenny J. (2019)  
 1090 Isotopic evidence for a young lunar magma ocean. *Earth and Planetary Science Letters*  
 1091 **523**, 115706.
- 1092 Borg L. E., Gaffney A. M. and Shearer C. K. (2015) A review of lunar chronology revealing a  
 1093 preponderance of 4.34–4.37 Ga ages. *Meteorit Planet Sci* **50**, 715–732.

- 1094 Borg L. E., Gaffney A. M., Shearer C. K., DePaolo D. J., Hutcheon I. D., Owens T. L., Ramon  
 1095 E. and Brennecka G. (2009) Mechanisms for incompatible-element enrichment on the  
 1096 Moon deduced from the lunar basaltic meteorite Northwest Africa 032. *Geochimica et*  
 1097 *Cosmochimica Acta* **73**, 3963–3980.
- 1098 Borst A. M., Foing B. H., Davies G. R. and van Westrenen W. (2012) Surface mineralogy and  
 1099 stratigraphy of the lunar South Pole-Aitken basin determined from Clementine UV/VIS  
 1100 and NIR data. *Planetary and Space Science* **68**, 76–85.
- 1101 Bottke W. F., Walker R. J., Day J. M. D., Nesvorny D. and Elkins-Tanton L. (2010) Stochastic  
 1102 Late Accretion to Earth, the Moon, and Mars. *Science* **330**, 1527–1530.
- 1103 Boyce J. M., Schaber G. G. and Dial Jr A. L. (1977) Age of Luna 24 mare basalts based on crater  
 1104 studies. *Nature* **265**, 38–39.
- 1105 Boyet M. and Carlson R. W. (2007) A highly depleted moon or a non-magma ocean origin for  
 1106 the lunar crust? *Earth and Planetary Science Letters* **262**, 505–516.
- 1107 Brandon A. D., Lapen T. J., Debaille V., Beard B. L., Rankenburg K. and Neal C. (2009) Re-  
 1108 evaluating 142Nd/144Nd in lunar mare basalts with implications for the early evolution  
 1109 and bulk Sm/Nd of the Moon. *Geochimica et Cosmochimica Acta* **73**, 6421–6445.
- 1110 Brown H. M., Boyd A. K., Denevi B. W., Henriksen M. R., Manheim M. R., Robinson M. S.,  
 1111 Speyerer E. J. and Wagner R. V. (2022) Resource potential of lunar permanently  
 1112 shadowed regions. *Icarus* **377**, 114874.
- 1113 Burgess R., Fernandes V. A., Irving A. J. and Bunch T. E. (2007) Ar-Ar Ages of NWA 2977 and  
 1114 NWA 3160 – Lunar Meteorites Paired with NWA 773. In Lunar and Planetary Science  
 1115 XXXVIII. The Lunar and Planetary Science Institute, The Woodlands, Texas. p. Abstract  
 1116 1603.
- 1117 Bussey D. B. J., McGovern J. A., Spudis P. D., Neish C. D., Noda H., Ishihara Y. and Sørensen  
 1118 S.-A. (2010) Illumination conditions of the south pole of the Moon derived using Kaguya  
 1119 topography. *Icarus* **208**, 558–564.
- 1120 Cao H., Ling Z., Chen J., Fu X., Zou Y. and Joy K. (2021) Petrography, mineralogy, and  
 1121 geochemistry of a new lunar magnesian feldspathic meteorite Northwest Africa 11460.  
 1122 *Meteorit Planet Sci* **56**, 1857–1889.
- 1123 Carlson R. W., Borg L. E., Gaffney A. M. and Boyet M. (2014) Rb-Sr, Sm-Nd and Lu-Hf  
 1124 isotope systematics of the lunar Mg-suite: the age of the lunar crust and its relation to the  
 1125 time of Moon formation. *Phil. Trans. R. Soc. A* **372**, 20130246.
- 1126 Černok A., White L. F., Anand M., Tait K. T., Darling J. R., Whitehouse M., Miljković K.,  
 1127 Lemelin M., Reddy S. M., Fougèrouse D., Rickard W. D. A., Saxey D. W. and Ghent R.  
 1128 (2021) Lunar samples record an impact 4.2 billion years ago that may have formed the  
 1129 Serenitatis Basin. *Commun Earth Environ* **2**, 1–9.

- 1130 Charlier B. L. A., Ginibre C., Morgan D., Nowell G. M., Pearson D. G., Davidson J. P. and  
 1131 Ottley C. J. (2006) Methods for the microsampling and high-precision analysis of  
 1132 strontium and rubidium isotopes at single crystal scale for petrological and  
 1133 geochronological applications. *Chemical Geology* **232**, 114–133.
- 1134 Che X., Nemchin A., Liu D., Long T., Wang C., Norman M. D., Joy K. H., Tartese R., Head J.,  
 1135 Jolliff B., Snape J. F., Neal C. R., Whitehouse M. J., Crow C., Benedix G., Jourdan F.,  
 1136 Yang Z., Yang C., Liu J., Xie S., Bao Z., Fan R., Li D., Li Z. and Webb S. G. (2021) Age  
 1137 and composition of young basalts on the Moon, measured from samples returned by  
 1138 Chang’e-5. *Science* **374**, 887–890.
- 1139 Cheek L. C., Donaldson Hanna K. L., Pieters C. M., Head J. W. and Whitten J. L. (2013) The  
 1140 distribution and purity of anorthosite across the Orientale basin: New perspectives from  
 1141 Moon Mineralogy Mapper data: CRYSTALLINE ANORTHOSITE ACROSS  
 1142 ORIENTALE. *J. Geophys. Res. Planets* **118**, 1805–1820.
- 1143 Cherniak D. J. and Watson E. B. (2001) Pb diffusion in zircon. *Chemical Geology* **172**, 5–24.
- 1144 Chew D., Drost K., Marsh J. H. and Petrus J. A. (2021) LA-ICP-MS imaging in the geosciences  
 1145 and its applications to geochronology. *Chemical Geology* **559**, 119917.
- 1146 Coan D. (2020) Exploration EVA System Concept of Operations.
- 1147 Cohen B. A., Swindle T. D. and Kring D. A. (2005) Geochemistry and  $^{40}\text{Ar}$ - $^{39}\text{Ar}$   
 1148 geochronology of impact-melt clasts in feldspathic lunar meteorites: Implications for  
 1149 lunar bombardment history. *Meteoritics & Planetary Science* **40**, 755–777.
- 1150 Cohen B. A., Swindle T. D. and Kring D. A. (2000) Support for the Lunar Cataclysm Hypothesis  
 1151 from Lunar Meteorite Impact Melt Ages. *Science* **290**, 1754–1756.
- 1152 Čuk M., Gladman B. J. and Stewart S. T. (2010) Constraints on the source of lunar cataclysm  
 1153 impactors. *Icarus* **207**, 590–594.
- 1154 Culler T. S., Becker T. A., Muller R. A. and Renne P. R. (2000) Lunar Impact History from  $^{40}$   
 1155  $\text{Ar}/^{39}\text{Ar}$  Dating of Glass Spherules. *Science* **287**, 1785–1788.
- 1156 Curran N. M., Joy K. H., Snape J. F., Pernet-Fisher J. F., Gilmour J. D., Nemchin A. A.,  
 1157 Whitehouse M. J. and Burgess R. (2019) The early geological history of the Moon  
 1158 inferred from ancient lunar meteorite Miller Range 13317. *Meteorit & Planetary Scien*  
 1159 **54**, 1401–1430.
- 1160 Dalrymple G. B. and Ryder G. (1993)  $^{40}\text{Ar}/^{39}\text{Ar}$  age spectra of Apollo 15 impact melt rocks by  
 1161 laser step-heating and their bearing on the history of lunar basin formation. *J. Geophys.*  
 1162 *Res.* **98**, 13085–13095.
- 1163 Dalrymple G. B. and Ryder G. (1991)  $^{40}\text{Ar}/^{39}\text{Ar}$  ages of six Apollo 15 impact melt rocks by  
 1164 laser step heating. *Geophysical Research Letters* **18**, 1163–1166.

- 1165 Dalrymple G. B. and Ryder G. (1996) Argon-40/argon-39 age spectra of Apollo 17 highlands  
 1166 breccia samples by laser step heating and the age of the Serenitatis basin. *J. Geophys.*  
 1167 *Res.* **101**, 26069–26084.
- 1168 Dauphas N., Hopp T., Craig G., J. Zhang Z., C. Valdes M., R. Heck P., A. Charlier B. L., A. Bell  
 1169 E., Mark Harrison T., M. Davis A., Dussubieux L., R. Williams P., J. Krawczynski M.,  
 1170 Bouman C., S. Lloyd N., Tollstrup D. and B. Schwieters J. (2022) In situ 87 Rb– 87 Sr  
 1171 analyses of terrestrial and extraterrestrial samples by LA-MC-ICP-MS/MS with double  
 1172 Wien filter and collision cell technologies. *Journal of Analytical Atomic Spectrometry* **37**,  
 1173 2420–2441.
- 1174 Day J. M., Floss C., Taylor L. A., Anand M. and Patchen A. D. (2006) Evolved mare basalt  
 1175 magmatism, high Mg/Fe feldspathic crust, chondritic impactors, and the petrogenesis of  
 1176 Antarctic lunar breccia meteorites Meteorite Hills 01210 and Pecora Escarpment 02007.  
 1177 *Geochimica et Cosmochimica Acta* **70**, 5957–5989.
- 1178 Deutsch A. N., Head J. W. and Neumann G. A. (2020) Analyzing the ages of south polar craters  
 1179 on the Moon: Implications for the sources and evolution of surface water ice. *Icarus* **336**,  
 1180 113455.
- 1181 Deutsch A. and Scharer U. (1994) Dating terrestrial impact events. *Meteoritics* **29**, 301–322.
- 1182 Deutsch A. and Stöffler D. (1987) Rb-Sr-analyses of Apollo 16 melt rocks and a new age  
 1183 estimate for the Imbrium basin: Lunar basin chronology and the early heavy  
 1184 bombardment of the moon. *Geochimica et Cosmochimica Acta* **51**, 1951–1964.
- 1185 Donaldson Hanna K. L., Cheek L. C., Pieters C. M., Mustard J. F., Greenhagen B. T., Thomas I.  
 1186 R. and Bowles N. E. (2014) Global assessment of pure crystalline plagioclase across the  
 1187 Moon and implications for the evolution of the primary crust: Pure Plagioclase on the  
 1188 Moon. *J. Geophys. Res. Planets* **119**, 1516–1545.
- 1189 Dressler B. O. and Reimold W. U. (2001) Terrestrial impact melt rocks and glasses. *Earth-*  
 1190 *Science Reviews* **56**, 205–284.
- 1191 Duncan A. R., Mckay S. M., Stoesser J. W., Lindstrom M. M., Lindstrom D. J., Fruchter J. S. and  
 1192 Goles G. G. (1975) Lunar polymict breccia 14321: a compositional study of its principal  
 1193 components. *Geochimica et Cosmochimica Acta* **39**, 247–260.
- 1194 Dymek R. F., Albee A. L. and Chodos A. A. (1975) Comparative petrology of lunar cumulate  
 1195 rocks of possible primary origin: dunitite 72415, troctolite 76535, norite 78235, and  
 1196 anorthosite 62237. In Lunar Science Conference VI. New York, Pergamon Press, Inc.,  
 1197 Houston, Texas. pp. 301–341.
- 1198 Edmunson J., Borg L. E., Nyquist L. E. and Asmerom Y. (2009) A combined Sm–Nd, Rb–Sr,  
 1199 and U–Pb isotopic study of Mg-suite norite 78238: Further evidence for early  
 1200 differentiation of the Moon. *Geochimica et Cosmochimica Acta* **73**, 514–527.

- 1201 Elardo S. M., Draper D. S. and Shearer C. K. (2011) Lunar Magma Ocean crystallization  
 1202 revisited: Bulk composition, early cumulate mineralogy, and the source regions of the  
 1203 highlands Mg-suite. *Geochimica et Cosmochimica Acta* **75**, 3024–3045.
- 1204 Elardo S. M., McCubbin F. M. and Shearer C. K. (2012) Chromite symplectites in Mg-suite  
 1205 troctolite 76535 as evidence for infiltration metasomatism of a lunar layered intrusion.  
 1206 *Geochimica et Cosmochimica Acta* **87**, 154–177.
- 1207 Elkins-Tanton L. T., Burgess S. and Yin Q.-Z. (2011) The lunar magma ocean: Reconciling the  
 1208 solidification process with lunar petrology and geochronology. *Earth and Planetary  
 1209 Science Letters* **304**, 326–336.
- 1210 Elkins-Tanton L. T., Van Orman J. A., Hager B. H. and Grove T. L. (2002) Re-examination of  
 1211 the lunar magma ocean cumulate overturn hypothesis: melting or mixing is required.  
 1212 *Earth and Planetary Science Letters* **196**, 239–249.
- 1213 Eugster O., Geiss J. and Grogler N. (1983) Dating of early regolith exposure and the evolution of  
 1214 trapped  $^{40}\text{Ar}/^{36}\text{Ar}$  with time. *14th Lunar and Planetary Science Conference*, 177–178.
- 1215 Eugster O., Groegler N., Eberhardt P. and Geiss J. (1980) Double drive tube 74001/2-  
 1216 Composition of noble gases trapped 3.7 AE ago. In In: Lunar and Planetary Science  
 1217 Conference, 11th, Houston, TX, March 17-21, 1980, Proceedings. Volume 2.(A82-22296  
 1218 09-91) New York, Pergamon Press, 1980, p. 1565-1592. Swiss National Science  
 1219 Foundation. pp. 1565–1592.
- 1220 Eugster O. and Polnau E. (1997) Further data for the calibration of the antiquity indicator Ar-  
 1221  $^{40}\text{Ar}/\text{Ar}-36$  for lunar soil. In Conference Paper, 28th Annual Lunar and Planetary Science  
 1222 Conference, p. 341. p. 341.
- 1223 Eugster O., Terribilini D., Polnau E. and Kramers J. (2001) The antiquity indicator argon-  
 1224  $^{40}\text{Ar}/\text{argon}-36$  for lunar surface samples calibrated by uranium-235-xenon-136 dating.  
 1225 *Meteoritics & Planetary Science* **36**, 1097–1115.
- 1226 Fagan A. L., Joy K. H., Bogard D. D. and Kring D. A. (2014) Ages of Globally Distributed  
 1227 Lunar Paleoregoliths and Soils from 3.9 Ga to the Present. *Earth Moon Planets* **112**, 59–  
 1228 71.
- 1229 Fairweather J. H., Lagain A., Servis K., Benedix G. K., Kumar S. S. and Bland P. A. (2022)  
 1230 Automatic Mapping of Small Lunar Impact Craters Using LRO-NAC Images. *Earth and  
 1231 Space Science* **9**.
- 1232 Fernandes V. A., Fritz J., Weiss B. P., Garrick-Bethell I. and Shuster D. L. (2013) The  
 1233 bombardment history of the Moon as recorded by  $^{40}\text{Ar}-^{39}\text{Ar}$  chronology. *Meteorit  
 1234 Planet Sci* **48**, 241–269.
- 1235 Gaffney A. M. and Borg L. E. (2014) A young solidification age for the lunar magma ocean.  
 1236 *Geochimica et Cosmochimica Acta* **140**, 227–240.

- 1237 Gagnepain-Beyneix J., Lognonné P., Chenet H., Lombardi D. and Spohn T. (2006) A seismic  
 1238 model of the lunar mantle and constraints on temperature and mineralogy. *Physics of the*  
 1239 *Earth and Planetary Interiors* **159**, 140–166.
- 1240 Ganapathy R., Morgan J., Higuchi H., Anders E. and Anderson Jr A. (1974) Meteoritic and  
 1241 volatile elements in Apollo 16 rocks and in separated phases from 14306 Lunar Science  
 1242 V. *The Lunar Science Institute. Part*, 257–259.
- 1243 Garrick-Bethell I., Miljković K., Hiesinger H., van der Bogert C. H., Laneuville M., Shuster D.  
 1244 L. and Korycansky D. G. (2020) Troctolite 76535: A sample of the Moon’s South Pole-  
 1245 Aitken basin? *Icarus* **338**, 113430.
- 1246 Garrick-Bethell I. and Zuber M. T. (2009) Elliptical structure of the lunar South Pole-Aitken  
 1247 basin. *Icarus* **204**, 399–408.
- 1248 Gawronska A. J., Barrett N., Boazman S. J., Gilmour C. M., Halim S. H., Harish, McCanaan K.,  
 1249 Satyakumar A. V., Shah J., Meyer H. M. and Kring D. A. (2020) Geologic context and  
 1250 potential EVA targets at the lunar south pole. *Advances in Space Research* **66**, 1247–  
 1251 1264.
- 1252 Gopalan K., Kaushal S., Lee-Hu C. and Wetherill G. (1970) Rb-Sr and U, Th-Pb ages of lunar  
 1253 materials. *Geochimica et Cosmochimica Acta Supplement* **2**, 1195–1205.
- 1254 Grieve R. A. F., Stöffler D. and Deutsch A. (1991) The Sudbury structure: Controversial or  
 1255 misunderstood? *J. Geophys. Res.* **96**, 22753.
- 1256 Grieve R. A., McKay G. A., Smith H. D. and Weill D. F. (1975) Lunar polymict breccia 14321:  
 1257 a petrographic study. *Geochimica et Cosmochimica Acta* **39**, 229–245.
- 1258 Gros J., Takahashi H., Hertogen J., Morgan J. W. and Anders E. (1976) Composition of the  
 1259 projectiles that bombarded the lunar highlands. In In: Lunar Science Conference, 7th,  
 1260 Houston, Tex., March 15-19, 1976, Proceedings. Volume 2.(A77-34651 15-91) New  
 1261 York, Pergamon Press, Inc., 1976, p. 2403-2425. pp. 2403–2425.
- 1262 Gross J., Hilton A., Prissel T. C., Setera J. B., Korotev R. L. and Calzada-Diaz A. (2020)  
 1263 Geochemistry and Petrogenesis of Northwest Africa 10401: A New Type of the Mg-Suite  
 1264 Rocks. *JGR Planets* **125**.
- 1265 Gross J., Treiman A. H. and Mercer C. N. (2014) Lunar feldspathic meteorites: Constraints on  
 1266 the geology of the lunar highlands, and the origin of the lunar crust. *Earth and Planetary*  
 1267 *Science Letters* **388**, 318–328.
- 1268 Halim S., Barrett N., Boazman S., Gawronska A., Gilmour C., Harish, McCanaan K.,  
 1269 Satyakumar A., Shah J. and Kring D. (2021) Numerical modeling of the formation of  
 1270 Shackleton crater at the lunar south pole. *Icarus* **354**, 113992.
- 1271 Hapke B. (1981) Bidirectional reflectance spectroscopy: 1. Theory. *J. Geophys. Res.* **86**, 3039–  
 1272 3054.

- 1273 Hapke B. (2001) Space weathering from Mercury to the asteroid belt. *J. Geophys. Res.* **106**,  
 1274 10039–10073.
- 1275 Haruyama J., Matsunaga T., Ohtake M., Morota T., Honda C., Yokota Y., Torii M., Ogawa Y.,  
 1276 and LISM Working Group (2008) Global lunar-surface mapping experiment using the  
 1277 Lunar Imager/Spectrometer on SELENE. *Earth, Planets and Space* **60**, 243–255.
- 1278 Haskin L. A. (1998) The Imbrium impact event and the thorium distribution at the lunar  
 1279 highlands surface. *J. Geophys. Res.* **103**, 1679–1689.
- 1280 Haskin L. A., Korotev R. L., Rockow K. M. and Jolliff B. L. (1998) The case for an Imbrium  
 1281 origin of the Apollo thorium-rich impact-melt breccias. *Meteoritics & Planetary Science*  
 1282 **33**, 959–975.
- 1283 Hawke B. R. (2003) Distribution and modes of occurrence of lunar anorthosite. *J. Geophys. Res.*  
 1284 **108**, 5050.
- 1285 Head J. W., Murchie S., Mustard J. F., Pieters C. M., Neukum G., McEwen A., Greeley R.,  
 1286 Nagel E. and Belton M. J. S. (1993) Lunar impact basins: New data for the western limb  
 1287 and far side (Orientale and South Pole-Aitken Basins) from the first Galileo flyby. *J.*  
 1288 *Geophys. Res.* **98**, 17149.
- 1289 Head J. W. and Wilson L. (1992) Lunar mare volcanism: Stratigraphy, eruption conditions, and  
 1290 the evolution of secondary crusts. *Geochimica et Cosmochimica Acta* **56**, 2155–2175.
- 1291 Hess P. C. (1994) Petrogenesis of lunar troctolites. *J. Geophys. Res.* **99**, 19083.
- 1292 Hess P. C. and Parmentier E. M. (1995) A model for the thermal and chemical evolution of the  
 1293 Moon's interior: implications for the onset of mare volcanism. *Earth and Planetary*  
 1294 *Science Letters* **134**, 501–514.
- 1295 Hiesinger H. (2006) New Views of Lunar Geoscience: An Introduction and Overview. *Reviews*  
 1296 *in Mineralogy and Geochemistry* **60**, 1–81.
- 1297 Hiesinger H., van der Bogert C. H., Pasckert J. H., Funcke L., Giacomini L., Ostrach L. R. and  
 1298 Robinson M. S. (2012) How old are young lunar craters? *Journal of Geophysical*  
 1299 *Research: Planets* **117**.
- 1300 Higuchi H. and Morgan J. W. (1975) Ancient meteoritic component in Apollo 17 boulders. In  
 1301 Lunar and Planetary Science Conference Proceedings. pp. 1625–1651.
- 1302 Horz F., Grieve R., Heiken G., Spudis P. and Binder A. (1991) Chapter 4: Lunar Surface  
 1303 Processes. In *The Lunar Sourcebook* Cambridge University Press/Lunar and Planetary  
 1304 Institute. pp. 61–120.
- 1305 Howard K. A., Wilhelms D. E. and Scott D. H. (1974) Lunar basin formation and highland  
 1306 stratigraphy. *Rev. Geophys.* **12**, 309.

- 1307 Huang (黄俊) J., Xiao (肖智勇) Z., Xiao (肖龙) L., Horgan B., Hu (胡晓依) X., Lucey P., Xiao  
 1308 (肖潇) X., Zhao (赵思源) S., Qian (钱煜奇) Y., Zhang (张昊) H., Li (李春来) C., Xu (徐  
 1309 睿) R., He (何志平) Z., Yang (杨建峰) J., Xue (薛彬) B., He (何琦) Q., Zhong (钟杰) J.,  
 1310 Lin (林宏宇) H., Huang (黄长宁) C. and Xie (谢剑锋) J. (2020) Diverse rock types  
 1311 detected in the lunar South Pole–Aitken Basin by the Chang’E-4 lunar mission. *Geology*  
 1312 **48**, 723–727.
- 1313 Hui H., Neal C. R., Shih C.-Y. and Nyquist L. E. (2013) Petrogenetic association of the oldest  
 1314 lunar basalts: Combined Rb–Sr isotopic and trace element constraints. *Earth and*  
 1315 *Planetary Science Letters* **373**, 150–159.
- 1316 Hult M., Vidmar T., Rosengård U., Marissens G., Lutter G. and Sahin N. (2014) Half-life  
 1317 measurements of lutetium-176 using underground HPGe-detectors. *Applied Radiation*  
 1318 *and Isotopes* **87**, 112–117.
- 1319 Huneke J. C. (1978) 40Ar-39Ar Microanalysis of single 74220 glass balls and 72435 breccia  
 1320 clasts. *Proceedings of the Lunar and Planetary Science Conference* **9**, 2345–2362.
- 1321 Hurley P. and Pinson, Jr. W. (1970) Whole-rock Rb-Sr isotopic age relationships in Apollo 11  
 1322 lunar samples. *Geochimica et Cosmochimica Acta Supplement* **2**, 1195–1205.
- 1323 Hurwitz D. M. and Kring D. A. (2014) Differentiation of the South Pole–Aitken basin impact  
 1324 melt sheet: Implications for lunar exploration. *J. Geophys. Res. Planets* **119**, 1110–1133.
- 1325 Ibanez-Mejia M., Gehrels G. E., Ruiz J., Vervoort J. D., Eddy M. P. and Li C. (2014) Small-  
 1326 volume baddeleyite (ZrO<sub>2</sub>) U–Pb geochronology and Lu–Hf isotope geochemistry by  
 1327 LA-ICP-MS. Techniques and applications. *Chemical Geology* **384**, 149–167.
- 1328 Jaffey A. H., Flynn K. F., Glendenin L. E., Bentley W. C. and Essling A. M. (1971) Precision  
 1329 Measurement of Half-Lives and Specific Activities of U 235 and U 238. *Phys. Rev. C* **4**,  
 1330 1889–1906.
- 1331 James O. (1996) Siderophile elements in lunar impact melts define nature of the impactors. In  
 1332 *Lunar and Planetary Science*, volume 27, page 603.
- 1333 James O. B. (2002) Distinctive Meteoritic Components in Lunar ‘‘Cataclysm’’ Impact-Melt  
 1334 Breccias. In *Lunar and Planetary Science Conference*. p. 1210.
- 1335 Johnston S., Brandon A., McLeod C., Rankenburg K., Becker H. and Copeland P. (2022) Nd  
 1336 isotope variation between the Earth–Moon system and enstatite chondrites. *Nature* **611**,  
 1337 501–506.
- 1338 Jolliff B. L., Gillis J. J., Haskin L. A., Korotev R. L. and Wieczorek M. A. (2000) Major lunar  
 1339 crustal terranes: Surface expressions and crust-mantle origins. *J. Geophys. Res.* **105**,  
 1340 4197–4216.

- 1341 Jolliff B. L., Korotev R. L. and Haskin L. A. (1993) An iridium-rich iron micrometeorite with  
 1342 silicate inclusions from the Moon. In Lunar and Planetary Inst., Twenty-Fourth Lunar  
 1343 and Planetary Science Conference. Part 2: GM.
- 1344 Jourdan F. (2012) The  $^{40}\text{Ar}/^{39}\text{Ar}$  dating technique applied to planetary sciences and terrestrial  
 1345 impacts. *Australian Journal of Earth Sciences* **59**, 199–224.
- 1346 Joy K. H., Crawford I. A., Anand M., Greenwood R. C., Franchi I. A. and Russell S. S. (2008)  
 1347 The petrology and geochemistry of Miller Range 05035: A new lunar gabbroic meteorite.  
 1348 *Geochimica et Cosmochimica Acta* **72**, 3822–3844.
- 1349 Joy K. H., Crawford I. A., Curran N. M., Zolensky M., Fagan A. F. and Kring D. A. (2016) The  
 1350 Moon: An Archive of Small Body Migration in the Solar System. *Earth Moon Planets*  
 1351 **118**, 133–158.
- 1352 Joy K. H., Kring D. A., Bogard D. D., McKay D. S. and Zolensky M. E. (2011) Re-examination  
 1353 of the formation ages of the Apollo 16 regolith breccias. *Geochimica et Cosmochimica*  
 1354 *Acta* **75**, 7208–7225.
- 1355 Joy K. H., Tartèse R., Messenger S., Zolensky M. E., Marrocchi Y., Frank D. R. and Kring D. A.  
 1356 (2020) The isotopic composition of volatiles in the unique Bench Crater carbonaceous  
 1357 chondrite impactor found in the Apollo 12 regolith. *Earth and Planetary Science Letters*  
 1358 **540**, 116265.
- 1359 Kenkmann T. and Artemieva N. (2021) The terrestrial impact crater record: A statistical analysis  
 1360 of morphologies, structures, ages, lithologies, and more. *Meteorit Planet Sci* **56**, 1024–  
 1361 1070.
- 1362 Kereszturi A., Tomka R., Gläser P. A., Pal B. D., Steinmann V. and Warren T. (2022)  
 1363 Characteristics of de Gerlache crater, site of girdlands and slope exposed ice in a lunar  
 1364 polar depression. *Icarus* **388**, 115231.
- 1365 Kettrup B., Deutsch A. and Masaitis V. L. (2003) Homogeneous impact melts produced by a  
 1366 heterogeneous target? *Geochimica et Cosmochimica Acta* **67**, 733–750.
- 1367 Korotev R. L., Gillis J. J., Haskin L. A. and Jolliff B. L. (2002) On the Age of the Nectaris  
 1368 Basin. In *The Moon Beyond 2002: Next Steps in Lunar Science and Exploration*. p. 31.
- 1369 Kraettli G., Schmidt M. W. and Liebske C. (2022) Fractional crystallization of a basal lunar  
 1370 magma ocean: A dense melt-bearing garnetite layer above the core? *Icarus* **371**, 114699.
- 1371 Kramer G. Y., Kring D. A., Nahm A. L. and Pieters C. M. (2013) Spectral and photogeologic  
 1372 mapping of Schrödinger Basin and implications for post-South Pole-Aitken impact deep  
 1373 subsurface stratigraphy. *Icarus* **223**, 131–148.
- 1374 Krasilnikov S. S., Ivanov M. A., Head J. W. and Krasilnikov A. S. (2023) Geologic history of  
 1375 the south circumpolar region (SCR) of the Moon. *Icarus* **394**, 115422.

- 1376 Kring D. A. (2008) Deciphering the Chronology and Implications of Impact Cratering on the  
 1377 Moon: A High Science Priority for Lunar Exploration. In *Lunar and Planetary Science*  
 1378 XXXIX. The Woodlands, TX.
- 1379 Kring D. A. (2006) Exploring Lunar Impact Craters and Their Implications for the Origin and  
 1380 Early Evolution of Life on Earth.
- 1381 Kring D. A. (2005) Hypervelocity collisions into continental crust composed of sediments and an  
 1382 underlying crystalline basement: comparing the Ries (~24 km) and Chicxulub (~180  
 1383 km) impact craters. *Geochemistry* **65**, 1–46.
- 1384 Kring D. A. (2019) Lunar South Pole Geology: Preparing for a Seventh Lunar Landing. In  
 1385 NASA Exploration Science Forum.
- 1386 Kring D. A. (2009) Targeting Complex Craters and Multi-Ring Basins to Determine the Tempo  
 1387 of Impact Bombardment while Simultaneously Probing the Lunar Interior. In *Lunar*  
 1388 *Reconnaissance Orbiter Science Targeting Meeting*.
- 1389 Kring D. A. (2007) Using the Moon to Determine the Magnitude of the Inner Solar System  
 1390 Cataclysm and Post-Cataclysm Impact Flux. In *NAC Lunar Meeting*.
- 1391 Kring D. A., Bickel V. T., Van Der Bogert C. H., Fagan A. L., Gaddis L. R., Hiesinger H.,  
 1392 Hurtado J. M., Joy K. H., Lemelin M., Looper C. A., Osinski G. R., Pösges G., Siegler  
 1393 M., Tikoo S. M. and Zacny K. (2023) Elevation Changes and Slope that May Affect EVA  
 1394 Workload Near Potential Artemis Landing Sites. In *2023 IEEE Aerospace Conference*  
 1395 *2023 IEEE Aerospace Conference*. IEEE, Big Sky, MT, USA. pp. 1–17.
- 1396 Kring D. A., Claeys P., Gulick S. P. S., Morgan J. V. and Collins G. S. (2017) Chicxulub and the  
 1397 Exploration of Large Peak-Ring Impact Craters through Scientific Drilling. *GSAT*, 4–8.
- 1398 Kring D. A. and Cohen B. A. (2002) Cataclysmic bombardment throughout the inner solar  
 1399 system 3.9–4.0 Ga. *J. Geophys. Res.* **107**.
- 1400 Kring D. A., Gruener J. E. and Eppler D. B. (2020) Artemis III EVA Opportunities on Malapert  
 1401 and Leibnitz B Massifs. *Science Definition Team for Artemis*.
- 1402 Kring D. A., Kramer G. Y., Bussey D. B. J., Hurley D. M., Stickle A. M. and van der Bogert C.  
 1403 H. (2021) Prominent volcanic source of volatiles in the south polar region of the Moon.  
 1404 *Advances in Space Research* **68**, 4691–4701.
- 1405 Kring D. A., Kramer G. Y., Collins G. S., Potter R. W. K. and Chandnani M. (2016) Peak-ring  
 1406 structure and kinematics from a multi-disciplinary study of the Schrödinger impact basin.  
 1407 *Nat Commun* **7**, 13161.
- 1408 Kring D. A., Lemelin M., van der Bogert C. H., Bickel V., Hiesinger H., Hurtado J. M., Petro N.,  
 1409 Siegler M. A., Looper C. A., Huning T., Osinski G. R. and Gaddis L. (2022) Geological  
 1410 EVA Science along a South Pole-Aitken (SPA) Basin Massif Ridge Cross-Cut by  
 1411 Shackleton Crater. In *Lunar and Planetary Science LIII*. The Woodlands, Texas.

- 1412 Kring D. A., Swindle T. D., Strom R. G., Ito T. and Yoshida F. (2005) Exploring Impact  
 1413 Cratering on the Moon and its Implications for the Biologic Evolution of, and Habitable  
 1414 Conditions on, the Earth. In *Space Resources Roundtable VII*. Golden, Colorado.
- 1415 Kruijer T. S. and Kleine T. (2017) Tungsten isotopes and the origin of the Moon. *Earth and*  
 1416 *Planetary Science Letters* **475**, 15–24.
- 1417 Kumari N., Bretzfelder J. M., Ganesh I., Lang A. and Kring D. A. (2022) Surface Conditions and  
 1418 Resource Accessibility at Potential Artemis Landing Sites 007 and 011. *Planet. Sci. J.* **3**,  
 1419 224.
- 1420 Lagain A., Kreslavsky M., Baratoux D., Liu Y., Devillepoix H., Bland P., Benedix G. K., Doucet  
 1421 L. S. and Servis K. (2022) Has the impact flux of small and large asteroids varied through  
 1422 time on Mars, the Earth and the Moon? *Earth and Planetary Science Letters* **579**,  
 1423 117362.
- 1424 Lally J. S., Christie J. M., Nord Jr. G. L. and Heuer A. H. (1976) Deformation, recovery and  
 1425 recrystallization of lunar dunite 72417. In *Lunar and Planetary Science VII* New York,  
 1426 Pergamon Press, Inc., Houston, Texas. pp. 1845–1863.
- 1427 Lapen T. J., Richter M., Brandon A. D., Debaille V., Beard B. L., Shafer J. T. and Peslier A. H.  
 1428 (2010) A Younger Age for ALH84001 and Its Geochemical Link to Shergottite Sources  
 1429 in Mars. *Science* **328**, 347–351.
- 1430 Le Feuvre M. and Wieczorek M. A. (2011) Nonuniform cratering of the Moon and a revised  
 1431 crater chronology of the inner Solar System. *Icarus* **214**, 1–20.
- 1432 Lemelin M., Lucey P. G. and Camon A. (2022) Compositional Maps of the Lunar Polar Regions  
 1433 Derived from the Kaguya Spectral Profiler and the Lunar Orbiter Laser Altimeter Data.  
 1434 *Planet. Sci. J.* **3**, 63.
- 1435 Lemelin M., Lucey P. G., Crites S. T. and Jha K. (2017) Mineralogy and Iron Content of the  
 1436 Lunar Polar Regions using the Kaguya Spectral Profiler and the Lunar Orbiter Laser  
 1437 Altimeter. In *New Views of the Moon 2 Europe*.
- 1438 Lemelin M., Lucey P. G., Miljković K., Gaddis L. R., Hare T. and Ohtake M. (2019) The  
 1439 compositions of the lunar crust and upper mantle: Spectral analysis of the inner rings of  
 1440 lunar impact basins. *Planetary and Space Science* **165**, 230–243.
- 1441 Lemelin M., Lucey P. G., Song E. and Taylor G. J. (2015) Lunar central peak mineralogy and  
 1442 iron content using the Kaguya Multiband Imager: Reassessment of the compositional  
 1443 structure of the lunar crust: LUNAR CENTRAL PEAK MINERALOGY AND IRON. *J.*  
 1444 *Geophys. Res. Planets* **120**, 869–887.
- 1445 Levinson A. A. (1970) Proceedings of the Apollo 11 Lunar Science Conference (issued as  
 1446 *Geochimica et Cosmochimica Acta*, supplement no. 1, vol. 34, 1970). *Geochimica et*  
 1447 *Cosmochimica Acta* **34**, 1367–1372.

- 1448 Li Q.-L., Zhou Q., Liu Y., Xiao Z., Lin Y., Li J.-H., Ma H.-X., Tang G.-Q., Guo S., Tang X.,  
 1449 Yuan J.-Y., Li J., Wu F.-Y., Ouyang Z., Li C. and Li X.-H. (2021) Two-billion-year-old  
 1450 volcanism on the Moon from Chang'e-5 basalts. *Nature* **600**, 54–58.
- 1451 Li S. and Milliken R. E. (2017) Water on the surface of the Moon as seen by the Moon  
 1452 Mineralogy Mapper: Distribution, abundance, and origins. *Sci. Adv.* **3**, e1701471.
- 1453 Lin Honglei, He Z., Yang W., Lin Y., Xu R., Zhang C., Zhu M.-H., Chang R., Zhang J., Li C.,  
 1454 Lin Hongyu, Liu Y., Gou S., Wei Y., Hu S., Xue C., Yang J., Zhong J., Fu X., Wan W.  
 1455 and Zou Y. (2020) Olivine-norite rock detected by the lunar rover Yutu-2 likely  
 1456 crystallized from the SPA impact melt pool. *National Science Review* **7**, 913–920.
- 1457 Lock S. J., Stewart S. T., Petaev M. I., Leinhardt Z., Mace M. T., Jacobsen S. B. and Cuk M.  
 1458 (2018) The Origin of the Moon Within a Terrestrial Synestia. *J. Geophys. Res. Planets*  
 1459 **123**, 910–951.
- 1460 Lovering J. F., Wark D. A., Gleadow A. J. W. and Britten R. (1974) Lunar monazite: A late-  
 1461 stage (mesostasis) phase in mare basalt. *Earth and Planetary Science Letters* **21**, 164–  
 1462 168.
- 1463 Lucey P. G., Taylor G. J., Hawke B. R. and Spudis P. D. (1998) FeO and TiO<sub>2</sub> concentrations in  
 1464 the South Pole-Aitken basin: Implications for mantle composition and basin formation. *J.*  
 1465 *Geophys. Res.* **103**, 3701–3708.
- 1466 Lucey P., Korotev R., Gillis J., Taylor L., Lawrence D., Campbell B., Elphic R., Feldman B.,  
 1467 Hood L., Hunten D., Mendillo M., Noble S., Papike J., Reedy R., Lawson S., Prettyman  
 1468 T., Gasnault O. and Maurice S. (2006) Understanding the Lunar Surface and Space-Moon  
 1469 Interactions. In *Reviews in Mineralogy and Geochemistry* Mineralogical Society of  
 1470 America. pp. 83–219.
- 1471 Marks N. E., Borg L. E., Shearer C. K. and Cassata W. S. (2019) Geochronology of an Apollo 16  
 1472 Clast Provides Evidence for a Basin-Forming Impact 4.3 Billion Years Ago. *JGR Planets*  
 1473 **124**, 2465–2481.
- 1474 Mazarico E., Neumann G. A., Smith D. E., Zuber M. T. and Torrence M. H. (2011) Illumination  
 1475 conditions of the lunar polar regions using LOLA topography. *Icarus* **211**, 1066–1081.
- 1476 Mazrouei S., Ghent R. R., Bottke W. F., Parker A. H. and Gernon T. M. (2019) Earth and Moon  
 1477 impact flux increased at the end of the Paleozoic. *Science* **363**, 253–257.
- 1478 McCallum I. S., Domeneghetti M. C., Schwartz J. M., Mullen E. K., Zema M., Cámara F.,  
 1479 McCammon C. and Ganguly J. (2006) Cooling history of lunar Mg-suite gabbro-norite  
 1480 76255, troctolite 76535 and Stillwater pyroxenite SC-936: The record in exsolution and  
 1481 ordering in pyroxenes. *Geochimica et Cosmochimica Acta* **70**, 6068–6078.
- 1482 McCubbin F. M. and Barnes J. J. (2020) The chlorine-isotopic composition of lunar KREEP  
 1483 from magnesian-suite troctolite 76535. *American Mineralogist* **105**, 1270–1274.

- 1484 McDougall I., Harrison T. M., McDougall P. of G. I. and Harrison P. of G. D. of E. and S. S. T.  
 1485 M. (1999) *Geochronology and Thermochronology by the  $^{40}\text{Ar}/^{39}\text{Ar}$  Method.*, Oxford  
 1486 University Press.
- 1487 McKay D. S., Bogard D. D., Morris R. V., Korotev R. L., Johnson P. and Wentworth S. J. (1986)  
 1488 Apollo 16 regolith breccias: Characterization and evidence for early formation in the  
 1489 mega-regolith. *J. Geophys. Res.* **91**, 277–303.
- 1490 McKay D. S., Heiken G., Basu A., Blanford G., Simon S., Reedy R., French B. M. and Papike J.  
 1491 (1991) Chapter 7: The Lunar Regolith. In *The Lunar Sourcebook* Cambridge University  
 1492 Press/Lunar and Planetary Institute. pp. 285–356.
- 1493 McLeod C. L., Brandon A. D. and Armytage R. M. G. (2014) Constraints on the formation age  
 1494 and evolution of the Moon from  $^{142}\text{Nd}$ – $^{143}\text{Nd}$  systematics of Apollo 12 basalts. *Earth*  
 1495 *and Planetary Science Letters* **396**, 179–189.
- 1496 McLeod C. L., Brandon A. D., Fernandes V. A., Peslier A. H., Fritz J., Lapen T., Shafer J. T.,  
 1497 Butcher A. R. and Irving A. J. (2016) Constraints on formation and evolution of the lunar  
 1498 crust from feldspathic granulitic breccias NWA 3163 and 4881. *Geochimica et*  
 1499 *Cosmochimica Acta* **187**, 350–374.
- 1500 McSween Jr H. Y. (1976) A new type of chondritic meteorite found in lunar soil. *Earth and*  
 1501 *Planetary Science Letters* **31**, 193–199.
- 1502 Mercer C. M. and Hodges K. V. (2016) ArAR — A software tool to promote the robust  
 1503 comparison of K–Ar and  $^{40}\text{Ar}/^{39}\text{Ar}$  dates published using different decay, isotopic, and  
 1504 monitor-age parameters. *Chemical Geology* **440**, 148–163.
- 1505 Mercer C. M., Hodges K. V., Jolliff B. L., Van Soest M. C., Wartho J. and Weirich J. R. (2019)  
 1506 Exploring the variability of argon loss in Apollo 17 impact melt rock 77135 using high-  
 1507 spatial resolution  $^{40}\text{Ar}/^{39}\text{Ar}$  geochronology. *Meteorit & Planetary Sci* **54**, 721–739.
- 1508 Mercer C. M., Young K. E., Weirich J. R., Hodges K. V., Jolliff B. L., Wartho J.-A. and Van  
 1509 Soest M. C. (2015) Refining lunar impact chronology through high spatial resolution  $^{40}$   
 1510  $\text{Ar}/^{39}\text{Ar}$  dating of impact melts. *Sci. Adv.* **1**, e1400050.
- 1511 Merle R. E., Nemchin A. A., Grange M. L., Whitehouse M. J. and Pidgeon R. T. (2014) High  
 1512 resolution U-Pb ages of Ca-phosphates in Apollo 14 breccias: Implications for the age of  
 1513 the Imbrium impact. *Meteorit Planet Sci* **49**, 2241–2251.
- 1514 Meyer H. M., Denevi B. W., Boyd A. K. and Robinson M. S. (2016) The distribution and origin  
 1515 of lunar light plains around Orientale basin. *Icarus* **273**, 135–145.
- 1516 Michaut C. and Pinel V. (2018) Magma Ascent and Eruption Triggered by Cratering on the  
 1517 Moon: MAGMA ASCENT BELOW IMPACT CRATERS. *Geophys. Res. Lett.* **45**,  
 1518 6408–6416.

- 1519 Miljković K., Wieczorek M. A., Laneuville M., Nemchin A., Bland P. A. and Zuber M. T.  
 1520 (2021) Large impact cratering during lunar magma ocean solidification. *Nat Commun* **12**,  
 1521 5433.
- 1522 Moore H. J., Hodges C. A. and Scott D. H. (1974) Multiringed basins- illustrated by Orientale  
 1523 and associated features. In *Proceedings of the Lunar and Planetary Science, V*  
 1524 Supplement 5, *Geochimica et Cosmochimica Acta*. Pergamon Press Inc., Houston, Texas.  
 1525 pp. 71–100.
- 1526 Morbidelli A., Marchi S., Bottke W. F. and Kring D. A. (2012) A sawtooth-like timeline for the  
 1527 first billion years of lunar bombardment. *Earth and Planetary Science Letters* **355–356**,  
 1528 144–151.
- 1529 Morgan J. W., Krahenbuhl U., Ganapathy R. and Anders E. (1972a) Trace elements in Apollo 15  
 1530 samples: implications for meteorite influx and volatile depletion on the moon.  
 1531 *Proceedings of the Third Lunar Science Conference* **2**, 1361–1376.
- 1532 Morgan J. W., Laul J. C., Krahenbuhl U., Ganapathy R. and Anders E. (1972b) Major impacts on  
 1533 the Moon: characterization from trace elements in Apollo 12 and 14 samples. *Proceedings*  
 1534 *of the Third Lunar Science Conference* **3**, 1377.
- 1535 Moriarty Daniel P., Dygert N., Valencia S. N., Watkins R. N. and Petro N. E. (2021) The search  
 1536 for lunar mantle rocks exposed on the surface of the Moon. *Nat Commun* **12**, 4659.
- 1537 Moriarty D. P. and Pieters C. M. (2018) The Character of South Pole-Aitken Basin: Patterns of  
 1538 Surface and Subsurface Composition. *J. Geophys. Res. Planets* **123**, 729–747.
- 1539 Moriarty D. P., Watkins R. N., Valencia S. N., Kendall J. D., Evans A. J., Dygert N. and Petro N.  
 1540 E. (2021) Evidence for a Stratified Upper Mantle Preserved Within the South Pole-  
 1541 Aitken Basin. *J Geophys Res Planets* **126**.
- 1542 Mukhametshin Ch. R., Semenov A. and Shpekin M. (2018) Experience of modeling relief of  
 1543 impact lunar crater Aitken based on high-resolution orbital images. *Journal of Physics:*  
 1544 *Conference Series* **1015**.
- 1545 Müller W. F. and Hornemann U. (1969) Shock-induced planar deformation structures in  
 1546 experimentally shock-loaded olivines and in olivines from chondritic meteorites. *Earth*  
 1547 *and Planetary Science Letters* **7**, 251–264.
- 1548 Nagaoka H., Takeda H., Karouji Y., Ohtake M., Yamaguchi A., Yoneda S. and Hasebe N.  
 1549 (2014) Implications for the origins of pure anorthosites found in the feldspathic lunar  
 1550 meteorites, Dhofar 489 group. *Earth, Planets and Space* **66**, 115.
- 1551 Nagurney A. B., Treiman A. H. and Spudis P. D. (2016) Petrology, Bulk Composition, and  
 1552 Provenance of Meteorite Northwest Africa 5000 (NWA 5000). In 47th Lunar and  
 1553 Planetary Science Conference. The Woodlands, TX.

- 1554 Nakamura R., Matsunaga T., Ogawa Y., Yamamoto S., Hiroi T., Saiki K., Hirata N., Arai T.,  
 1555 Kitazato K., Takeda H., Sugihara T., Kodama S., Ohtake M., Haruyama J. and Yokota Y.  
 1556 (2009) Ultramafic impact melt sheet beneath the South Pole–Aitken basin on the Moon.  
 1557 *Geophys. Res. Lett.* **36**, L22202.
- 1558 NASA (2022) NASA Identifies Candidate Regions for Landing Next Americans on Moon.  
 1559 *NASA*.
- 1560 NASA (2021) NASA Prompts Companies for Artemis Lunar Terrain Vehicle Solutions. *Press*  
 1561 *Release*.
- 1562 NASA (2023) NASA Pursues Lunar Terrain Vehicle Services for Artemis Missions. *Press*  
 1563 *Release*.
- 1564 NASA (2020a) NASA’s lunar exploration program overview. *NASA’s lunar exploration*  
 1565 *program overview*.
- 1566 NASA (2020b) *NASA’s Plan for Sustained Lunar Exploration and Development.*, National  
 1567 Aeronautics and Space Administration.
- 1568 Nelson W. S., Hammer J. E., Shea T., Hellebrand E. and Jeffrey Taylor G. (2021) Chemical  
 1569 heterogeneities reveal early rapid cooling of Apollo Troctolite 76535. *Nat Commun* **12**,  
 1570 7054.
- 1571 Nemchin A., Timms N., Pidgeon R., Geisler T., Reddy S. and Meyer C. (2009) Timing of  
 1572 crystallization of the lunar magma ocean constrained by the oldest zircon. *Nature Geosci*  
 1573 **2**, 133–136.
- 1574 Neukum G. (1984) *Meteorite bombardment and dating of planetary surfaces, Translation of:*  
 1575 *Meteoritenbombardement und Datierung planetarer Oberflächen, Tenure Thesis,*  
 1576 *Ludwig-Maximilians University, Munich, Germany.*, NASA, NASA Headquarters  
 1577 Washington, DC United States.
- 1578 Neukum G., Ivanov B. A. and Hartmann W. K. (2001) Cratering Records in the Inner Solar  
 1579 System in Relation to the Lunar Reference System. In *Chronology and Evolution of Mars*  
 1580 (eds. R. Kallenbach, J. Geiss, and William K. Hartmann). Space Sciences Series of ISSI.  
 1581 Springer Netherlands, Dordrecht. pp. 55–86.
- 1582 Neukum G., König B. and Arkani-Hamed J. (1975) A study of lunar impact crater size-  
 1583 distributions. *The Moon* **12**, 201–229.
- 1584 Niihara T., Beard S. P., Swindle T. D., Schaffer L. A., Miyamoto H. and Kring D. A. (2019)  
 1585 Evidence for multiple 4.0–3.7 Ga impact events within the Apollo 16 collection. *Meteorit*  
 1586 *Planet Sci* **54**, 675–698.
- 1587 Niihara T., Kaiden H., Misawa K. and Sekine T. (2009) U-Pb Isotopic Systematics of  
 1588 Experimentally Shocked Baddeleyite. In id. 1562. 40th Lunar and Planetary Science  
 1589 Conference. Lunar and Planetary Institute, The Woodlands, Texas.

- 1590 Norman M. D., Bennett V. C. and Ryder G. (2002) Targeting the impactors: siderophile element  
 1591 signatures of lunar impact melts from Serenitatis. *Earth and Planetary Science Letters*  
 1592 **202**, 217–228.
- 1593 Norman M. D., Borg L. E., Nyquist L. E. and Bogard D. D. (2003) Chronology, geochemistry,  
 1594 and petrology of a ferroan noritic anorthosite clast from Descartes breccia 67215: Clues  
 1595 to the age, origin, structure, and impact history of the lunar crust. *Meteoritics &*  
 1596 *Planetary Science* **38**, 645–661.
- 1597 Norman M. D., Duncan R. A. and Huard J. J. (2006) Identifying impact events within the lunar  
 1598 cataclysm from  $40\text{Ar}$ – $39\text{Ar}$  ages and compositions of Apollo 16 impact melt rocks.  
 1599 *Geochimica et Cosmochimica Acta* **70**, 6032–6049.
- 1600 Norman M. D., Jourdan F. and Hui S. S. M. (2019) Impact History and Regolith Evolution on  
 1601 the Moon: Geochemistry and Ages of Glasses from the Apollo 16 Site. *JGR Planets* **124**,  
 1602 3167–3180.
- 1603 NRC (2007) *The Scientific Context for Exploration of the Moon.*,
- 1604 Nyquist L., Bogard D., Yamaguchi A., Shih C.-Y., Karouji Y., Ebihara M., Reese Y., Garrison  
 1605 D., McKay G. and Takeda H. (2006) Feldspathic clasts in Yamato-86032: Remnants of  
 1606 the lunar crust with implications for its formation and impact history. *Geochimica et*  
 1607 *Cosmochimica Acta* **70**, 5990–6015.
- 1608 Nyquist L. E., Bogard D. D., Shih C.-Y., Greshake A., Stöffler D. and Eugster O. (2001) Ages  
 1609 and Geologic Histories of Martian Meteorites. In *Chronology and Evolution of Mars*  
 1610 (eds. R. Kallenbach, J. Geiss, and W. K. Hartmann). Space Sciences Series of ISSI.  
 1611 Springer Netherlands, Dordrecht. pp. 105–164.
- 1612 Nyquist L. E. and Shih C. Y. (1992) The isotopic record of lunar volcanism. *Geochimica et*  
 1613 *Cosmochimica Acta* **56**, 2213–2234.
- 1614 Nyquist L. E., Wiesmann H., Bansal B., Shih C.-Y., Keith J. E. and Harper C. L. (1995)  $146\text{Sm}$ -  
 1615  $142\text{Nd}$  formation interval for the lunar mantle. *Geochimica et Cosmochimica Acta* **59**,  
 1616 2817–2837.
- 1617 Ohtake M., Matsunaga T., Haruyama J., Yokota Y., Morota T., Honda C., Ogawa Y., Torii M.,  
 1618 Miyamoto H., Arai T., Hirata N., Iwasaki A., Nakamura R., Hiroi T., Sugihara T., Takeda  
 1619 H., Otake H., Pieters C. M., Saiki K., Kitazato K., Abe M., Asada N., Demura H.,  
 1620 Yamaguchi Y., Sasaki S., Kodama S., Terazono J., Shirao M., Yamaji A., Minami S.,  
 1621 Akiyama H. and Josset J.-L. (2009) The global distribution of pure anorthosite on the  
 1622 Moon. *Nature* **461**, 236–240.
- 1623 Ostertag R. (1983) Shock experiments on feldspar crystals. *J. Geophys. Res.* **88**, B364.
- 1624 Papanastassiou D. A., Wasserburg G. J. and Burnett D. S. (1970) Rb-Sr ages of lunar rocks from  
 1625 the sea of tranquillity. *Earth and Planetary Science Letters* **8**, 1–19.

- 1626 Papike J. J., Burger P. V., Bell A. S. and Shearer C. K. (2018) Mn-Fe Systematics in Martian  
 1627 Olivine: Effect of Mantle Source, Oxygen Fugacity, and Temperature of Crystallization.  
 1628 In *Lunar and Planetary Science XLIX*. The Woodlands, Texas.
- 1629 Papike J., Ryder G. and Shearer C. (2006) Lunar Samples. In *Planetary Materials Reviews in*  
 1630 *Mineralogy*. Mineralogical Society of America. pp. 5–103 to 5–161.
- 1631 Patchett P. J. and Tatsumoto M. (1981) A routine high-precision method for Lu-Hf isotope  
 1632 geochemistry and chronology. *Contr. Mineral. and Petrol.* **75**, 263–267.
- 1633 Patchett P. J. and Tatsumoto M. (1980) Lu–Hf total-rock isochron for the eucrite meteorites.  
 1634 *Nature* **288**, 571–574.
- 1635 Patterson R. V., Frizzell K. R., Kodikara G. R. L., Kopp M., Luchsinger K. M., Madera A.,  
 1636 Meier M. L., Paladino T. G., Tai Udovicic C. J., Wroblewski F. B. and Kring D. A.  
 1637 (2022) In situ resource utilization investigations of potential Artemis landing site 105,  
 1638 lunar south pole. In *Lunar and Planetary Science LIII*. The Woodlands, Texas.
- 1639 Petro N. E. and Pieters C. M. (2008) The lunar-wide effects of basin ejecta distribution on the  
 1640 early megaregolith. *Meteoritics & Planetary Science* **43**, 1517–1529.
- 1641 Phinney W. (2015) *Science Training History of the Apollo Astronauts.*, NASA.
- 1642 Pieters C. M., Head J. W., Gaddis L., Jolliff B. and Duke M. (2001) Rock types of South Pole-  
 1643 Aitken basin and extent of basaltic volcanism. *J. Geophys. Res.* **106**, 28001–28022.
- 1644 Pieters C. M., Staid M. I., Fischer E. M., Tompkins S. and He G. (1994) A Sharper View of  
 1645 Impact Craters from Clementine Data. *Science* **266**, 1844–1848.
- 1646 Potter R. W. K., Collins G. S., Kiefer W. S., McGovern P. J. and Kring D. A. (2012)  
 1647 Constraining the size of the South Pole-Aitken basin impact. *Icarus* **220**, 730–743.
- 1648 Prissel T. C. and Prissel K. B. (2021) A lunar sample renaissance. *Nat Commun* **12**, 7053.
- 1649 Puchtel I. S., Walker R. J., James O. B. and Kring D. A. (2008) Osmium isotope and highly  
 1650 siderophile element systematics of lunar impact melt breccias: implications for the late  
 1651 accretion history of the Moon and Earth. *Geochimica et Cosmochimica Acta* **72**, 3022–  
 1652 3042.
- 1653 Rankenburg K., Brandon A. D. and Norman M. D. (2007) A Rb–Sr and Sm–Nd isotope  
 1654 geochronology and trace element study of lunar meteorite LaPaz Icefield 02205.  
 1655 *Geochimica et Cosmochimica Acta* **71**, 2120–2135.
- 1656 Rankenburg K., Brandon A. and Neal C. (2006) Constraints on the formation of the Moon from  
 1657 high-precision and Nd-isotopic measurements of lunar basalts. In *Lunar and Planetary*  
 1658 *Science Conference*. Lunar and Planetary Institute, The Woodlands, Texas.

- 1659 Rapp J. F. and Draper D. S. (2018) Fractional crystallization of the lunar magma ocean:  
 1660 Updating the dominant paradigm. *Meteorit & Planetary Scienc* **53**, 1432–1455.
- 1661 Rasmussen B., Fletcher I. R. and Muhling J. R. (2008) Pb/Pb geochronology, petrography and  
 1662 chemistry of Zr-rich accessory minerals (zirconolite, tranquillityite and baddeleyite) in  
 1663 mare basalt 10047. *Geochimica et Cosmochimica Acta* **72**, 5799–5818.
- 1664 Reimold W. U. and Stöffler D. (1978) Experimental shock metamorphism of dunite. In Lunar  
 1665 and Planetary Science Conference IV. The Woodlands, Texas. pp. 2805–2824.
- 1666 Renne P. R., Balco G., Ludwig K. R., Mundil R. and Min K. (2011) Response to the comment by  
 1667 W.H. Schwarz et al. on “Joint determination of 40K decay constants and 40Ar\*/40K for  
 1668 the Fish Canyon sanidine standard, and improved accuracy for 40Ar/39Ar  
 1669 geochronology” by P.R. Renne et al. (2010). *Geochimica et Cosmochimica Acta* **75**,  
 1670 5097–5100.
- 1671 Rubin A. E. (1997) The Hadley Rille enstatite chondrite and its agglutinate-like rim: Impact  
 1672 melting during accretion to the Moon. *Meteoritics & Planetary Science* **32**, 135–141.
- 1673 Schaal R. B., Hörz F., Thompson T. D. and Bauer J. F. (1979) Shock metamorphism of  
 1674 granulated lunar basalt. *Lunar and Planetary Science Conference X*, 2547–2571.
- 1675 Schaen A. J., Jicha B. R., Hodges K. V., Vermeesch P., Stelten M. E., Mercer C. M., Phillips D.,  
 1676 Rivera T. A., Jourdan F., Matchan E. L., Hemming S. R., Morgan L. E., Kelley S. P.,  
 1677 Cassata W. S., Heizler M. T., Vasconcelos P. M., Benowitz J. A., Koppers A. A. P., Mark  
 1678 D. F., Niespolo E. M., Sprain C. J., Hames W. E., Kuiper K. F., Turrin B. D., Renne P.  
 1679 R., Ross J., Nomade S., Guillou H., Webb L. E., Cohen B. A., Calvert A. T., Joyce N.,  
 1680 Ganerød M., Wijbrans J., Ishizuka O., He H., Ramirez A., Pfänder J. A., Lopez-Martínez  
 1681 M., Qiu H. and Singer B. S. (2020) Interpreting and reporting <sup>40</sup>Ar/<sup>39</sup>Ar geochronologic  
 1682 data. *GSA Bulletin*.
- 1683 Scherer E., Münker C. and Mezger K. (2001) Calibration of the Lutetium-Hafnium Clock.  
 1684 *Science* **293**, 683–687.
- 1685 Schoene B. (2014) U-Th-Pb Geochronology. In *Treatise on Geochemistry* Elsevier. pp. 341–377.
- 1686 Schoene B., Crowley J. L., Condon D. J., Schmitz M. D. and Bowring S. A. (2006) Reassessing  
 1687 the uranium decay constants for geochronology using ID-TIMS U–Pb data. *Geochimica*  
 1688 *et Cosmochimica Acta* **70**, 426–445.
- 1689 Schultz P. H. and Spudis P. D. (1983) Beginning and end of lunar mare volcanism. *Nature* **302**,  
 1690 233–236.
- 1691 Shaulis B. J., Righter M., Lapen T. J., Jolliff B. L. and Irving A. J. (2017) 3.1 Ga crystallization  
 1692 age for magnesian and ferroan gabbro lithologies in the Northwest Africa 773 clan of  
 1693 lunar meteorites. *Geochimica et Cosmochimica Acta* **213**, 435–456.

- 1694 Shearer C., Hess P., Wieczorek M., Pritchard M., Parmentier E., Borg L., Longhi J., Elkins-  
 1695 Tanton L., Neal C., Antonenko I., Canup R., Halliday A., Grove T., Hager B., Lee D. and  
 1696 Wiechert U. (2006) Thermal and Magmatic Evolution of the Moon. In *New Views on the*  
 1697 *Moon* Mineralogical Society of America. pp. 365–518.
- 1698 Shearer C. K., Elardo S. M., Petro N. E., Borg L. E. and McCubbin F. M. (2015) Origin of the  
 1699 lunar highlands Mg-suite: An integrated petrology, geochemistry, chronology, and  
 1700 remote sensing perspective. *American Mineralogist* **100**, 294–325.
- 1701 Shearer C. K. and Papike J. J. (2005) Early crustal building processes on the moon: Models for  
 1702 the petrogenesis of the magnesian suite. *Geochimica et Cosmochimica Acta* **69**, 3445–  
 1703 3461.
- 1704 Shih C.-Y., Nyquist L. E., Dasch E. J., Bogard D. D., Bansal B. M. and Wiesmann H. (1993)  
 1705 Ages of pristine noritic clasts from lunar breccias 15445 and 15455. *Geochimica et*  
 1706 *Cosmochimica Acta* **57**, 915–931.
- 1707 Shirley M. and Balaban E. (2022) An Overview of Mission Planning for the VIPER Rover.
- 1708 Silver L. T. (1970) Uranium-Thorium-Lead Isotope Relations in Lunar Materials. *Science* **167**,  
 1709 468–471.
- 1710 Snape J. F., Curran N. M., Whitehouse M. J., Nemchin A. A., Joy K. H., Hopkinson T., Anand  
 1711 M., Bellucci J. J. and Kenny G. G. (2018) Ancient volcanism on the Moon: Insights from  
 1712 Pb isotopes in the MIL 13317 and Kalahari 009 lunar meteorites. *Earth and Planetary*  
 1713 *Science Letters* **502**, 84–95.
- 1714 Söderlund U., Patchett P. J., Vervoort J. D. and Isachsen C. E. (2004) The  $^{176}\text{Lu}$  decay constant  
 1715 determined by Lu–Hf and U–Pb isotope systematics of Precambrian mafic intrusions.  
 1716 *Earth and Planetary Science Letters* **219**, 311–324.
- 1717 Spangler R. R., Warasila R. and Delano J. W. (1984)  $^{39}\text{Ar}$ - $^{40}\text{Ar}$  ages for the Apollo 15 green  
 1718 and yellow volcanic glasses. *J. Geophys. Res.* **89**, B487.
- 1719 Speyerer E. J. and Robinson M. (2013) Persistently illuminated regions at the lunar poles: Ideal  
 1720 sites for future exploration. *ICARUS* **222**, 122–136.
- 1721 Sprung P., Kleine T. and Scherer E. E. (2013) Isotopic evidence for chondritic Lu/Hf and Sm/Nd  
 1722 of the Moon. *Earth and Planetary Science Letters* **380**, 77–87.
- 1723 Spudis P. D., Bussey B., Plescia J., Josset J.-L. and Beauvivre S. (2008) Geology of Shackleton  
 1724 Crater and the south pole of the Moon. *Geophysical Research Letters* **35**.
- 1725 Spudis P. D. and Davis P. A. (1986) A chemical and petrological model of the lunar crust and  
 1726 implications for lunar crustal origin. *J. Geophys. Res.* **91**, E84.

- 1727 Spudis P. D., Hawke B. R. and Lucey P. G. (1988) Materials and formation of the Imbrium  
 1728 Basin. In *A89-10851 01-91 Proceedings of the Lunar and Planetary Science XVIII*.  
 1729 Cambridge University Press/Lunar and Planetary Institute, Houston, Texas. pp. 155–168.
- 1730 Srivastava Y., Basu Sarbadhikari A., Day J. M. D., Yamaguchi A. and Takenouchi A. (2022) A  
 1731 changing thermal regime revealed from shallow to deep basalt source melting in the  
 1732 Moon. *Nat Commun* **13**, 7594.
- 1733 Staudacher T., Jessberger E., Dominik B., Kirsten T. and Schaefferh O. (1982) Ar-40-Ar-39 ages  
 1734 of rocks and glasses from the Noerdlinger Ries Crater and the temperature history of  
 1735 impact breccias. *Journal of Geophysics* **51**, 1–11.
- 1736 Steele I. M. and Smith J. V. (1971) Mineralogy of Apollo 15415 “Genesis Rock” : Source of  
 1737 Anorthosite on Moon. *Nature* **234**, 138–140.
- 1738 Steiger R. H. and Jäger E. (1977) Subcommittee on geochronology: Convention on the use of  
 1739 decay constants in geo- and cosmochronology. *Earth and Planetary Science Letters* **36**,  
 1740 359–362.
- 1741 Stephan T. and Jessberger E. K. (1992) Isotope systematics and shock-wave metamorphism: III.  
 1742 K-Ar in experimentally and naturally shocked rocks; the Haughton impact structure,  
 1743 Canada. *Geochimica et Cosmochimica Acta* **56**, 1591–1605.
- 1744 Stöffler D. (1974) Deformation and transformation of rock forming minerals by natural and  
 1745 experimental shock processes. *Fortschr Mineral* **II**, 256–289.
- 1746 Stöffler D., Bischoff A., Borchardt R., Burgehele A., Deutsch A., Jessberger E. K., Ostertag R.,  
 1747 Palme H., Spettel B., Reimold W. U., Wacker K. and Wänke H. (1985) Composition and  
 1748 evolution of the lunar crust in the Descartes Highlands, Apollo 16. *J. Geophys. Res.* **90**,  
 1749 C449.
- 1750 Stöffler D. and Hornemann U. (1972) Quartz and feldspar glasses produced by natural and  
 1751 experimental shock. *Meteoritics* **7**, 371–394.
- 1752 Stöffler D., Knoll H. D. and Maerz U. (1979) Genetic Classification and Nomenclature of Lunar  
 1753 Highland Rocks Based on the Texture and Geological Setting of Terrestrial Impact  
 1754 Breccias. In *Lunar and Planetary Science X*. Houston, Texas.
- 1755 Stöffler D., Knoll H. D., Marvin U. B., Simonds C. H. and Warren P. H. (1980) *Recommended*  
 1756 *Classification and Nomenclature of Lunar Highland Rocks- a Committee Report.*, Lunar  
 1757 and Planetary Institute.
- 1758 Stöffler D. and Ryder G. (2001) Stratigraphy and Isotope Ages of Lunar Geologic Units:  
 1759 Chronological Standard for the Inner Solar System. In *Chronology and Evolution of Mars*  
 1760 (eds. R. Kallenbach, J. Geiss, and W. K. Hartmann). Space Sciences Series of ISSI.  
 1761 Springer Netherlands, Dordrecht. pp. 9–54.

- 1762 Stöffler D., Ryder G., Ivanov B. A., Artemieva N. A., Cintala M. J. and Grieve R. A. F. (2006)  
 1763 Cratering History and Lunar Chronology. In *New Views of the Moon Reviews in*  
 1764 *Mineralogy and Geochemistry*. Mineralogical Society of America. pp. 519–596.
- 1765 Swindle T. D., Isachsen C. E., Weirich J. R. and Kring D. A. (2009) <sup>40</sup>Ar-<sup>39</sup>Ar ages of H-  
 1766 chondrite impact melt breccias. *Meteoritics & Planetary Science* **44**, 747–762.
- 1767 Tai Udovicic C. J., Frizzell K. R., Kodikara G. R. L., Kopp M., Luchsinger K. M., Madera A.,  
 1768 Meier M. L., Paladino T. G., Patterson R. V., Wroblewski F. B. and Kring D. A. (2022)  
 1769 Modeling the Effects of Basin Impacts and Ballistic Sedimentation on Ice in Lunar Cold  
 1770 Traps. In 53rd Lunar and Planetary Science Conference. The Woodlands, TX.
- 1771 Tatsumoto M. and Rosholt J. N. (1970) Age of the Moon: An Isotopic Study of Uranium-  
 1772 Thorium-Lead Systematics of Lunar Samples. *Science* **167**, 461–463.
- 1773 Taylor D. J., McKeegan K. D. and Harrison T. M. (2009) Lu–Hf zircon evidence for rapid lunar  
 1774 differentiation. *Earth and Planetary Science Letters* **279**, 157–164.
- 1775 Tera F., Papanastassiou D. A. and Wasserburg G. J. (1974) Isotopic evidence for a terminal lunar  
 1776 cataclysm. *Earth and Planetary Science Letters* **22**, 1–21.
- 1777 Touboul M., Kleine T., Bourdon B., Palme H. and Wieler R. (2007) Late formation and  
 1778 prolonged differentiation of the Moon inferred from W isotopes in lunar metals. *Nature*  
 1779 **450**, 1206–1209.
- 1780 Turner G. (1972) <sup>40</sup>Ar-<sup>39</sup>Ar age and cosmic ray irradiation history of the Apollo 15 anorthosite,  
 1781 15415. *Earth and Planetary Science Letters* **14**, 169–175.
- 1782 Turner G. (1970) Argon-40/ Argon-39 Dating of Lunar Rock Samples. *Science* **167**, 466–468.
- 1783 Turner G. and Cadogan P. H. (1975) The history of lunar bombardment inferred from <sup>40</sup>Ar-<sup>39</sup>Ar  
 1784 dating of highland rocks. *Lunar and Planetary Science Conference Proceedings* **2**, 1509–  
 1785 1538.
- 1786 Turner G., Cadogan P. H. and Yonge C. J. (1973) Argon selenochronology. *Lunar and Planetary*  
 1787 *Science Conference Proceedings* **4**, 1889.
- 1788 Tye A. R., Fassett C. I., Head J. W., Mazarico E., Basilevsky A. T., Neumann G. A., Smith D. E.  
 1789 and Zuber M. T. (2015) The age of lunar south circumpolar craters Haworth, Shoemaker,  
 1790 Faustini, and Shackleton: Implications for regional geology, surface processes, and  
 1791 volatile sequestration. *Icarus* **255**, 70–77.
- 1792 Uemoto K., Ohtake M., Haruyama J., Matsunaga T., Yokota Y., Morota T., Nakamura R.,  
 1793 Yamamoto S. and Iwata T. (2010) Purest anorthosite distribution in the lunar South Pole-  
 1794 Aitken Basin derived from SELENE Multiband Imager. In 41st Lunar and Planetary  
 1795 Science Conference. The Woodlands, TX.

- 1796 Unruh D. M., Stille P., Patchett P. J. and Tatsumoto M. (1984) Lu-Hf and Sm-Nd evolution in  
1797 lunar mare basalts. *J. Geophys. Res.* **89**, B459.
- 1798 Vaughan W. M. and Head J. W. (2014) Impact melt differentiation in the South Pole-Aitken  
1799 basin: Some observations and speculations. *Planetary and Space Science* **91**, 101–106.
- 1800 Villa I. M., De Bièvre P., Holden N. E. and Renne P. R. (2015) IUPAC-IUGS recommendation  
1801 on the half life of 87Rb. *Geochimica et Cosmochimica Acta* **164**, 382–385.
- 1802 Villa I. M., Holden N. E., Possolo A., Ickert R. B., Hibbert D. B. and Renne P. R. (2020)  
1803 IUPAC-IUGS recommendation on the half-lives of 147Sm and 146Sm. *Geochimica et*  
1804 *Cosmochimica Acta* **285**, 70–77.
- 1805 Villa I. M., Holden N. E., Possolo A., Ickert R. B., Hibbert D. B., Renne P. R., Bonardi M. L.  
1806 and Bièvre P. D. (2022) IUGS–IUPAC recommendations and status reports on the half-  
1807 lives of 87Rb, 146Sm, 147Sm, 234U, 235U, and 238U (IUPAC Technical Report). *Pure*  
1808 *and Applied Chemistry* **94**, 1085–1092.
- 1809 Wang S.-J. (2022) First Location And Characterization Of Lunar Highland Clasts In Chang'E-5  
1810 Breccias Using TIMA-SEM-EPMA. *At.Spectrosc.* **43**, 351–362.
- 1811 Warren P. H. and Korotev R. L. (2022) Ground truth constraints and remote sensing of lunar  
1812 highland crust composition. *Meteorit & Planetary Scien* **57**, 527–557.
- 1813 Weirich J. R., Wittmann A., Isachsen C. E., Rumble D., Swindle T. D. and Kring D. A. (2010)  
1814 The Ar-Ar age and petrology of Miller Range 05029: Evidence for a large impact in the  
1815 very early solar system: Ar-Ar age and petrology of MIL 05029. *Meteoritics & Planetary*  
1816 *Science* **45**, 1868–1888.
- 1817 White L. F., Tait K. T., Kamo S. L., Moser D. E. and Darling J. R. (2020) Highly accurate dating  
1818 of micrometre-scale baddeleyite domains through combined focused ion beam extraction  
1819 and U–Pb thermal ionization mass spectrometry (FIB-TIMS). *Geochronology* **2**, 177–  
1820 186.
- 1821 Wieczorek M. A. and Zuber M. T. (2001) The composition and origin of the lunar crust:  
1822 Constraints from central peaks and crustal thickness modeling. *Geophys. Res. Lett.* **28**,  
1823 4023–4026.
- 1824 Wilhelms D. E., McCauley J. F. and Trask N. J. (1987) *The geologic history of the Moon.*,
- 1825 Wilshire H. G., Schaber G. G., Silver L. T., Phinney W. C. and Jackson E. D. (1972) Geologic  
1826 Setting and Petrology of Apollo 15 Anorthosite (15415). *Geol Soc America Bull* **83**,  
1827 1083.
- 1828 Wilson L. and Head J. W. (1981) Ascent and eruption of basaltic magma on the Earth and Moon.  
1829 *J. Geophys. Res.* **86**, 2971–3001.

- 1830 Wittmann A., Friedrich J. M., Troiano J., Macke R. J., Britt D. T., Swindle T. D., Weirich J. R.,  
 1831 Rumble D., Lasue J. and Kring D. A. (2011) H/L chondrite LaPaz Icefield 031047 – A  
 1832 feather of Icarus? *Geochimica et Cosmochimica Acta* **75**, 6140–6159.
- 1833 Wood J. A. (1970) Petrology of the lunar soil and geophysical implications. *J. Geophys. Res.* **75**,  
 1834 6497–6513.
- 1835 Wood J. A., Dickey J. S., Marvin U. B. and Powell B. N. (1970) Lunar Anorthosites. *Science*  
 1836 **167**, 602–604.
- 1837 Wu B., Wang Y., Lin T. J., Hu H. and Werner S. C. (2019) Impact cratering in and around the  
 1838 Orientale Basin: Results from recent high-resolution remote sensing datasets. *Icarus* **333**,  
 1839 343–355.
- 1840 Xie M., Liu T. and Xu A. (2020) Ballistic Sedimentation of Impact Crater Ejecta: Implications  
 1841 for the Provenance of Lunar Samples and the Resurfacing Effect of Ejecta on the Lunar  
 1842 Surface. *Journal of Geophysical Research: Planets* **125**, e2019JE006113.
- 1843 Xu Xiaoqing, Hui H., Chen W., Huang S., Neal C. R. and Xu Xisheng (2020) Formation of lunar  
 1844 highlands anorthosites. *Earth and Planetary Science Letters* **536**, 116138.
- 1845 Yamamoto S., Nakamura R., Matsunaga T., Ogawa Y., Ishihara Y., Morota T., Hirata N., Ohtake  
 1846 M., Hiroi T., Yokota Y. and Haruyama J. (2012) Massive layer of pure anorthosite on the  
 1847 Moon: Pure anorthosite on the Moon. *Geophys. Res. Lett.* **39**, n/a-n/a.
- 1848 Yamamoto S., Nakamura R., Matsunaga T., Ogawa Y., Ishihara Y., Morota T., Hirata N., Ohtake  
 1849 M., Hiroi T., Yokota Y. and Haruyama J. (2010) Possible mantle origin of olivine around  
 1850 lunar impact basins detected by SELENE. *Nature Geosci* **3**, 533–536.
- 1851 Yokota Y., Matsunaga T., Ohtake M., Haruyama J., Nakamura R., Yamamoto S., Ogawa Y.,  
 1852 Morota T., Honda C., Saiki K., Nagasawa K., Kitazato K., Sasaki S., Iwasaki A., Demura  
 1853 H., Hirata N., Hiroi T., Honda R., Iijima Y. and Mizutani H. (2011) Lunar photometric  
 1854 properties at wavelengths 0.5–1.6  $\mu\text{m}$  acquired by SELENE Spectral Profiler and their  
 1855 dependency on local albedo and latitudinal zones. *Icarus* **215**, 639–660.
- 1856 Yue Z., Shi K., Di K., Lin Y. and Gou S. (2022) Progresses and prospects of impact crater  
 1857 studies. *Sci. China Earth Sci.*
- 1858 Zellner N. E. B. and Delano J. W. (2015)  $^{40}\text{Ar}/^{39}\text{Ar}$  ages of lunar impact glasses: Relationships  
 1859 among Ar diffusivity, chemical composition, shape, and size. *Geochimica et*  
 1860 *Cosmochimica Acta* **161**, 203–218.
- 1861 Zellner N. E. B., Delano J. W., Swindle T. D., Barra F., Olsen E. and Whittet D. C. B. (2009)  
 1862 Apollo 17 regolith, 71501,262: A record of impact events and mare volcanism in lunar  
 1863 glasses. *Meteoritics & Planetary Science* **44**, 839–851.

- 1864 Zhang B., Lin Y., Moser D. E., Warren P. H., Hao J., Barker I. R., Shieh S. R. and Bouvier A.  
1865 (2021) Timing of lunar Mg-suite magmatism constrained by SIMS U-Pb dating of Apollo  
1866 norite 78238. *Earth and Planetary Science Letters* **569**, 117046.
- 1867 Zhang J., Yang W., Hu S., Lin Y., Fang G., Li C., Peng W., Zhu S., He Z., Zhou B., Lin H.,  
1868 Yang J., Liu E., Xu Y., Wang J., Yao Z., Zou Y., Yan J. and Ouyang Z. (2015) Volcanic  
1869 history of the Imbrium basin: A close-up view from the lunar rover Yutu. *Proc. Natl.*  
1870 *Acad. Sci. U.S.A.* **112**, 5342–5347.
- 1871 Zhang W. (2022) In Situ Rb-Sr Dating Of Lunar Meteorites Using Laser Ablation MC-ICP-MS.  
1872 *At.Spectrosc.* **43**.
- 1873 Zhu M.-H., Artemieva N., Morbidelli A., Yin Q.-Z., Becker H. and Wünnemann K. (2019)  
1874 Reconstructing the late-accretion history of the Moon. *Nature* **571**, 226–229.
- 1875 Zolensky M. E. (1997) Structural water in the Bench Crater chondrite returned from the Moon.  
1876 *Meteoritics & Planetary Science* **32**, 15–18.
- 1877 Zolensky M. E., Weisburg M. K. and Buchanan P. C. (1996) Mineralogy of carbonaceous  
1878 chondrite clasts in HED achondrites and the Moon. *Meteoritics & Planetary Science* **31**,  
1879 537.
- 1880 Zuber M. T., Head J. W., Smith D. E., Neumann G. A., Mazarico E., Torrence M. H., Aharonson  
1881 O., Tye A. R., Fassett C. I., Rosenburg M. A. and Melosh H. J. (2012) Constraints on the  
1882 volatile distribution within Shackleton crater at the lunar south pole. *Nature* **486**, 378–  
1883 381.
- 1884

1 **Lithologies and Chronologic Opportunities of Materials to be Returned from the**  
2 **Artemis Exploration Zone**

3

4 **Ruby V. Patterson<sup>1</sup>, Thomas J. Lapen<sup>1</sup>, David A. Kring<sup>2</sup>, Myriam Lemelin<sup>3</sup>, and McKayla**  
5 **L. Meier<sup>4</sup>**

6 <sup>1</sup>University of Houston.<sup>2</sup>Lunar and Planetary Institute.<sup>3</sup>Université de Sherbrooke.<sup>4</sup>University of  
7 Florida.

8 Corresponding author: Ruby Patterson (rubypatterson1@gmail.com)

9 \*Alternate affiliation: Jacobs at NASA Johnson Space Center, 2101 NASA Parkway, Building 31,  
10 Room 156, Houston, TX, 77058; ruby.v.patterson@nasa.gov.

11 **Key Points:**

- 12 • The Artemis lunar missions will explore a feldspathic impact terrain and return samples  
13 from unexplored terrain.
- 14 • Likely lithologies, ages, and chronometers are discussed for six potential landing sites.
- 15 • Artemis return samples from will be unique from Apollo samples and have the possibility  
16 of determining absolute ages of significant events in lunar history.  
17

## 18 **Abstract**

19 The Artemis exploration zone is a geologically-complex region likely hosting some of the oldest  
20 and as-yet-unstudied materials on the Moon. We review six potential Artemis landing sites (001,  
21 004, 007, 011, 102, and 105) within candidate Artemis III landing regions ‘Connecting Ridge,’  
22 ‘Peak Near Shackleton,’ ‘Leibnitz Beta Plateau,’ ‘de Gerlache Rim,’ and ‘de Gerlache Rim 2.’  
23 Kaguya Spectral Profiler mineral data were used to determine average lithological composition at  
24 each landing site. Potentially accessible geologic materials, their ages and significance, and  
25 appropriate application of radiometric chronometers are discussed in reference to return samples  
26 from each potential landing site. Chronologic analyses of return samples from the Artemis  
27 exploration zone will enable the anchoring of the lunar impact flux curve, determine the absolute  
28 timing of pivotal events in lunar geologic history, and reveal geological diversity of the  
29 differentiated lunar body.

30

## 31 **Plain Language Summary**

32 Artemis astronauts will bring new samples from the Moon back to Earth. We discuss the  
33 geology of some landing sites the astronauts might visit, what types of rocks they may encounter,  
34 and how to examine them using geochronology. The application of geochronology to Moon rocks  
35 is essential to know the absolute timing of major events in lunar and early Solar system history.

## 36 **1 Introduction**

37 The Artemis exploration zone (AEZ) includes terrain dominated by photogeologically-mapped  
38 and stratigraphically-determined Nectarian and pre-Nectarian age surfaces. These surfaces have  
39 materials that can help answer important questions regarding impact chronology, history of major  
40 lunar events such as formation and differentiation, and an opportunity to sample deeply excavated  
41 materials. To answer these questions, detailed petrologic analyses coupled with chronologic  
42 analyses of specimens collected from the AEZ are required.

43

44 Examination of impact-cratered surfaces can determine fluxes in impact events in lunar history  
45 (Neukum et al., 1975; Boyce et al., 1977; Kring, 2008; Mazrouei et al., 2019; Lagain et al., 2022;  
46 Fairweather et al., 2022). Establishing the ages of specific impact craters and basins is important  
47 because these ages can anchor a crater chronology of the lunar surface (Arvidson et al., 1979;  
48 Neukum, 1984; Neukum et al., 2001; Che et al., 2021; Yue et al., 2022) and better define the  
49 bombardment history of the inner solar system (Kring et al., 2005; Kring, 2006, 2007, 2008, 2009).  
50 The returned lunar samples by the Apollo program were subjected to radioisotope dating, but many  
51 of the sampling sites might be part of the perturbed megaregolith formed by ejecta of large impact  
52 basins (Howard et al., 1974; Moore et al., 1974; Head et al., 1993; Haskin, 1998; Haskin et al.,  
53 1998; Petro and Pieters, 2008) and many studied specimens cannot be reliably attributed to a  
54 specific impact event (Korotev et al., 2002). The Imbrium basin is dated at roughly ~3.5 Ga  
55 (Deutsch and Stöffler, 1987; Spudis et al., 1988; Merle et al., 2014; Zhang et al., 2015), but ages  
56 of other significant lunar basins, such as the Orientale Basin, have yet to be firmly established  
57 (Stöffler et al., 2006; Meyer et al., 2016; Wu et al., 2019). The mapped ages of features in Figure  
58 1 are in flux based on crater-counting ages determined from orbit (Tye et al., 2015; Deutsch et al.,  
59 2020). While Spudis et al. (2008) mapped Shackleton crater with a 3.6 Ga age, Zuber et al. (2012),  
60 Tye et al. (2015), and Kring et al. (2021) reported Imbrian ages of ~3.69 Ga, 3.51 +0.05/-0.08 Ga,

61 and  $3.43 \pm 0.04/-0.05$  Ga, respectively. Moreover, while Spudis et al. (2008) mapped Shoemaker  
62 and Faustini craters with Nectarian ages, Tye et al. (2015) report pre-Nectarian ages, similar to  
63 those at Haworth. The variable age estimates illustrate the need for sample return and radiometric  
64 analyses in Earth-based laboratories. The age of the South Pole-Aitkin (SPA) basin, thought to be  
65 the oldest and largest basin on the Moon and, thus, a key anchor point in defining the lunar  
66 chronology, is still not precisely known (Wilhelms et al., 1987; Hiesinger et al., 2012). The South  
67 Pole-Aitken Terrane has not yet been directly sampled but it is the focus for the crewed Artemis  
68 missions (Jolliff et al., 2000) (Figure 1).  
69

70 Sampling impact-generated pre-Nectarian- and Nectarian-age materials in the Artemis  
 71 exploration zone also provides a way to test the crater counting calibration curve and refine the  
 72 impact flux during the first billion years of Earth-Moon history; i.e., testing the lunar cataclysm

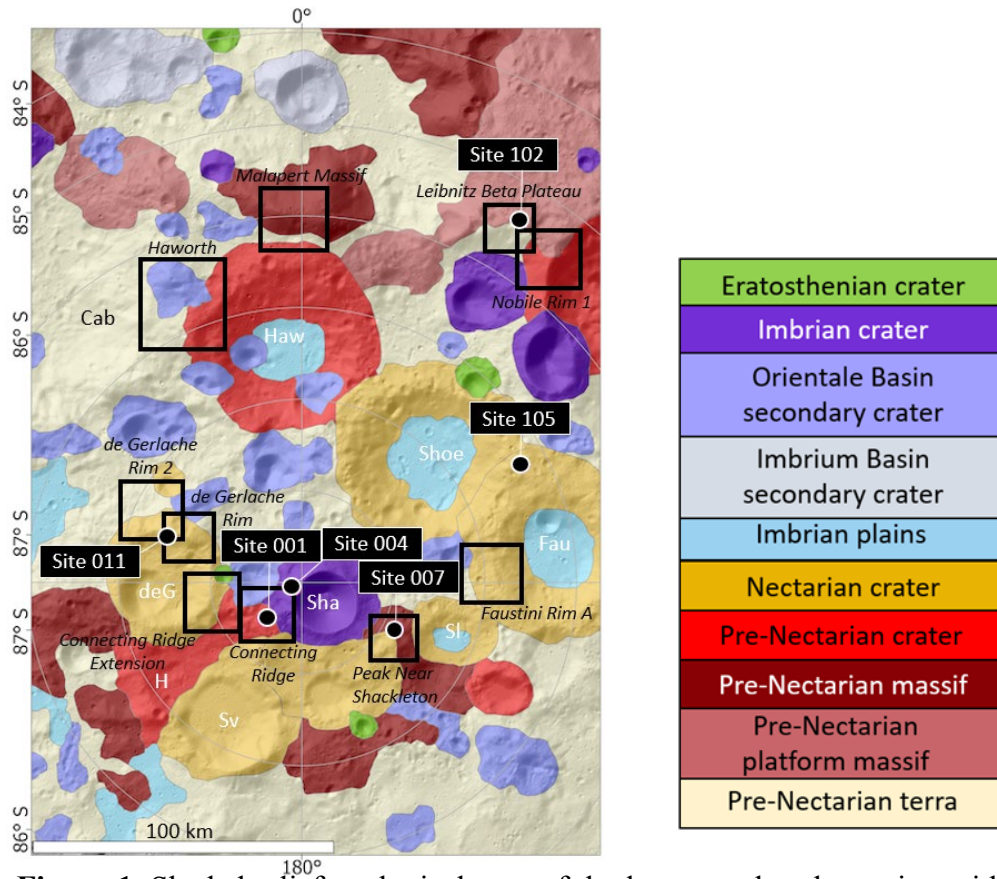


**Figure 1.** Shaded relief geological map of the lunar south polar region with the locations of several potential Artemis landing sites (001, 004, 007, 011, 102, and 105). Base map by Allender et al. (2019) in the LPI Lunar South Pole Atlas using geology of Spudis et al. (2008) and Lunar Orbiter Laser Altimeter data. The mapped ages of features are in flux based on crater-counting ages determined from orbit. For example, while Spudis et al. (2008) mapped Shackleton crater with a 3.6 Ga age, Zuber et al. (2012), Tye et al. (2015), and Kring et al. (2021) reported Imbrian ages of  $\sim 3.69$  Ga,  $3.51 \pm 0.05/-0.08$  Ga, and  $3.43 \pm 0.04/-0.05$  Ga, respectively. Moreover, while Spudis et al. (2008) mapped Shoemaker and Faustini craters with Nectarian ages, Tye et al. (2015) report pre-Nectarian ages, similar those that of Haworth. Those disparate ages illustrate the need for sample return and radiometric analyses in Earth-based laboratories. Cab- Cabeus; Haw- Haworth; Shoe- Shoemaker; Fau- Faustini; deG- de Gerlache; Sha- Shackleton; Sl- Slater; H- Henson; Sv- Sverdrup.

73 hypothesis, which is the highest priority science objective as defined by the National Research  
 74 Council (NRC) (2007). In addition, the region may contain debris from the SPA basin. Recovering  
 75 debris with an SPA impact-reset age will provide an opportunity to address the second highest  
 76 priority science objective (NRC, 2007): to provide an anchor to the basin-forming epoch on the  
 77 Moon. Currently, ages for SPA range from 4.39 Ga to 4.25 Ga (Hiesinger et al., 2012; Morbidelli  
 78 et al., 2012). Collectively, those data will refine the crater calibration curve, which can then be  
 79 applied to surfaces around the entire Moon and other planetary surfaces in the Solar system. The

80 pre-Nectarian and Nectarian impact events in the Artemis exploration zone excavated and  
81 produced breccias composed, in part, of unusually old highland terrain crust. Samples of that  
82 material could provide additional opportunities to constrain the timing of the giant Moon-forming  
83 impact, lunar differentiation, crustal formation, and subsequent magmatism, which are tied to  
84 several other important scientific objectives (NRC, 2007; Artemis III Science Definition Team  
85 Report).

86  
87 The impact cratering process is critical for excavating materials from depth and allows access  
88 to materials that may otherwise be deeply buried. Exhumed lithologies also provide information  
89 on the local stratigraphy (Pieters et al., 1994; Kring, 2009; Kenkmann and Artemieva, 2021), for  
90 example, at Shackleton crater (Gawronska et al., 2020). Because SPA is the largest and oldest  
91 impact basin on the Moon (Wilhelms et al., 1987), it may contain rare upper mantle materials at  
92 the surface in select locations (Moriarty et al., 2021). Thus, a cross-section of lunar crust up to 10's  
93 of kilometers deep may be developed if the return sample collection strategy includes samples  
94 collected from varied crater features (e.g., modification zones, central uplifts, etc.) and impact  
95 breccias (Kring, 2009). Impact crater ejecta may also allow for the determination of the average  
96 composition of impacted crust from the sampling of homogenized subsurface lithologies in the  
97 form of impact melt materials (Kring, 2009). The environmental consequences (e.g., dust lofting,  
98 ejecta blanketing, flood basalts, rockfall; mountain-forming, etc.) of these impacts may also be  
99 inferred through orbital, field, and sample observation of impact craters (Mukhametshin et al.,  
100 2018; Michaut and Pinel, 2018; Xie et al., 2020; Bickel et al., 2020). The delivery and abundance  
101 of elements through impacts may also be determined and used to piece together a history of the  
102 chemical evolution of the lunar interior and crust (Bottke et al., 2010; Barnes et al., 2016; Joy et  
103 al., 2016, 2020; Zhu et al., 2019). Finally, investigations and sampling of heavily impact-cratered  
104 terrain may also provide access to impact melt samples from other craters (Kring et al., 2005;  
105 Kring, 2007, 2009).

106  
107 This study reviews six potential Artemis landing sites (001, 004, 007, 011, 102, and 105) within  
108 candidate Artemis III landing regions 'Connecting Ridge,' 'Peak Near Shackleton,' 'Leibnitz Beta  
109 Plateau,' 'de Gerlache Rim,' and 'de Gerlache Rim 2' (NASA, 2020b, 2022). The numbered  
110 potential landing sites correspond to the illumination sites identified in previous work (Bussey et  
111 al., 2010; Mazarico et al., 2011; Speyerer and Robinson, 2013). Kaguya Spectral Profiler mineral  
112 count data were used to determine average lithological composition at each landing site. Potential  
113 accessible geologic materials, their ages and significance, and appropriate application of  
114 radiometric chronometers are discussed in reference to return samples from each potential landing  
115 site. Chronologic analyses of return samples from the Artemis exploration zone will enable the  
116 anchoring of the lunar impact flux curve, determine the absolute timing of pivotal events in lunar  
117 geologic history, and reveal geological diversity of the differentiated lunar body.

## 118 **1.1 Input Data**

119 Kayuga Spectral Profiler (SP) is a visible to near infrared spectrometer with a ~500 m spatial  
120 footprint acquiring data via three spectral bands (one visible, two near infrared) between 500 and  
121 2600 nm (Haruyama et al., 2008). However, topography in the polar regions causes different  
122 surfaces to receive widely uneven solar illumination, from no direct incident sunlight in  
123 topographic depressions (such as permanently shaded regions) to abundant sunlight on steep Sun-  
124 facing slopes, which makes spectral interpretation challenging. Lemelin et al. (2022) converted

125 the SP radiance data (level 2B1) measured in each SP orbit into bidirectional reflectance using the  
 126 photometric function of Yokota et al. (2011), which allowed the conversion of radiance data into  
 127 reflectance data at a standard viewing geometry of 30° incidence angle and 0° emission angle.  
 128 However, as the photometric function of Yokota et al. (2011) assumes a flat sphere, reflectance  
 129 measurements higher or lower than expected occur on sloped surfaces. The Lunar Orbiter Laser  
 130 Altimeter (LOLA) onboard LRO acquires reflectance data at 1064 nm and is unaffected by slope  
 131 effects as it sends its own illumination. Lemelin et al. (2022) thus scaled the gridded SP reflectance  
 132 data to the gridded and calibrated LOLA data at their common wavelength of 1064 nm. They could  
 133 then calculate FeO abundances using reflectance data at 750 and 950 nm, and use Hapke radiative  
 134 model (e.g., Hapke, 1981, 2001) to estimate the abundance of olivine, low-calcium pyroxene  
 135 (LCP), high-calcium pyroxene (HCP), and plagioclase on continuum removed spectra, using FeO  
 136

	Potential Landing Site					
	001	004	007	011	102	105
<b>Copernican</b> < 0.80 Ga						
<b>Eratosthenian</b> 0.8 to 3.20 Ga						
<b>Upper Imbrian</b> 3.20 to 3.80 Ga	Shackleton	Shackleton				
<b>Lower Imbrian</b> 3.80 to 3.85 Ga	Shackleton Spudis, Marvin, Orientale (Secondary)	Shackleton Spudis + Orientale (Secondary)		Orientale (Secondary)		Malinkin + Orientale (Secondary)
<b>Nectarian</b> 3.85 to 3.92 Ga	de Gerlache, Unnamed?			de Gerlache		Shoemaker + Faustini
<b>pre-Nectarian</b> > 3.92 Ga	Henson, Sverdrup, Marvin	Sverdrup	Slater Massif Terra	Terra	Nobile Platform Massif Terra	Terra

**Figure 2.** Summary of age units at each potential landing site in accordance with Figure 1. Upper and lower age limits of each time period are from Stöffler et al. (2006). Although not visible at the scale mapped in Figure 1, all sites will contain small Copernican-age craters.

137  
 138 as a constraint. We used these gridded mineral maps and the gridded abundance of FeO to study  
 139 the probable geology of the Artemis region.

## 140 1.2 Potential Landing Sites

141 The Artemis III mission will not be supported with a rover, so crew will be limited to walking  
 142 extravehicular activities (EVAs) within 2 km distance of the Human Landing System (HLS)  
 143 (Coan, 2020; Kring et al., 2023). An unpressurized Lunar Terrain Vehicle (LTV) will be deployed

144 for later missions (NASA, 2021, 2023) and should provide an exploration range up to 10 km radial  
 145 distance from a lander. For the purposes of our study, we utilize that 10 km radial distance around  
 146 potential Artemis landing sites to evaluate the types of samples available for collection and return  
 147 to Earth.

#### 148 1.2.1 Site 001 (‘Connecting Ridge’ region)

149 Potential Artemis landing site 001 (NASA, 2020a) (Site “SP-1” at (-89.45, 222.69) in Mazarico  
 150 et al. (2011); “Point B” at (89.44°S, 141.8°W) in Bussey et al. (2010)) is within the Artemis III  
 151 candidate landing region called “Connecting Ridge” and located on a massif ridge connecting  
 152 Shackleton and Henson craters (Figure 1a). This ridge itself is roughly pre-Nectarian in age  
 153 (Stöffler et al., 2006) but is cross-cut by Shackleton crater and secondary crater ejecta believed to  
 154 be of significantly younger Imbrian age (3.51 to  $3.69 \pm 0.4$  Ga) (Spudis et al., 2008; Zuber et al.,  
 155 2012). The ridge will be covered with Shackleton ejecta, potentially including fragments of the  
 156 original highland crust, components from the lunar magma ocean and later intrusive rocks,  
 157 cryptomare from SPA, plus impact melts from Shackleton, SPA, and other pre-Nectarian impacts  
 158 (Kring, 2019; Halim et al., 2021; Kring et al., 2022). Anticipated dominant lithologies are  
 159 anorthosite below the Shackleton crater rim down to ~900 m, regolith, and breccia (Gawronska et  
 160 al., 2020). Lowest FeO values within the Artemis exploration region determined by Kaguya SP  
 161 (~5 to 7 wt. %) are found in the 89° to 90°S region near Shackleton crater (applies to Site 004 as  
 162 well) (Lemelin et al., 2022).

#### 163 1.2.2 Site 004 (along margin of ‘Connecting Ridge’ region)

164 Potential Artemis landing site 004 (NASA, 2020a) ( Site “SP-4” at (-89.78, 204.27) in  
 165 Mazarico et al. (2011); “Point A” at (89.68°S, 166.0°W) in Bussey et al. (2010)) is along the  
 166 margin of Artemis III candidate landing region called “Connecting Ridge” on a portion of  
 167 Shackleton crater (ridge is pre-Nectarian age, 4.52 to 3.92 Ga, (Stöffler et al., 2006); crater is  
 168 Imbrian age;  $3.6 \pm 0.4$  Ga (Spudis et al., 2008; Zuber et al., 2012; Tye et al., 2015; Halim et al.,  
 169 2021)) rim and is nearly coincident with the geographic south pole of the Moon (Figure 1).  
 170 Imbrium secondary crater materials and pre-Nectarian ejecta from Henson crater are accessible  
 171 within a 10 km radial distance (Figure 2). This site contains multiple rock exposures (Gawronska  
 172 et al., 2020). Anticipated lithologies include pure anorthosite exposures (Yamamoto et al., 2012;  
 173 Lemelin et al., 2017). Sites 001 and 004 provide a unique opportunity to sample rays from Tycho  
 174 crater that reach directly between the two sites (Lemelin et al., 2022). Both sites provide an  
 175 opportunity to sample pre-Nectarian crater, Imbrian crater, and Imbrian secondary crater materials.

#### 176 1.2.3 Site 007 (‘Peak near Shackleton’ region)

177 Potential Artemis landing site 007 (NASA, 2020a) (Site “SP-7” at (-88.81, 123.64) in Mazarico  
 178 et al. (2011); “Point D” at (88.79°S, 124.5°E) in Bussey et al. (2010)) is within the Artemis III  
 179 candidate landing region “Peak near Shackleton” located on a massif ridge between Shackleton  
 180 and Slater craters (Figure 1a). Within a 10 km radial distance, Site 007 would enable the sampling  
 181 of materials from the pre-Nectarian massif, Nectarian crater, and Imbrian crater (Figure 2). This  
 182 site may provide the possibility to observe layered strata from Shackleton and compare ejecta and  
 183 stratigraphy with Slater crater. Layered terrain is 10 to 50 m thick in Shackleton (Halim et al.,  
 184 2021). The lateral extent of these layers is difficult to observe due to poor illumination conditions,  
 185 but they may be ejecta produced from older impacts (i.e., Haworth, Shoemaker, Faustini).

186 Interestingly, numerical modeling efforts have determined the top bed in this stratigraphic  
187 sequence may contain over ~150 m of Shackleton ejecta (Halim et al., 2021). Kumari et al. (2022)  
188 identified 3,204 resolvable boulders (ranging from 0.7 to 14 m diameter) within a 10 km radius of  
189 site 007.

#### 190 1.2.4 Site 011 (‘de Gerlache Rim 1’ and ‘de Gerlache Rim 2’ regions)

191 Potential Artemis landing site 011 (NASA, 2020a) (Site “SP-11” at (-88.67, 291.90) in  
192 Mazarico et al. (2011); “Point C” at (88.71°S, 68.7°W) in Bussey et al. (2010)) is within the  
193 Artemis III candidate landing region “de Gerlache Rim”. De Gerlache Rim 1 is approximately  
194 centered on the crater rim, while de Gerlache Rim 2 is mostly north of the crater rim (Figure 1).  
195 Based on absolute crater counting models, de Gerlache is believed to be Nectarian in age (Tye et  
196 al., 2015; Deutsch et al., 2020) and, just beyond de Gerlache Rim 1, its rim is cross-cut by an  
197 Eratosthenian-age Marvin crater. The de Gerlache impact appears to be younger than the pre-  
198 Nectarian ‘Connecting Ridge’ massif (Spudis et al., 2008) and, thus, may have covered the massif  
199 with ejecta prior to the Shackleton impact. Pre-Nectarian terra, Nectarian crater, and Imbrian  
200 secondary crater materials are present within a 10 km radial distance from Site 011 (Figure 2).  
201 This site may allow for volatile sampling within secondary craters and comparison to Apollo  
202 permanently shadowed region (PSR) crater samples (Li and Milliken, 2017; Kereszturi et al.,  
203 2022). The de Gerlache ejecta within the region may provide samples of anorthositic crustal  
204 lithologies and SPA ejecta. Within a 10 km radial distance around site 011, over 3,774 boulders  
205 from 0.7 to 26 m in diameter have been identified (Kumari et al., 2022).

#### 206 1.2.5 Site 102 (‘Leibnitz Beta Plateau’ region)

207 Potential Artemis landing site 102 (NASA, 2020a) (Site “SP-20” at (-85.43, 31.73) in Mazarico  
208 et al. (2011)) is within the Artemis III candidate landing region called “Leibnitz Beta Plateau”  
209 located atop informally-named Mons Leibnitz Beta, which is now called Mons Mouton (Figure 1).  
210 The Leibnitz Mountains lie on the topographically-high ring outlining the SPA basin (Garrick-  
211 Bethell and Zuber, 2009). This plateau is bounded by a nearly vertical cliff facing south-poleward.  
212 The cliff may provide a unique opportunity to access a roughly 8-km-thick cross-section of lunar  
213 crust. Massifs like Mons Mouton may also provide an opportunity to identify additional lithologies  
214 produced by early lunar magmatic processes. This site may allow for sampling from adjacent pre-  
215 Nectarian and Nectarian aged impacts Haworth ( $4.18 \pm 0.02$  Ga), Shoemaker ( $4.15 \pm 0.02$  Ga),  
216 and Faustini ( $4.10 \pm 0.03$  Ga) craters (Figure 2; Tye et al., 2015). NASA’s VIPER rover is set to

217 land and traverse near this site to search for and sample volatiles up to approximately 1 meter deep  
218 within the regolith (Shirley and Balaban, 2022).

### 219 1.2.6 Site 105

220 Potential Artemis landing site 105 (NASA, 2020a) ((-87.18, 62.84) in Patterson et al. (2022)  
221 is located between pre-Nectarian aged Shoemaker ( $4.15 \pm 0.02$  Ga) and Faustini ( $4.10 \pm 0.03$  Ga)  
222 craters (Tye et al., 2015) (Figures 1, 2). Site 105 is downslope from Site 102. This region contains  
223 many large blocks and boulders (1.5 to 9 m diameter) (Patterson et al., 2022) and the floors of  
224 Shoemaker and Faustini likely have icy volatile deposits (Tye et al., 2015; Patterson et al., 2022;  
225 Brown et al., 2022), and the ridge bisecting Faustini and Shoemaker crater rims has ejecta deposits  
226 likely to be up to Nectarian in age (Tai Udovicic et al., 2022). This site contains the lowest FeO  
227 values ( $\sim 5$ -7 wt. %) of all of the  $84^\circ$  to  $90^\circ$  S region (Figure 1a; Lemelin et al., 2022).

**Table 1.** Commonly applied radiogenic isotope systems and the methods by which they may be analyzed.

Isotope System	Analytical Technique				
	Bulk sample or glass	Mineral/bulk rock isochron	Single mineral	In-situ (Laser ablation/secondary ion)	Wet chemistry
$^{40}\text{K} \rightarrow ^{40}\text{Ar}$ ( $^{40}\text{Ar} - ^{39}\text{Ar}$ )	X		X	X	
$^{87}\text{Rb} \rightarrow ^{87}\text{Sr}$		X		X	X
$^{147}\text{Sm} \rightarrow ^{143}\text{Nd}$		X			
$^{146*}\text{Sm} \rightarrow ^{142}\text{Nd}$		X			
$^{176}\text{Lu} \rightarrow ^{176}\text{Hf}$		X	X	X	X
$^{187}\text{Re} \rightarrow ^{187}\text{Os}$		X			
$^{232}\text{Th} \rightarrow ^{208}\text{Pb}$		X	X	X	X
$^{235}\text{U} \rightarrow ^{207}\text{Pb}$		X	X	X	X
$^{238}\text{U} \rightarrow ^{206}\text{Pb}$		X	X	X	X

## 228 2 Isotope Chronology

229 The timing of major events, including the timing of lunar differentiation, duration of igneous  
230 activity, and impact history, can be constrained with isotope chronology of lunar materials (e.g.,  
231 Nyquist and Shih, 1992). Foundational chronologic analyses of Apollo 11 samples are  
232 summarized in the Proceedings of the Apollo 11 Lunar Science Conference (1970) and “The Moon  
233 Issue” of the journal *Science* (Abelson, 1970, and articles in the issue) and laid the groundwork  
234 for all future studies of lunar return samples. The commonly applied isotope systems are  
235 summarized in Table 1 and described below. Each radiometric system is best suited to a particular  
236 subset of geologic events and temperatures. For example, some approaches are best suited to date  
237 high-temperature igneous crystallization, whereas other systems best reflect cooling below 300 to  
238  $500^\circ\text{C}$ . Furthermore, the radiometric systems may require specific minerals and/or chemical  
239 compositions. Thus, some chronologic approaches may be more suitable to different lunar  
240 lithologies than others, simply by the nature of the texture and/or mineralogy of the sample. The

241 ages of secondary processes, such as impact metamorphism, may also be determined, depending  
242 on the material and degree of metamorphism/melting.

## 243 2.1 U-Th-Pb

244 The  $^{238}\text{U}$ - $^{206}\text{Pb}$ ,  $^{235}\text{U}$ - $^{207}\text{Pb}$ , and  $^{232}\text{Th}$ - $^{208}\text{Pb}$  isotope systems are some of the most versatile  
245 isotope systems that can be applied to a wide variety of lunar lithologies. These systems were  
246 developed prior to the Apollo 11 mission and were applied to the first returned specimens (e.g.,  
247 Silver, 1970; Tatsumoto and Rosholt, 1970). Because  $^{238}\text{U}$ - $^{206}\text{Pb}$  and  $^{235}\text{U}$ - $^{207}\text{Pb}$  reflect two isotope  
248 systems in the U-Pb system, ages can be determined using multiple approaches including standard  
249 U-Pb isochrons, inverse Pb-Pb isochrons, and U-Pb concordia diagrams (e.g., Wetherill and Tera-  
250 Wasserburg diagrams). The  $^{238}\text{U}$ ,  $^{235}\text{U}$ , and  $^{232}\text{Th}$  half-lives are 4.468, 0.704, and 14.01 Ga,  
251 respectively (Steiger and Jäger, 1977). Despite recent studies that refine the decay constants (e.g.,  
252 Amelin and Zaitsev, 2002; Schoene et al., 2006), the IUGS-IUPAC recommends the decay  
253 constants of Jaffey et al. (1971) for  $^{238}\text{U}$  and  $^{235}\text{U}$  (Villa et al., 2022). Uranium and Th-rich and  
254 high U/Pb and/or Th/Pb ratio trace phases such as zircon, baddeleyite, zirconolite, tranquillityite,  
255 apatite, merrillite, and monazite are documented in many lunar lithologies and have the potential  
256 for precise chronology (e.g., Lovering et al., 1974; Rasmussen et al., 2008; Barboni et al., 2017;  
257 Shaulis et al., 2017). Even in materials without these trace phases, many lunar rocks and/or their  
258 sources have relatively high  $^{238}\text{U}/^{204}\text{Pb}$  ratios (denoted as  $\mu$ ) of about 360 to over 2600 for lunar  
259 basaltic rocks (e.g., Snape et al., 2018) whereas the  $\mu$ -value of the terrestrial mantle is about 8  
260 (e.g., Ballhaus et al., 2013).

261  
262 Since most lunar rocks have experienced secondary processes such as thermal and/or impact  
263 metamorphism, some mineral hosts are more resilient to disturbances of the U-Th-Pb systems than  
264 others. For example, zircon has the potential to preserve the U-Th-Pb systematics of crystallization  
265 from a melt and will retain those characteristics even through metamorphic events that would  
266 disturb U-Th-Pb in other materials (Cherniak and Watson, 2001). Zircon is considered one of the  
267 most robust time capsules nature has to offer. Uranium and Pb in baddeleyite also has the potential  
268 to record igneous events despite the host rock being subjected to high-grade metamorphic  
269 conditions (Niihara et al., 2009). Microstructural analyses of trace phases such as baddeleyite can  
270 reveal relict polymorphs that provide additional context for age data (White et al., 2020). Other U  
271 and/or Th-rich mineral hosts such as apatite, however, are less resistant to disturbances than zircon  
272 for any given temperature-time (T-t) history (Chew et al., 2021) and can record the timing of  
273 metamorphic events (Nemchin et al., 2009).

274  
275 Analytical approaches for U-Th-Pb analyses include in-situ (minimally destructive) or wet  
276 chemical (fully destructive). In-situ analyses usually involve either a laser or secondary ion source  
277 that samples the material of interest at spatial resolutions between 5 and 100  $\mu\text{m}$ . The advantages  
278 of in-situ approaches are that analyses often have petrological context through microstructural  
279 and/or mineral textural data. Age data can be collected from very small specimens (Che et al.,  
280 2021) and clasts (Snape et al., 2018). One disadvantage of in-situ analyses is that the measurement  
281 precision is often significantly less than that of wet chemical approaches such as isotope-dilution  
282 thermal ionization mass spectrometry (ID TIMS; see Schoene (2014) for a full treatment of the  
283 methods). In lithologies that do not typically contain U and Th-rich trace phases, measurement of  
284 the  $^{207}\text{Pb}/^{206}\text{Pb}$  and  $^{204}\text{Pb}/^{206}\text{Pb}$  ratios of other phases such as pyroxene can yield precise ages. For  
285 example, Borg et al. (2011) measured an age of  $4359.2 \pm 2.4$  Ma for sequentially-dissolved

286 pyroxene in ferroan anorthosite 60025. Overall, with modern analytical techniques, the ages of  
 287 most lunar lithologies can be precisely determined with the U-Th-Pb systems.

## 288 2.2 Rb-Sr

289 The Rb-Sr isotope system has been applied to Apollo lunar materials since they were collected  
 290 (Gopalan et al., 1970; Hurley and Pinson, Jr., 1970; Papanastassiou et al., 1970) and has the  
 291 potential for precise chronology (Rankenburg et al., 2007) and chemical/isotopic tracing (Borg et  
 292 al., 2022). The IUGS-IUPAC-recommended decay constant for  $^{87}\text{Rb}$  is  $(1.3972 \pm 0.0045) \times 10^{-11}\text{a}^{-1}$   
 293 (Villa et al., 2015). Great care must be taken in comparing data because many studies used  
 294 and/or still use the value of  $1.42 \times 10^{-11}\text{a}^{-1}$  reported in Steiger and Jäger (1977) and other studies  
 295 may adopt the new decay constants. In any case, most published age data can be recalculated to  
 296 the same or updated decay constant.

297

298 Strontium isotopic and  $^{87}\text{Rb}/^{86}\text{Sr}$  ratios of rock, glass, and/or mineral materials are typically  
 299 measured with wet chemical approaches (destructive analyses) where the materials are digested  
 300 and Rb and Sr are chemically purified and analyzed (Charlier et al., 2006). Common lunar rock-  
 301 forming minerals such as pyroxene, plagioclase, K-feldspar, and olivine have highly variable  
 302 Rb/Sr ratios making them amenable for dating using the isochron approach. Very recent  
 303 advancements in mass spectrometry have enabled in-situ analysis of  $^{87}\text{Sr}/^{86}\text{Sr}$  and  $^{87}\text{Rb}/^{86}\text{Sr}$  by  
 304 laser ablation plasma-source mass spectrometry (Dauphas et al., 2022) opening a vast new area for  
 305 investigation with a minimally-destructive, high-spatial resolution ( $\sim 100\ \mu\text{m}$ ) technique.

306

307 In addition to chronology, the Rb-Sr system can be used as an isotope tracer. For example,  
 308 Borg et al. (2022) model the Rb-Sr isotope systematics of the Earth, Moon, and Theia (the proto-  
 309 Earth impactor) to constrain the timing of volatile addition and the timing of the Moon-forming  
 310 event. The Rb-Sr isotope system can also be used to trace potential mixing relationships and the  
 311 sources of lunar igneous rocks (Hui et al., 2013), and potentially define model age constraints in  
 312 materials that cannot otherwise be dated (McLeod et al., 2016).

## 313 2.3 Sm-Nd

314 Similar to U-Pb, Sm-Nd consists of two isotope systems ( $^{146}\text{Sm}-^{142}\text{Nd}$  and  $^{147}\text{Sm}-^{143}\text{Nd}$ ) in one  
 315 element system, except  $^{146}\text{Sm}$  is now extinct. The Sm-Nd system has been applied to most lunar  
 316 lithologies for chronology and tracers of magma sources (Nyquist et al., 1995; Brandon et al.,  
 317 2009; Carlson et al., 2014; Borg et al., 2015; Johnston et al., 2022). The IUGS-IUPAC  
 318 recommended half-lives of  $^{146}\text{Sm}$  and  $^{147}\text{Sm}$  are 0.068 – 0.103 and  $106.25 \pm 0.38\ \text{Ga}$ , respectively  
 319 (Villa et al., 2020). Given the uncertainty of the  $^{146}\text{Sm}$  decay rate, recent papers (McLeod et al.,  
 320 2014) use both half-life values of 0.068 and 0.103 Ga in their model calculations.

321

322 High-precision analyses of Sm-Nd requires wet chemical approaches and relatively large  
 323 samples with minimum mass requirements of 0.05 to 1 g, depending on Sm and Nd concentrations,  
 324 mineralogy, and grain size. Most lunar rocks and minerals have overall low concentrations of Sm  
 325 and Nd (ppb to ppm concentrations) and limited natural variations in Sm/Nd ratios due to their  
 326 similar geochemical characteristics in most materials. The range in  $^{147}\text{Sm}/^{144}\text{Nd}$  ratios in most  
 327 lunar minerals (feldspar, pyroxene, olivine, phosphate) is limited between about 0.14 to 0.30,  
 328 unlike Rb-Sr, U-Th-Pb, and Lu-Hf where the range in parent/daughter ratios can be orders of  
 329 magnitude greater. Despite the limited range in Sm/Nd ratios and resulting limited variations in

330 radiogenic Nd isotopic compositions, advancements in mass spectrometry allow very high  
 331 precision (few ppm) measurements of  $^{143}\text{Nd}/^{144}\text{Nd}$  and  $^{142}\text{Nd}/^{144}\text{Nd}$  ratios (Rankenburg et al., 2006;  
 332 Boyet and Carlson, 2007). These high-precision measurements are also required to accurately  
 333 measure and ultimately correct neutron capture effects from cosmic ray exposure that can alter the  
 334 Sm and Nd isotopic compositions (Nyquist et al., 1995; Brandon et al., 2009).

335  
 336 Measured Sm and Nd isotopic compositions corrected for neutron capture effects have yielded  
 337 many robust ages of lunar materials (Carlson et al., 2014; Borg and Carlson, 2023). As opposed  
 338 to the other isotope systems listed in Table 1, Sm and Nd are geochemically similar lanthanide  
 339 elements that are relatively immobile during periods of shock metamorphism. Other elements,  
 340 such as the alkalis (Rb), can be more easily mobilized than Sm-Nd. This is evident in some studies  
 341 that compare Sm-Nd and Rb-Sr measured on the same sample aliquots where there can be greater  
 342 scatter about a Rb-Sr isochron than for a Sm-Nd isochron (Edmunson et al., 2009). In addition to  
 343 standard isochron chronology, coupled  $^{146-147}\text{Sm}$ - $^{142-143}\text{Nd}$  isotope systematics can be used to  
 344 assess the mantle closure ages (i.e., the duration of lunar magma ocean crystallization) for the  
 345 sources of lunar basalts (Boyet and Carlson, 2007; Brandon et al., 2009; McLeod et al., 2014).  
 346 Finally, the nature and compositions of lunar mantle source compositions and potential mixtures  
 347 can be assessed with the Sm-Nd system (Borg et al., 2009; Srivastava et al., 2022).

#### 348 2.4 Lu-Hf

349 The Lu-Hf isotope system was first applied to lunar materials by Patchett and Tatsumoto  
 350 (1981) and Unruh et al. (1984). Few subsequent papers presented Lu-Hf data (Beard et al., 1998)  
 351 until the application of plasma-source mass spectrometry; now the Lu-Hf isotope system is  
 352 routinely applied to lunar materials (Taylor et al., 2009; Sprung et al., 2013; Gaffney and Borg,  
 353 2014; Carlson et al., 2014; Melanie Barboni et al., 2017). The  $^{176}\text{Lu}$  half-life used by the isotope  
 354 geochemistry community changed from the value of 35.82 Ga (Patchett and Tatsumoto, 1980) to  
 355 a value of about 37.12 Ga (Scherer et al., 2001; Söderlund et al., 2004), so care must be taken  
 356 when comparing Lu-Hf isotope data and models in the literature. Hult et al. (2014) summarize  
 357 many  $^{176}\text{Lu}$  half-life measurements and propose a value of  $37.22 \pm 0.29$  Ga.

358  
 359 The Lu-Hf isotope system is enhanced by the different geochemical behavior of Lu and Hf and  
 360 resultant large range in  $^{176}\text{Lu}/^{177}\text{Hf}$  ratios in many lunar materials. For example, most zircon has  
 361 1-3 wt% Hf and Lu in ppm concentrations resulting in  $^{176}\text{Lu}/^{177}\text{Hf}$  ratios typically  $< 0.002$ .  
 362 Combined with its robust retention of U-Th-Pb isotopes for precise chronology, zircon is also a  
 363 powerful Lu-Hf isotope tracer requiring minimal age corrections (Taylor et al., 2009; Barboni et  
 364 al., 2017). Phosphate minerals have the potential for  $^{176}\text{Lu}/^{177}\text{Hf}$  ratios of over 100 (Amelin, 2005).  
 365 Overall, in addition to zircon, many oxide minerals can have very low  $^{176}\text{Lu}/^{177}\text{Hf}$  ratios of  $< 0.01$ ,  
 366 whereas phosphates and garnet have the potential for  $^{176}\text{Lu}/^{177}\text{Hf}$  ratios greater than 1.0. Therefore,  
 367 Lu-Hf mineral isochron chronology has the potential for relatively large spreads in Lu/Hf ratios  
 368 even in lithologies with a simple mineralogy (e.g., Lapen et al., 2010).

369  
 370 Modern analytical methods for Lu-Hf chronology and/or isotope tracer studies include both  
 371 in-situ laser ablation mass spectrometry and wet chemical approaches applied to bulk rock and/or  
 372 mineral separates. Because Hf concentrations are in the ppb to ppm range for most rock-forming  
 373 minerals, wet chemical approaches are required for analysis with minimum sample sizes typically  
 374 of 0.05 to 0.10 g. Hafnium-rich minerals such as zircon and baddeleyite can be analyzed for Lu-

375 Hf isotopes by in-situ approaches (Ibanez-Mejia et al., 2014). All Lu-Hf isotope data of lunar  
 376 materials should be assessed for neutron capture effects and corrected (Sprung et al., 2013; Gaffney  
 377 and Borg, 2014; Barboni et al., 2017).

### 378 2.5 Ar-Ar

379 Turner (1970) presented some of the first applications of the  $^{40}\text{Ar}/^{39}\text{Ar}$  method to Apollo 11  
 380 samples. Since then,  $^{40}\text{Ar}/^{39}\text{Ar}$  data have been essential for unraveling the timing of primary and  
 381 secondary lunar events such as protolith formation and impact metamorphism, respectively.  
 382 Depending on the material and its temperature-time history, the  $^{40}\text{Ar}/^{39}\text{Ar}$  method has the potential  
 383 to provide precise dates of a wide-range of lunar materials (Turner et al., 1973; Turner and  
 384 Cadogan, 1975; Dalrymple and Ryder, 1991, 1993, 1996; Jourdan, 2012; Fernandes et al., 2013).  
 385 Impact events that produced melt can be precisely dated and help build impact flux estimates  
 386 (Dalrymple and Ryder, 1993, 1996; Culler et al., 2000; Cohen et al., 2000; Kring and Cohen, 2002;  
 387 Norman et al., 2006; Mercer et al., 2015, 2019; Zellner and Delano, 2015). The timing of lunar  
 388 volcanism, often expressed as fine-grained and/or amorphous materials (e.g., lunar orange glass  
 389 beads in 74220 soil), can be precisely dated (Huneke, 1978; Spangler et al., 1984; Zellner et al.,  
 390 2009) whereas other isotope systems that rely on mineral-liquid fractionation processes would not  
 391 typically yield precise age determinations of these bulk materials.

392  
 393 Potassium-40 has a branched decay to  $^{40}\text{Ca}$  (89.32%) and  $^{40}\text{Ar}$  (10.68%) with a total decay  
 394 constant of about  $5.53 \times 10^{-10} \text{ yr}^{-1}$  (Renne et al., 2011). Associated  $^{40}\text{K}$ - $^{40}\text{Ca}$  chronology of felsic  
 395 lunar materials (Shih et al., 1993) is possible for specialized applications. Analytical details of the  
 396  $^{40}\text{Ar}$ - $^{39}\text{Ar}$  method are complex (McDougall et al., 1999; Cohen et al., 2000, 2005; Swindle et al.,  
 397 2009; Weirich et al., 2010; Wittmann et al., 2011; Mercer and Hodges, 2016; Niihara et al., 2019;  
 398 Schaen et al., 2020; Beard et al., 2022). Recent advancements in in-situ analytical approaches  
 399 (Mercer et al., 2015) make it easier for analyses of critical petrographic contexts.

400  
 401 Argon-Ar thermochronology is especially useful for understanding the potentially complex  
 402 temperature-time (T-t) history of lunar materials. For short T-t histories relative to the diffusivity  
 403 of Ar in a particular material, Ar-Ar data may have remained a closed system since the last Ar-  
 404 degassing event such as melting (Cohen et al., 2000). For T-t histories that are long and/or extreme  
 405 enough to facilitate Ar loss, the timing of these Ar-loss events may be recorded in the measured  
 406 Ar isotope data (Niihara et al., 2019; Schaen et al., 2020). Overall, Ar-Ar approaches, both in-situ  
 407 and conventional, are a critical tool for unraveling primary and secondary processes operative on  
 408 the Moon.

409

### 410 3 Lunar Lithologies

411 The Artemis exploration zone is a feldspathic highland terrain that was originally anorthositic  
 412 crust, covered and/or mixed with more mafic lithologies excavated by the SPA and other basin-  
 413 forming events producing a mixed - nominally noritic - composition (Pieters et al., 2001; Hawke,  
 414 2003; Spudis et al., 2008; Lin et al., 2020; Huang et al., 2020; Krasilnikov et al., 2023). Major  
 415 minerals in the surface regolith are plagioclase, pyroxene, and olivine, in that order. Reflectance  
 416 spectra suggest the region has an average anorthite abundance of ~80 to 90 wt% and ~5 to 10 wt  
 417 % Fe) (Lemelin et al., 2022).

418

419

420

421

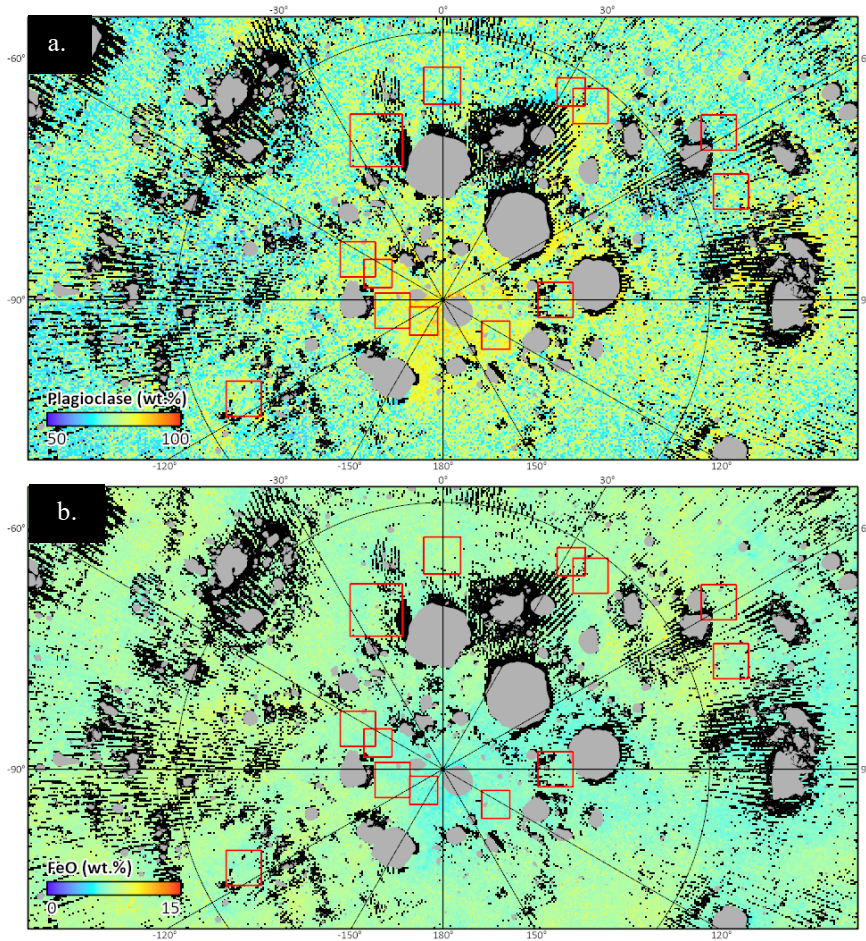


**Figure 3.** Colorized counts of Kaguya SP mineral data used to determine average lithological composition at each of the candidate landing regions (red squares). Gray areas represent permanently shadowed regions, which were masked during analyses. Black areas are areas with no mineral count data available. **(a)** Colorized counts of plagioclase from 50 to 100 wt. %. **(b)** Colorized counts of iron from 0 to 15 wt. %.

**Table 2.** Artemis zonal statistics of mineralogy at each landing site within an exploration zone of 10 radial kilometers. The values below contain minerals modeled from Spectral Profiler data with all PSRs masked from Lemelin et al. (2022). The four sites closest to the south pole (001, 004, 007, and 011) have similar mineralogy. The mineral error is on the order of  $\pm 8$  wt. % and FeO about 2 wt. %. SD = standard deviation.

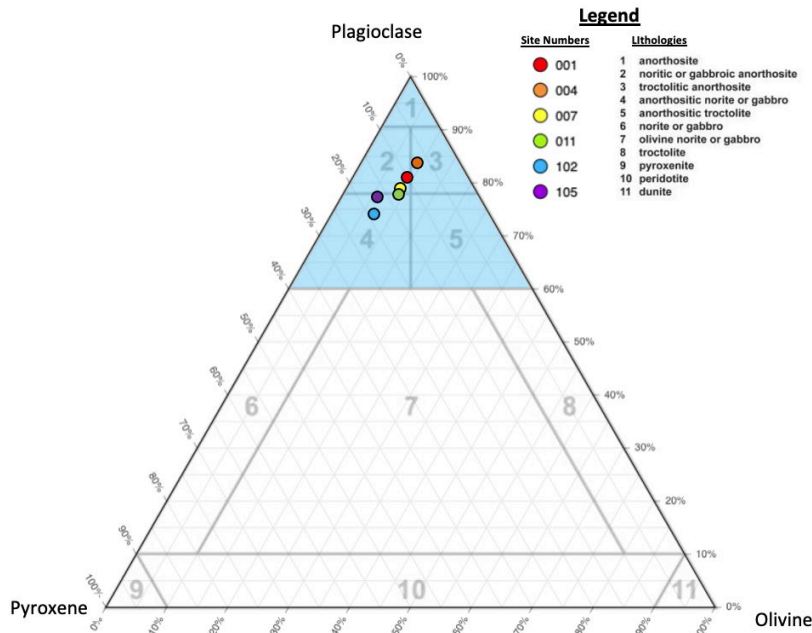
Site #	Lat.	Long.	FeO		Plagioclase		Low-Ca Pyroxene		High-Ca Pyroxene		Olivine	
			Mean	1 SD	Mean	1 SD	Mean	1 SD	Mean	1 SD	Mean	1 SD
001	-89.45	-137.31	6.2	0.4	81	5	10	6	0	2	9	6
004	-89.78	-155.73	6.1	0.4	83	4	8	5	0	1	9	6
007	-88.81	123.64	6.5	0.4	79	5	12	6	0	1	9	6
011	-88.67	-68.1	6.7	0.4	78	5	13	7	0	2	9	6
102	-85.55	37.57	7.2	0.3	74	5	19	7	0	1	7	5
105	-88.8	123.95	6.4	0.3	78	5	16	8	0	0	6	5

422

423 The basin-forming event that created SPA would have been an exceptionally violent impact  
 424 (Potter et al., 2012) that excavated material from depth where mafic to ultramafic materials likely  
 425 existed (Kring, 2005; Hurwitz and Kring, 2014), produced melt, fallback ejecta, and brecciated  
 426 basin floor materials (Petro and Pieters, 2008; Moriarty et al., 2021). This, coupled with billions  
 427 of years of subsequent impacts results in a complicated and varied lithological suite of outcrops  
 428 and potential return sample targets. The lithologies discussed here are those which were defined  
 429 by Stöffler et al. (1980) (Figure 4, Table 3). They may exist as homogenous hand samples (e.g., ~  
 430 5 to 20 cm) or even at the outcrop scale, although there is a strong likelihood of polymict breccias  
 431 housing a multitude of lithologies, much like NWA 5000 and various Apollo samples (Duncan et  
 432 al., 1975; Grieve et al., 1975; Stöffler et al., 1985; Nagurney et al., 2016; Marks et al., 2019; Cao  
 433 et al., 2021). Some lithologies, such as dunite (Shearer et al., 2015), are exceedingly rare within  
 434 the Apollo collection and exist as chips and fragments within brecciated samples. Because it  
 435 crystallizes at depth, dunite solely relies on impact excavation processes or incorporation into  
 436 magmas as xenoliths to be exposed on the lunar surface. The spatial resolution of this study (>500  
 437 m) preclude identification of litho-fragments within an individual sample, driving the need for  
 438 polymict breccia return samples.

439  
 440 We understand lunar rocks exist within a continuum of lithologies, however they are discussed  
 441 below in accordance with the classification schema outlined in Figure 4. With the exception of  
 442 impact melts or fine-grained basaltic clasts, we predict most lithologies in the Artemis exploration  
 443 zone to be relatively coarse-grained (~1 to 3 mm grain size; Joy et al., 2008).

444



445

446

447 **Figure 4.** Average landing site lithological composition displayed relative to plagioclase,  
 448 pyroxene, and olivine. Blue shaded region represents the zone of statistical uncertainty from our  
 449 analysis. Modified after Stöffler et al. (1980).

450

451 **Table 3.** List of lunar lithologies that might be included in the regolith within each site. (List of  
 452 lithologies from Hiesinger (2006)). Gray-filled boxes: within the standard deviation range of

453 average composition calculated from this study (PSRs not masked); X: presence of lithology  
 454 recognized; Y= existence of lithology likely, but below detection limit of current instrumentation;  
 455 Z: lithology possibly present as clasts. References: [1] Gawronska et al. (2020); [2] Lemelin et al.  
 456 (2022); [3] Yamamoto et al. (2012); [4] Uemoto et al. (2010); [5] Halim et al. (2021); [6] Ohtake  
 457 et al. (2009); [7] Borst et al. (2012); [8] Kraettli et al. (2022); [9] Gagnepain-Beyneix et al. (2006);  
 458 [10] Kring (2019); [11] Kring et al. (2022).  
 459

Lithology	Sites					
	001	004	007	011	102	105
Purest Anorthosite (PAN) <sup>[1-4]</sup>	Y	X	Y	Y	X	X
Anorthosite <sup>[1-3,5,6]</sup>	X	X	X	X	X	X
Noritic or Gabbroic Anorthosite <sup>[2]</sup>	X	X	X	X	X	X
Troctolitic Anorthosite <sup>[2]</sup>	X	X	X	X	X	X
Anorthositic Norite or Gabbro <sup>[2]</sup>	X	X	X	X	X	X
Anorthositic Troctolite <sup>[2]</sup>	X	X	X	X	X	X
Norite or Gabbro <sup>[2]</sup>	X	X	X	X	X	X
Olivine Norite or Gabbro <sup>[2]</sup>	X	X	X	X	X	X
Troctolite <sup>[7]</sup>	Y	Y	Y	Y	Y	Y
Pyroxenite <sup>[8,9]</sup>	Z	Z	Z	Z	Z	Z
Peridotite <sup>[7]</sup>	Z	Z	Z	Z	Z	Z
Dunite <sup>[7]</sup>	Z	Z	Z	Z	Z	Z
Basaltic material <sup>[7,10]</sup>	Z	Z	Z	Z	Z	Z

Impact Melt <sup>[10,11]</sup>	Z	Z	Z	Z	Z	Z
Impact Breccia <sup>[1,11]</sup>	Z	Z	Z	Z	Z	Z

460

## 461 3.1 Anorthositic Lithologies

462 Anorthositic lithologies include anorthosite (and ‘purest anorthosite’) and noritic, gabbroic,  
 463 and troctolitic anorthosite. These lithologies are all characterized by having high proportions of  
 464 plagioclase with low, but variable proportions of pyroxene and olivine. Anorthitic plagioclase  
 465 tends to have relatively low concentrations of REE, K, Rb, and U, making direct chronometric  
 466 analyses difficult. The complex thermal and impact histories for many lunar anorthositic rocks  
 467 (see Shearer et al., 2006, and references therein) further compromises the accuracy and precision  
 468 of chronologic measurements. Despite these challenges, chronology of anorthositic rocks by U-  
 469 Pb of mafic phases, mineral and bulk-rock Sm-Nd, and Ar-Ar have been successfully  
 470 accomplished (e.g., Norman et al., 2003; Borg et al., 2011; Marks et al., 2019). Given the overall  
 471 low concentrations in alkali elements, Rb/Sr ratios are low, making Rb-Sr analyses of anorthositic  
 472 rocks useful as a petrogenetic tracer and for calculating model ages (e.g., Borg et al., 2022).

## 473 3.1.1 Anorthosite

474 Anorthosites are coarse-grained igneous rocks that may record early lunar differentiation  
 475 processes. Anorthositic lithologies are common on the Moon because they may have formed from  
 476 early differentiation and crust-forming processes (Anderson et al., 1970; Wood et al., 1970; Wood,  
 477 1970; Ohtake et al., 2009). They are mineralogically defined as > 90 % by volume of plagioclase  
 478 (Figure 4), suggesting they are cumulates produced from an ancient melt (Lucey et al., 2006).  
 479 Mafic minerals in some lunar anorthosites have relatively low Mg/(Mg+Fe) ratios (Lucey et al.,  
 480 2006), and plagioclase within them is typically An<sub>96</sub> which may reflect the Moon’s depletion in  
 481 sodium and other volatile elements (Borg et al., 2022).

## 482 3.1.2 Purest Anorthosite

483 A particularly pure anorthosite exists in the south polar region and is composed of >97 wt. %  
 484 anorthite with <2 wt. % pyroxene (Ohtake et al., 2009). Because it is almost pure anorthite, this  
 485 variant is known as ‘purest anorthosite’ (PAN) (Ohtake et al., 2009). Outcrops that correspond to  
 486 PAN spectra are recognized at the geographic south pole and extend into the massif bridging  
 487 Shackleton to de Gerlache crater (toward the west) and Slater crater (toward the east) (Gawronska  
 488 et al., 2020). The physical extent of the PAN unit is debated because no significant samples of  
 489 PAN were identified within the Apollo collection (Lemelin et al., 2015). Exposures of anorthosites  
 490 (90 to 100 wt. % plagioclase) are somewhat rare in the Artemis region, with a few concentrated  
 491 around Shackleton crater and on or near the ridge between Shackleton and Henson craters (~88.5  
 492 °S, 128 °W, near Site 004) (Lemelin et al., 2022). In this region, PAN could be intact and  
 493 crystalline, or potentially comprise portion of megabreccia with blocks 100 m in size (Gawronska  
 494 et al., 2020).

495 Small clasts of PAN might exist within lunar meteorites (Nagaoka et al., 2014), but PAN is not  
 496 known to exist within the Apollo collection. Some attribute the remote detection of PAN to an  
 497 erroneous calibration of spectral data (Warren and Korotev, 2022). The closest representative

498 sample is 97.6% An (mode) ferroan anorthosite 15415 ('Genesis Rock') (Steele and Smith, 1971;  
499 Wilshire et al., 1972; Turner, 1972), which formed after the Moon's crust solidified and, therefore,  
500 not representative of the LMO flotation crust remnants present in the south polar region (Ohtake  
501 et al., 2009). For direct testing of the earliest flotation crust products of lunar crust formation, PAN  
502 samples should be collected from the SPA, the oldest impact structure on the Moon.

503  
504 PAN is mineralogically-pure in a scale detectable by remote sensing (Ohtake et al., 2009;  
505 Cheek et al., 2013; Donaldson Hanna et al., 2014; Lemelin et al., 2019). A potential opportunity  
506 to study the petrogeneses PAN materials could greatly improve the understanding of early lunar  
507 differentiation processes (Yamamoto et al., 2012; Gawronska et al., 2020; Kring et al., 2022).  
508 Return samples of PAN composition would help determine the spatial extent and composition of  
509 the primary feldspathic crust, improve our inventory of the variety of age, distribution, and origin  
510 of lunar rock types, aid in determining the composition of the lower crust and bulk Moon, and  
511 clarify the local and regional complexity of the current lunar crust (NRC Concepts 3a, 3b, 3c, 3d).  
512 Study of PAN return samples would aid understanding of how massifs were generated from the  
513 SPA basin-forming impact (Kring et al., 2020), and the successive geologic evolution of the region  
514 (NRC Concepts 1b, 1c). PAN samples may also provide an anchor to the early Earth-Moon impact  
515 flux curve by determining the age of the oldest lunar basin (SPA) (Kring, 2007; Mazrouei et al.,  
516 2019), establish a precise chronology of lunar geologic events (Marks et al., 2019), help determine  
517 the thickness of the lunar crust (Spudis and Davis, 1986), aid characterization of lunar crust  
518 variability on regional and global scales (NRC Concepts 1b, 1c, 2a). If anorthosite were to be  
519 collected in-situ from strata exposed on the massif cliff (pole-ward) side of Site 102, this would  
520 directly enable the investigation of the structure and composition of the lunar crust (Spudis and  
521 Davis, 1986; Kring et al., 2020) (NRC Concepts 2a, 2d). It would also reveal more about the multi-  
522 ring impact basin structure of SPA, quantify the effects of planetary characteristics (composition,  
523 density, impact velocities) on crater formation and morphology, and allow the extent of lateral and  
524 vertical mixing of local and ejecta material to be measured (NRC Concepts 6b, 6c, 6d).

### 525 3.1.3 Noritic, Gabbroic, or Troctolitic Anorthosite

526 Noritic/gabbroic anorthosites belong to the ferroan anorthosite (FAN) suite of lunar rocks and  
527 have been confirmed to exist within the SPA farside Highlands by analyses of the Chang'E-5  
528 return sample CE5C0800YJYX132GP (Wang, 2022). Noritic/gabbroic anorthosite or troctolitic  
529 anorthosite (77.5 to 90 wt. % plagioclase, Figure 4) are the second most abundant lithologies in  
530 the south polar region (Lemelin et al., 2022). The parent melts of noritic/gabbroic anorthosites are  
531 believed to be produced during the lunar magma ocean (LMO) overturn by the decompression  
532 melting of upwelling Mg cumulates and coincident mixing with incompatible element enriched  
533 materials (e.g., potassium, rare earth elements, and phosphorous-rich; KREEP) (Hess and  
534 Parmentier, 1995; Elkins-Tanton et al., 2002, 2011). However, Apollo FANs are not representative  
535 of all lunar highland-type crust (Gross et al., 2014, 2020; Xu et al., 2020), so further study of  
536 noritic/gabbroic anorthosites returned by Artemis astronauts would provide information about the  
537 early evolution of the Moon as relevant to the LMO hypothesis.

538  
539 Troctolitic anorthosite is an anorthosite with a minor olivine component (Figure 4) and the  
540  $Mg\# = 87 \pm 5$  (Lucey et al., 2006). Troctolitic anorthosite is a member of the magnesian suite (Mg-  
541 suite) of lunar lithologies and does not belong to the ferroan anorthosite (FAN) group of lunar  
542 lithologies (Lucey et al., 2006). It is representative of the average lithological composition of Site

543 004 (Lemelin et al., 2022). The collection of noritic or gabbroic anorthosite samples from the lunar  
544 surface would enable a more in-depth understanding of lunar crust formation and differentiation  
545 through the study of coexisting pyroxene and plagioclase, which is rare in other early LMO  
546 cumulates (Elardo et al., 2011). A better understanding of LMO crystallization trends from a more  
547 complete suite of materials that record this process will better inform thermal models of the Moon  
548 and the thermal state of the interior during early crustal formation periods (Shearer and Papike,  
549 2005; Elardo et al., 2011) (NRC Concepts 2a, 2d) (NRC, 2007).

550

551 Noritic/gabbroic return samples would improve our understanding of the extent and  
552 composition of the primary feldspathic crust and other products of planetary differentiation, in turn  
553 quantifying the local and regional complexity of the current lunar crust (NRC Concepts 3a, 3c,  
554 3d). This can be most accurately accomplished by collecting samples with known impact crater  
555 sources (i.e., in ejecta blankets with a clear crater source or in-situ from strata within crater walls).  
556 Certain samples may also enable clarification of the lateral rock type variability on regional and  
557 global scales.

558

559 Geochronological analyses of noritic/gabbroic anorthosites would improve the established  
560 global lunar time scale and timing of large impact basin formation (Wood et al., 1970; Hawke,  
561 2003) (NRC Concepts 1b, 1c). Noritic/gabbroic samples will add to our efforts to inventory the  
562 diversity of lunar crustal rocks with respect to composition, age, distribution, and origin (NRC  
563 Concepts 3b, 3c). For example, should troctolitic anorthosite be collected from Shackleton ejecta,  
564 it would improve the understanding of early mafic cumulate products from the Lunar Magma  
565 Ocean (LMO), in particular the precipitation and equilibration of olivine within the lunar crust  
566 (Elkins-Tanton et al., 2011; Elardo et al., 2011) (NRC Concepts 3a, 3b, 3c, 3d). Direct sampling  
567 of troctolitic anorthosite could show how it was generated and preserved relative to the SPA basin-  
568 forming impact (Miljković et al., 2021) (NRC Concepts 1b, 1c, 2a, 3a, 3b, 3c, 3d), and the later  
569 geologic evolution of the region (NRC Concepts 1b, 1c) (NRC, 2007).

## 570 3.2 Mafic Lithologies

571 Lunar mafic lithologies include troctolite, norite, and gabbro, including anorthositic and  
572 olivine-bearing norite and gabbro. Many of these lithologies, especially coarse-grained varieties,  
573 contain a mineralogic diversity that allows for most chronologic systems in Table 1 to be applied.  
574 Methods involving Rb-Sr, Sm-Nd, and Lu-Hf isochron approaches have been applied (e.g., Borg  
575 and Carlson, 2023, and references therein). In many cases, important U-rich accessory phases such  
576 as zircon, baddeleyite, and phosphate group minerals are present, allowing for in-situ chronology  
577 by laser ablation and ion probe (e.g., Shaulis et al, 2017; Merle et al., 2020).

### 578 3.2.1 Anorthositic Norite, Gabbro, or Troctolite

579 The regolith of the south polar region is dominated by anorthositic noritic/gabbroic and  
580 anorthositic troctolitic mineral spectra (Lemelin et al., 2022). Of that regolith, anorthositic  
581 norite/gabbro and anorthositic troctolite (60 to 77.5 wt. % plagioclase with varying proportions of  
582 clino- to orthopyroxene, Figure 4) were identified at sites 011, 102, and 105 (Lemelin et al., 2022).  
583 Anorthositic troctolite is an igneous rock with more plagioclase component than traditional  
584 troctolite (Figure 4) It is still unknown if anorthositic troctolites from the AEZ will be coarse- or

585 fine-grained. Anorthositic troctolites from SPA may signify lithologies formed very early on in  
586 lunar history (Lucey et al., 2006).

587

588 If anorthositic norite/gabbro or anorthositic troctolite were to be collected from the Artemis  
589 region, those samples may illuminate how differentiation occurred after the overturn of the LMO  
590 including a better characterization of the thermal state of the interior (Elkins-Tanton et al., 2011;  
591 Elardo et al., 2011) (NRC Concepts 2a, 2b, 2d). These differentiation products are valuable tools  
592 to understand more details of the extent and composition of varied lithologies, and to quantify our  
593 inventory of the nuanced complexities therein (i.e., variety, age, distribution, origin) (NRC  
594 Concepts 3a, 3b, 3d) (NRC, 2007). Anorthositic norite/gabbros may also aid in the understanding  
595 of the bombardment history of the inner solar system recorded within the uniquely preserved lunar  
596 crust in samples with impact-reset ages (Kring, 2019). This would allow for the anchoring of the  
597 impact flux curve, determining the cadence of the creation of lunar basins (Kring, 2007), and  
598 establishing a precise absolute chronology of the geologic evolution of the lunar south pole region  
599 (NRC Concepts 1a, 1b, 1c).

### 600 3.2.2 Gabbro and Norite

601 Gabbro is a general term for a coarse-grained (typically plutonic) mafic igneous rock composed  
602 of plagioclase, Ca-rich clinopyroxene (augite), and <5 wt% of each of olivine and orthopyroxene  
603 (Figure 4). Norite is an orthopyroxene-bearing gabbro, with < 5 wt. % clinopyroxene or olivine  
604 (Figure 4). Lunar norites are distinguished from lithologies termed ‘gabbro-norites’ by the absence  
605 of a discrete high-Ca pyroxene phase and presence of a wider variety of trace phases (Papike et  
606 al., 2006). Because Shackleton crater is on the edge of the SPA basin, target material of Shackleton  
607 may be ancient noritic crust which may be exposed within crater walls (Gawronska et al., 2020).  
608 Gabbro/norite lithologies in SPA are believed to originate from upper mantle ejecta and contain a  
609 high abundance of Th- and K-bearing materials (Moriarty et al., 2021).

610

611 Gabbros and other mafic lunar lithologies can be used to define magmatic periods and chemical  
612 characteristics of mantle components contributing to the sources of the magmas (Papike et al.,  
613 2006). Gabbroic/noritic cumulates may not have participated in the gravitational overturn during  
614 the time of SPA formation (Moriarty et al., 2021), so return samples of this type would reveal  
615 critical information about magmatic differentiation events in early lunar history (NRC Concepts  
616 2a, 2b, 2d, 3a, 3b, 3d).

617

618 If gabbro or norite were to be collected from the Artemis region, it would aid in understanding  
619 the diversity of lunar crustal rocks through the comparison with Apollo samples of similar  
620 composition (NRC Concepts 3a, 3b, 3c, 3d, 6c, 6d). The large-scale lateral and vertical distribution  
621 of gabbro/norite lithologies could be better determined through in-situ observations of strata in  
622 crater walls and determination of source magmas via geochemical study (Shaulis et al., 2017).  
623 Defining isochron ages from analyses of these pyroxene-rich lithologies would aid in the  
624 understanding of the bombardment history of the inner solar system recorded within the lunar crust  
625 (Shih et al., 1993; Norman et al., 2003; Carlson et al., 2014; Zhang et al., 2021) (NRC Concepts  
626 1a, 1b, 1c, 3a, 3b, 3c, 3d). Gabbro/norite analyses could also show how magmatic events, including  
627 differentiation, transpired after the LMO overturn (NRC Concepts 2a, 2b, 2d, 3a, 3b, 3d) (NRC,  
628 2007).

### 629 3.2.3 Olivine Norite or Gabbro

630 Olivine norite or gabbro are composed of 10 to 50 wt. % plagioclase with varying proportions  
631 of olivine and pyroxene (Figure 4). This lithology is included in the Mg-suite of lunar rocks, which  
632 is representative of the crustal growth and basaltic magmatism period in lunar history (Shearer and  
633 Papike, 2005). The Chinese lunar farside mission Chang'E-4 identified a rock of olivine norite  
634 composition that is believed to have crystallized from the SPA impact pool using a visible and  
635 near-infrared spectrometer aboard the Yutu-2 rover (Lin et al., 2020). Although olivine  
636 norite/gabbro is not a dominant lithology within a 10-km radial exploration zone from any of the  
637 six potential crewed Artemis landing sites, fragments of it could be entrained in breccias. The  
638 Yutu-2 rover discovery of an olivine norite greatly increases the likelihood of finding others like  
639 it within SPA on the lunar nearside. Compositions consistent with olivine norite have been  
640 recognized but those compositions can also represent clast contamination in breccia (Lemelin et  
641 al., 2019). Olivine norite has also been recognized to exist as the most abundant host lithology of  
642 olivine on the edges of the innermost ring material of several basins (e.g., Moscoviense, Humorum,  
643 Imbrium, and Serentitatis), although may represent 'contamination' from basaltic materials  
644 (Yamamoto et al., 2010; Lemelin et al., 2019).

645  
646 If olivine norite/gabbro were to be collected from the Artemis region, it would shed light on  
647 impact kinematics and 'contamination' effects within impact structures (Lemelin et al., 2019),  
648 reveal a more detailed record of the bombardment history of the inner solar system recorded within  
649 the lunar crust (NRC Concepts 1a, 1b, 1c, 3a, 3b, 3c, 3d), and add valuable information to the  
650 diversity of lunar crustal rocks in an impact terrane (NRC Concepts 3a, 3b, 3c, 3d, 6c, 6d) (NRC,  
651 2007). The higher proportions of olivine within an olivine norite or gabbro would allow for more  
652 opportunities to investigate early differentiation processes within the lunar crust.

### 653 3.2.4 Troctolite

654 Troctolite is composed of plagioclase and olivine, with < 5 wt. % of pyroxene (Stöffler et al.,  
655 1980; Prissel and Prissel, 2021). Troctolites are included in the "Mg-suite" of nonmare lunar rocks  
656 and analyzed specimens contain a whole rock composition of  $Mg \# = 87 \pm 5$ . Troctolites are the  
657 most abundant Mg-suite sample type in the Apollo collection (Shearer et al., 2015), but the spatial  
658 distribution on a global scale is not well understood.

659  
660 Troctolites may represent the start of mantle materials in a subsurface depth profile (Hess,  
661 1994). An olivine-bearing lithology, possibly troctolite, is abundant in the peak-ring of the  
662 Shrodingier basin near the Artemis exploration zone. The original spectroscopy was published by  
663 Kramer et al. (2013). An LRO picture showing many kilometers of rock exposure in the peak ring  
664 was published by Kring et al. (2017). Hydrocode calculations indicate the olivine-bearing lithology  
665 was uplifted from depths of 20 to 30 km (Kring et al., 2016). Previous study of phosphorous  
666 diffusion patterns within olivine grains within lunar troctolite 76535 revealed a two-stage cooling  
667 model (initial rapid cooling at high temperatures, then slow cooling at lower temperatures) (Nelson  
668 et al., 2021). Therefore, continued study of lunar troctolites in impact ejecta or fragments of  
669 troctolites harvested from polymict breccias would lead to greater understanding of the thermal  
670 history of the Moon. However, if troctolite were to be collected from in-situ outcrops within crater  
671 walls, it would provide the most detailed context of the specific landing site's history through the  
672 observation of geologic relationships and large-scale textures. Because the global distribution of

673 Mg-suite lithologies is still unknown, the sampling of troctolite (or another in-situ mafic lithology)  
 674 could bring more understanding to their spatial extent and source regions (Shearer et al., 2015).

675  
 676 If troctolite were to be collected from impact ejecta or otherwise, it would allow for the creation  
 677 of a more detailed absolute chronology of serial magmatism, crust/mantle formation and evolution,  
 678 and impact and degassing events (McCallum et al., 2006; Elardo et al., 2012; Shearer et al., 2015;  
 679 McCubbin and Barnes, 2020) (NRC Concepts 1a, 1b, 1c, 1e). Troctolite samples would improve  
 680 the understanding of the structure and composition of the lunar interior, including a potentially  
 681 stratified upper mantle (Moriarty et al., 2021) (NRC Concepts 2a, 2b, 2d), and elucidate the nature  
 682 of the lower crust-mantle boundary (NRC Concepts 3a, 3b, 3c, 3d) (NRC, 2007).

### 683 3.3 Ultramafic Lithologies

684 Lunar ultramafic lithologies include pyroxenite, peridotite, and dunite. These lithologies are  
 685 typically incompatible trace-element (ITE) depleted, thus rock and mineral compositions can be  
 686 low in REE, U, K, and Rb. Depending on the mineralogy and ITE compositions, Rb-Sr, Sm-Nd,  
 687 and Lu-Hf have been applied to certain martian and terrestrial ultramafic specimens (e.g., Lapen et  
 688 al. 2005; 2010). Currently, lunar ultramafic rock specimens are extremely rare but are extremely  
 689 important for unraveling the timing of early lunar differentiation.

#### 690 3.3.1 Pyroxenites

691 Pyroxenite is a cumulate, igneous rock comprised of >90 wt. % pyroxene (Figure 4). It is  
 692 believed to be representative of lunar upper mantle layers crystallized directly from the LMO, and  
 693 thus difficult to observe in-situ due to a mostly subsurface existence (Gagnepain-Beyneix et al.,  
 694 2006; Kraettli et al., 2022). Despite the presence of deep craters within SPA, pyroxenite is not  
 695 currently known to be present at outcrop-scale within the Artemis region, which may be a relic of  
 696 the generally coarse spatial resolution of spectral data. Pyroxenite may, however, have been  
 697 excavated from depth and exist at the surface as lithic fragments within brecciated hand samples  
 698 within the Artemis region.

699  
 700 If pyroxenite were to be collected from impact ejecta, it would improve the understanding of  
 701 the structure and composition of the lunar interior (NRC Concepts 2a, 2b, 2d), elucidate the nature  
 702 of the lower crust-mantle boundary (NRC Concepts 3a, 3b, 3c, 3d), and reveal a more detailed  
 703 absolute chronology of impact events that led to the formation of SPA (NRC Concepts 1a, 1b, 1c,  
 704 1e) (NRC, 2007).

#### 705 3.3.2 Peridotite

706 Peridotite is an olivine-rich (Figure 4) cumulate igneous rock that is not yet known to exist  
 707 within the SPA region, however olivine-rich exposures have been identified throughout SPA  
 708 (Pieters et al., 2001; Yamamoto et al., 2010, 2012). Although it is not yet known to exist in sizable  
 709 deposits identifiable by current detection limitations, the possibility of a peridotite fragment  
 710 existing in a brecciated sample remains.

711  
 712 If peridotite were to be collected from impact ejecta, it would improve the understanding of  
 713 the composition of the lunar mantle and therefore, increase knowledge of structure and  
 714 differentiation in the lunar interior (NRC Concepts 2a, 2b, 2d), allow interpretation of the nature

715 of the lower crust-mantle boundary (NRC Concepts 3a, 3b, 3c, 3d), and reveal a more detailed  
716 absolute chronology of impact events, specifically the formation kinematics of the SPA basin  
717 (NRC Concepts 1a, 1b, 1c, 1e) (NRC, 2007).

### 718 3.3.3 Dunite

719 Dunite is composed of 90 to 100 vol. % olivine (Figure 4). Olivine exposures have been  
720 detected within walls, ejecta, and peaks of craters within the SPA basin (Yamamoto et al., 2010).  
721 It is unclear whether the exposures were excavated upper mantle (dunite) material or Mg-rich  
722 plutonic material (troctolite) in the Moon's lower crust (Yamamoto et al., 2010). Deep-seated  
723 olivine-rich layers would be hidden by a differentiated impact melt sheet (Grieve et al., 1991;  
724 Nakamura et al., 2009; Hurwitz and Kring, 2014), but later impacts could have excavated and  
725 exposed the olivine. This olivine-rich lithology is best observed at young, fresh craters in the  
726 concentric regions around large basins (Yamamoto et al., 2010). It is possible the SPA impact may  
727 have excavated into the mantle (Lucey et al., 1998), although it would have reprocessed the  
728 material in some manner (e.g., giant, differentiated impact melt sheet (Hurwitz and Kring, 2014).  
729

730 Very little ultramafic material exists within the Apollo collection. The only sample large  
731 enough to make the parent rock known (dunite fragments 72415-72418) has been extensively  
732 crushed and shows a complex history of shock, deformation, and recrystallization (Albee et al.,  
733 1974; Dymek et al., 1975; Lally et al., 1976; Papike et al., 2006). Dunite is representative of lunar  
734 mantle materials. The collection and return of in-situ lunar dunite to Earth would be a significant  
735 finding, as none of this yet exists in the lunar collections and is only hypothesized to exist in select  
736 areas within SPA. If dunite were to be collected from outcrop, it would improve the understanding  
737 of the structure and composition of the lunar interior (NRC Concepts 2a, 2b, 2c, 2d), however this  
738 scenario is unlikely because dunite exists at depth and would not easily be exhumed. If dunite is  
739 present within the Artemis exploration zone, it most likely exists as fragments and chips within  
740 ejecta blankets produced via impact cratering processes significant enough to reach the lunar  
741 mantle depths (Vaughan and Head, 2014; Moriarty and Pieters, 2018).  
742

743 Any lunar dunite would be a unique and rare addition to the lunar collection and could increase  
744 our knowledge of the diversity of lunar crustal rocks (NRC Concepts 3a, 3b, 3c, 3d). Because it  
745 would have been excavated from depth via large impactor, it could a) act as a 'probe' to examine  
746 mantle lithologies and petrologic evolution of the lunar interior, and b) highlight information about  
747 the bombardment history of the inner solar system (NRC Concepts 1a, 1b, 1c, 1e) (NRC, 2007).

### 748 3.4 Basaltic Materials

749 Basaltic materials are fine-grained mafic rocks that display a wide range in compositions  
750 similar to the suite of mafic plutonic rocks described earlier. Understanding the ages of these  
751 materials constrains the volcanic history of the Moon. Some basaltic materials have U-rich  
752 accessory phases that can be dated in-situ or can be dated by the Pb isotope systematics of other  
753 igneous phases (e.g., Curran et al., 2019; Li et al., 2021). In many cases, and where the rock has  
754 a relatively simple thermal history, Ar-Ar chronology has the potential for precise determinations  
755 of eruption ages.  
756

757 Photogeologic studies and return samples confirmed the lunar mare areas are formed by large  
758 volumes of flood basaltic lava, like the Columbia River Basalts on Earth (Wilson and Head, 1981).

759 Although no traditional mare materials are confirmed to exist at the surface in SPA, it likely resides  
 760 in considerable quantities at depth in this region and is known as cryptomare. Cryptomare is  
 761 basaltic in composition and represents some of the earliest volcanism on the Moon that has been  
 762 buried by the later emplacement of crater ejecta material and basin-forming events (Head and  
 763 Wilson, 1992). Cryptomare within SPA is estimated to cover a minimum area of  $2.5 \times 10^5 \text{ km}^2$ , be  
 764 at least 400 m thick, volumetrically encompass  $>1.0 \times 10^5 \text{ km}^3$ , and be 3.63 to 4.1 Ga (Shearer et  
 765 al., 2006). Cryptomare is observed within SPA through examination of dark-haloed craters  
 766 (Schultz and Spudis, 1983) which enable the darker albedo cryptomare to be studied against the  
 767 lighter albedo regolith materials. In-situ cryptomare exposures may not be present or accessible at  
 768 any of the six potential landing regions but may still be present within the Artemis exploration  
 769 zone as hashed fragments within crater ejecta. Impact melt ponds also exist on the margins of  
 770 craters and are composed of basaltic ‘mare’ material, though they are not the classical mare  
 771 deposits we were familiarized with from the Apollo landing sites.

772

773 If basaltic materials were to be collected in-situ from ‘cryptomaria’ strata within crater walls,  
 774 application of geochronology methods would primarily reveal vital information about early lunar  
 775 volcanism including the lunar volcanic flux, mantle sources, and compositional variability of  
 776 basalts (NRC Concepts 5a, 5b, 5d). Impact melt ponds may also be sampled in-situ from the outer  
 777 margins of craters within the Artemis region but would be more telling of the bombardment history  
 778 of a region than a distinct new type of volcanism generated from depth (NRC Concepts 1a, 1b, 1c,  
 779 1e). Collecting ‘mare’ type materials from impact ejecta would also prove useful toward  
 780 establishing absolute chronology (NRC Concept 1c), broaden our understanding of the diversity  
 781 of lunar crustal rocks (NRC Concept 3a, 3b, 3d), and reveal limited information on lunar volcanism  
 782 (NRC Concept 5a, 5b, 5d) (NRC, 2007).

### 783 3.5 Impact Melts

784 Impact melt is created by intense shock pressures and temperatures that result in instantaneous  
 785 melting and rapid quenching of a rock during impact. The original rock bulk chemistry is  
 786 preserved, but the mineralogy and petrography is destroyed to varying degrees (Kettrup et al.,  
 787 2003). Chronology of these materials typically rely on systems that are susceptible to thermal  
 788 disturbances and systems (e.g., Ar-Ar) that can be applied to melts (Turner, 1972; Turner et al.,  
 789 1973; Dalrymple and Ryder, 1993, 1996; Zellner and Delano, 2015; Norman et al., 2019) .  
 790 Distinctions between impact melt, impact glasses, and volcanic glasses are important. Impact  
 791 glasses are similar to volcanic glasses but are instead associated with shock and metamorphosed  
 792 lithic fragments. Impact melt fragments are found in breccia deposits within and outside impact  
 793 craters (‘suevite’), and as spherules in distal ejecta (‘tektites’) (Dressler and Reimold, 2001).  
 794 Impact melt rocks differ from impact glasses in that they occur as massive bodies of rock  
 795 crystallized from melt bodies, commonly in the form of sheet-like masses, in the interior of some  
 796 impact craters.

797

798 Most impact-melt rocks contain lithic and mineral clasts from the target (Dressler and  
 799 Reimold, 2001 and references therein; Stahle, 1972), which show clear shock and thermal effects  
 800 (Bischoff and Stöffler, 1984). Complete homogenization of a target rock is only achieved in  
 801 impacts by vaporization and whole-rock melting. The shock pressures required to produce whole-  
 802 rock melting of gabbro is  $>75\text{-}80 \text{ GPa}$ , dunite is  $>60\text{-}70 \text{ GPa}$ , and most relevant to SPA, anorthosite  
 803 is  $>45\text{-}50 \text{ GPa}$  (Müller and Hornemann, 1969; Stöffler and Hornemann, 1972; Stöffler, 1974;

804 Reimold and Stöffler, 1978; Schaal et al., 1979; Ostertag, 1983; Bischoff and Stöffler, 1992).  
805 Material identified as impact melt composes 30-50% of all hand-specimen-sized rocks returned  
806 from highland landing sites and ~50% of all lunar soil materials, including non-mare collections  
807 (Ryder, 1981). Impact-melt rocks from the parent crater are the most reliable for dating the time  
808 of impact (Staudacher et al., 1982; Stephan and Jessberger, 1992; Deutsch and Scharer, 1994) and  
809 should be the first choice for any dating effort.

810

811 The SPA impact likely formed from a 170 km diameter impactor with an energy of  
812  $\sim 4 \times 10^{26}$  J, replacing the basin center with a melt pool of mantle-dominated composition (Potter  
813 et al., 2012). This large melt pond would have cooled slow enough to differentiate within itself,  
814 creating a differentiated melt sheet within SPA, and therefore the Artemis region (Hurwitz and  
815 Kring, 2014). Sampling of different locations (e.g., quenched margins vs. strongly differentiated  
816 center) of the SPA impact melt sheet would reveal a more detail about the impact, its age, and  
817 thermal history of the Moon.

818

819 Sampling of varied locations of a differentiated melt sheet within SPA would uniquely enable  
820 fundamental information about impact processes including melt sheet differentiation (Hurwitz and  
821 Kring, 2014) (NRC Concepts 6a, 6b, 6c, and 6d), make a distinct and diverse addition to our current  
822 sample collection of lunar crustal rocks (NRC Concepts 3a, 3b, 3d), aid in untangling the  
823 bombardment history of the inner solar system (Kettrup et al., 2003; Lin et al., 2020) (NRC  
824 Concepts 1a, 1b, 1c), and better constrain the thickness and variability of the lunar crust within  
825 SPA (Wieczorek and Zuber, 2001; Besserer et al., 2014) (NRC Concepts 2a, 2b). Impact melt  
826 fragments collected from ejecta would reveal impact event timing in the Artemis region, although  
827 in some cases it may be difficult to identify the source crater of the melt.

### 828 3.6 Impact Breccias

829 Impact breccias can contain a wide assortment of lithologies, a range in textures, materials with  
830 wide ranges in thermal histories, and contain clasts from various locations/levels in the Moon.  
831 Because of this variability, thus the chronologic opportunities can be rock/clast specific. Due to  
832 the classification of SPA as an impact terrain, a significant fraction of the surface lithologies  
833 available to Artemis astronauts and robotic assets will be breccias. Impact breccias are composed  
834 of older rocks that have been broken or melted by meteoroid impact (Stöffler et al., 1979). The  
835 components of breccias may be mineral and lithic fragments, crystallized impact melt, or glassy  
836 impact melt. Despite their randomized nature of rock and mineral components generated by  
837 impacts, they are lithified by the heat and shock associated with the impact. Most of the rock  
838 fragments in breccias of the distal part of the continuous ejecta deposits are from the local bedrock  
839 (Deutsch and Stöffler, 1987; Stöffler and Ryder, 2001).

840

841 A melt rock with clasts of unmelted (potentially shock-metamorphosed) targeted material is  
842 an 'impact melt breccia.' These melt bodies may intrude into fractures on the crater floor as veins  
843 and dikes that have been resampled by later impact events (Dressler and Reimold, 2001).  
844 Conversely, breccias composed of exclusively clastic components are 'fragmental' or 'lithic', and  
845 allow for the possibility to identify the nature of their dominant source rock types (Dressler and  
846 Reimold, 2001). The lithology, texture, and clast-types within breccias can be so widely varied  
847 that they, as a group, host the potential to address a majority of the NRC (2007) concepts. For  
848 example, a single polymict impact breccia could contain fragments from units with the ability

849 reveal the age of the SPA basin (NRC Concepts 1b, 1c), record a history of the ancient thermal  
850 state of the lunar interior (NRC Concept 2d), contain a wide diversity of lithologies (e.g., polymict  
851 breccias) (NRC Concepts 3a, 3b, 3c, 3d), host a cryptomare clast (NRC Concepts 5a, 5b, 5d), host  
852 a clast from a specific impact-associated unit such as a differentiated melt sheet (NRC Concepts  
853 6a, 6b, 6c), and exist as a mixture of units from depth and local ejecta and regolith materials (NRC  
854 Concepts 6d, 7a, 7c, 7d). Breccias are common to find in impact terrains but vary greatly in their  
855 contents. Each brecciated sample will require a highly individualized approach to the analyses and  
856 assessment of applicable NRC Concepts (2007).

857

### 858 3.7 Regolith Breccias and Soils

859 The lunar regolith was created by large impacts which reduced the grain size of the underlying  
860 bedrock (Horz et al., 1991; McKay et al., 1991). This regolith layer records the Moon's impact  
861 history and the nature and timing of material delivered to the Moon's surface (e.g., Lucey et al.,  
862 2006). Due to the high velocity of impact (e.g., Le Feuvre and Wieczorek, 2011) and resultant  
863 melting and/or vaporization, a projectile imparts its geochemical signature into impact melt  
864 deposits it creates (Morgan et al., 1972a, b; Ganapathy et al., 1974; Higuchi and Morgan, 1975;  
865 Gros et al., 1976; James, 1996, 2002; Norman et al., 2002; Puchtel et al., 2008). However, some  
866 impactors completely or partially survive the lunar impact process intact, as evidenced by  
867 unmelted fragments of meteorites that have been found in lunar rocks and soils (e.g., McSween Jr,  
868 1976; Jolliff et al., 1993; Zolensky et al., 1996; Rubin, 1997; Zolensky, 1997; Day et al., 2006).  
869 When paired with a time of impact, these partially unmelted samples help to provide better  
870 geochemical and chronological constraints for models of Solar system dynamics and causes of  
871 impact spikes to the Earth-Moon system (Turner et al., 1973; Tera et al., 1974; Dalrymple and  
872 Ryder, 1993, 1996; Cohen et al., 2000; Kring and Cohen, 2002; Kring et al., 2005; Norman et al.,  
873 2006; Čuk et al., 2010). Geochemical and chronological evidence from lunar samples informs our  
874 understanding of the Earth-Moon system, and the wider inner Solar system. Ages of lunar regolith  
875 breccias and soils can be estimated from the trapped  $^{40}\text{Ar}/^{36}\text{Ar}$  ratio of a sample. The abundances  
876 of trapped  $^{40}\text{Ar}$  within a regolith sample is normalized to  $^{36}\text{Ar}$  as an indicator of the point in time  
877 of the last exposure to solar wind (i.e., the space environment), before closure of the system  
878 through burial by an ejecta blanket or a basalt flow. Variations of trapped Ar with time has been  
879 used to estimate the ages of lunar regolith samples (Eugster et al., 1980, 1983, 2001; McKay et al.,  
880 1986; Eugster and Polnau, 1997). A model age representing breccia closure represents the last time  
881 grain-size components of the breccia were exposed to solar wind and may be used to calculate the  
882 formation time of the breccia (Joy et al., 2011, after Eugster et al., 2001). The technique was used  
883 to determine the ages of 191 lunar regolith samples from Apollo, Luna, and meteorite collections  
884 (Fagan et al., 2014).

885

886 In addition to what was stated in the impact breccia section, regolith breccias and lunar soils  
887 have the potential to address physical properties of the extremely cold (and possible volatile-rich)  
888 polar regolith (NRC Concept 4d), measure the extent of lateral and vertical mixing of local and  
889 ejecta material (NRC Concept 6d), and utilize the Moon as a natural laboratory for regolith  
890 processes and weathering on anhydrous airless bodies (NRC Concepts 7a, 7b, 7c, 7d).

## 891 4 Chronologic Applications: Limitations and Opportunities

892 In the previous sections, the Artemis exploration zone lithologies are described and the science  
893 potential for these returned materials is discussed. Applications of chronologic approaches to these  
894 lithologies and some specific and unresolved major questions are informed by previous  
895 chronologic studies (Nyquist and Shih, 1992; Nyquist et al., 2001; Carlson et al., 2014; Borg et  
896 al., 2015; Barboni et al., 2017; Papike et al., 2018; Borg and Carlson, 2023). A primary question  
897 is: what is the age of the Moon? This seemingly simple question has been exceedingly difficult to  
898 answer.

899

### 900 4.1 Age of the Moon and timing of the LMO

901

902 In the context of a Moon-forming impact model of Lock et al. (2018), the violence of this event  
903 served to destroy most, if not all evidence of the impactor and proto-Earth. The Moon would have  
904 formed from a terrestrial synestia and undergone a magma ocean phase (Elkins-Tanton et al., 2011;  
905 Elardo et al., 2011). During the lunar magma ocean (LMO) crystallization phase, metal-silicate  
906 differentiation would take place. The timing of lunar core formation is robustly constrained to have  
907 occurred after 4.51 to 4.50 Ga based on the short-lived  $^{182}\text{Hf}$ - $^{182}\text{W}$  isotope system (Touboul et al.,  
908 2007; Kruijjer and Kleine, 2017). Thus, the Moon formed *after* 4.51 – 4.50 Ga. Constraints on the  
909 first silicate minerals to form in the crust and mantle during the magma ocean crystallization phase  
910 is where significant debate exists. Prominent, accessible lithologies that should reflect LMO  
911 fractionation products are anorthositic flotation cumulate rocks that form after about 75% of the  
912 LMO crystallized (Rapp and Draper, 2018). As discussed in Borg and Carlson (2023), numerous  
913 attempts to date lunar anorthosites have yielded many different results. They discuss many issues  
914 that could result in ‘excess’ scatter about an isochron (meaning that the scatter is greater than  
915 predicted from analytical uncertainties alone) and initial isotopic compositions that suggest open-  
916 system behavior or variable effects of secondary processes. Thus, Borg and Carlson (2023) suggest  
917 that the most reliable ages are those that are supported by independent confirmation with another  
918 isotopic system and from these criteria conclude that anorthosites related to LMO crystallization  
919 are likely no older than about 4.36 Ga. There are, however, other studies that show relatively robust  
920 isochrons indicative of older ages but lack independent confirmation. These include a Sm-Nd  
921 mineral and whole rock isochron age of  $4.463 \pm 0.040$  Ga in Descartes breccia 67215 (Norman et  
922 al., 2003), an Sm-Nd isochron age of  $4.436 \pm 0.034$  for an anorthositic clast in Y-86032 (Nyquist  
923 et al., 2006). The oldest reliable age determined directly from a ferroan anorthosite constrains how  
924 late the Moon-forming event was. The potential for additional anorthositic materials from the  
925 Artemis explorations areas, especially the potential PAN lithologies, may provide materials that  
926 could help better constrain the timing of LMO crystallization and the age of lunar formation,  
927 overall. Other constraints on the age of the Moon come from Lu-Hf model ages of lunar zircon  
928 (Barboni et al., 2017). These data provide strong evidence that the Moon-forming event occurred  
929 at about 4.50-4.51 Ga and highlight an ‘old versus young’ Moon formation debate. Collection of  
930 any materials containing zircon (e.g., gabbroic clasts) in the exploration zone can further test the  
931 Lu-Hf constraints on lunar formation.

932

933 In addition to the sample return of materials that may help directly date the Moon-forming  
934 event through an expanded sample suite, new analytical opportunities are evolving. These include  
935 advances in in-situ Rb-Sr isotopic analyses (Dauphas et al., 2022; Zhang, 2022). Because  
936 anorthositic lithologies are susceptible to disturbance and have experienced protracted thermal

937 histories that may have resulted in isotopic disequilibrium (Borg and Carlson, 2023), in-situ  
938 approaches have the potential for identifying sample areas (e.g., in a thick or thin section) that are  
939 disturbed and those that are more pristine. This information will be invaluable for identifying lunar  
940 materials that best preserve their primary or protolith components and target those areas for dating.  
941 Robust ages, as defined by Borg and Carlson (2023), determined directly from LMO products will  
942 have major implications for lunar age models and the timing and duration of the LMO.

943  
944 Another way to date the LMO is to assess the formation timing of lunar mantle sources. A  
945 robust method to determine when the lunar mantle ceased evolving through LMO crystallization  
946 processes is to investigate the  $^{146}\text{Sm}$ - $^{142}\text{Nd}$  and  $^{147}\text{Sm}$ - $^{143}\text{Nd}$  isotopic compositions of lunar  
947 materials (Nyquist et al., 1995; Boyet and Carlson, 2007; Borg et al., 2019). These studies show  
948 that the lunar mantle closed to fractionation at about 4.33 Ga, but these data do not constrain when  
949 LMO crystallization began. Thus, additional constraints on the timing of LMO crystallization can  
950 be made if additional LMO products were collected and returned, such as those that may have been  
951 excavated from depth during the SPA impact (Potter et al., 2012; Hurwitz and Kring, 2014;  
952 Garrick-Bethell et al., 2020; Lin et al., 2020; Moriarty et al., 2021).

#### 953 954 4.2 Timing of Lunar Magmatism

955  
956 Lunar magmatism has been ongoing until at least  $2.030 \pm 0.003$  Ga (Li et al., 2021). Models  
957 that explain the evolution of lunar magmatism through time are underpinned by robust chronology.  
958 While anorthositic rocks are often associated with LMO processes, lunar magmatism is often  
959 associated with materials that are more basaltic in composition. Because these materials (which  
960 include mare basalt, cryptomare, and most Mg-suite rocks) have more diverse mineralogies than  
961 anorthositic rocks, the chronologic opportunities are far greater and essentially encapsulate all of  
962 the systems and approaches listed in Table 1. Of critical note, trace U-rich phases such as zircon  
963 and baddeleyite have the potential for precise U-Pb ages, even in thermally and chemically  
964 disturbed specimens. In thermally undisturbed specimens and/or fine-grained or amorphous  
965 specimens, precise Ar-Ar chronology can yield precise magmatic age determinations (e.g.,  
966 Jourdan, 2012 and references therein). Precise mineral isochrons have been successfully applied  
967 to numerous basaltic lunar compositions coarse enough for mineral separations (Nyquist and Shih,  
968 1992; Rankenburg et al., 2007; Carlson et al., 2014). Given that most of the compositional mapping  
969 noted in section 2 indicates anorthositic compositions, mafic clasts could be present that are below  
970 the spatial resolution of spectral mapping. Thus, mafic lithologies have relatively high probabilities  
971 of success for chronology and these data can better inform models for the magmatic evolution of  
972 the Moon and help develop thermal models that explain at least  $\sim 2.5$  billion years of lunar  
973 magmatic activity.

#### 974 975 4.3 Impact Processes and the Age of SPA

976  
977 The Artemis exploration zones are located within the SPA basin and within heavily impacted  
978 terrain. It is expected that most materials collected from these regions will have been affected to  
979 some degree by impact processes. Figure 2 summarizes some of the predicted geology and unit  
980 ages that might be encountered in the exploration zones. Critical to assessing the source(s) of  
981 ejecta and their impact ages, dating impact metamorphism and/or impact melting is required.  
982 Standard approaches involve Ar-Ar analyses of impact glass or material that experienced  
983 significant Ar-loss during impact metamorphism. Materials that crystallized from an impact melt

983 can have U-rich phases that can be dated by in-situ U-Pb analyses or can be dated by mineral  
984 isochron approaches. In most cases, specimens that developed through impact processes can be  
985 dated in a variety of ways depending on the severity of impact metamorphism/melting; often, both  
986 the age of the protolith and the age of thermal metamorphism can be established (Burgess et al.,  
987 2007; Fernandes et al., 2013; Shaulis et al., 2017; Černok et al., 2021). The opportunity that impact  
988 materials would be collected from mapped terrains, connections between ejecta and impact basin  
989 can be strengthened. For impact chronology, the limit on science return is not the analytical  
990 techniques, it's the nature and types of samples collected from the surface and how they relate to  
991 the surface geology.

## 992 **5 Sampling Strategy**

993 The lithologies detected in the Artemis region by numerous previous studies (Yamamoto et  
994 al., 2012; Lemelin et al., 2017, 2022) were identified at relatively coarse spatial resolutions (1  
995 km/pixel; 500 m/pixel). It should be noted that two upcoming instruments with improved spatial  
996 resolution (Imaging Infrared Spectrometer aboard Chandrayaan-2; High-Resolution Volatiles and  
997 Minerals Moon Mapper aboard Lunar Trailblazer) will launch prior to crewed Artemis activities.  
998 Both instruments will produce data at a spatial resolution of 70 to 80 m/pixel, which will  
999 dramatically increase the mineralogical detail available to identify less abundant lithologies (i.e.,  
1000 PAN, olivine-rich units, mafic lithologies, etc.).

1001  
1002 The Apollo astronauts were instructed to collect the greatest diversity of samples with the  
1003 coarsest grain sizes to allow for easier mineral separation in laboratory analyses on Earth (Phinney,  
1004 2015). This practice does not need to hold true for the Artemis astronauts. There is benefit in  
1005 collecting the greatest diversity of samples possible with respect to grain size and composition. To  
1006 broaden the potential science impact from returned samples, the Artemis astronauts should focus  
1007 on material diversity and areas that may contain deeply excavated materials, among other activities  
1008 and sampling related to the broader mission goals.

## 1009 **6 Concluding Remarks**

1010 The Artemis exploration zone contains several regions that may be explored by future crewed  
1011 and uncrewed surface missions. Lithologies in this region were created from igneous and impact  
1012 processes that have persisted over billions of years. Some brecciated samples may contain clasts  
1013 petrogenetically unrelated to one another, which could be an efficient strategy to study a greater  
1014 variety of lunar lithologies without venturing over large spatial regions on the surface. The  
1015 potential for such breadth of lithological variety in an as-yet-unexplored region of the Moon will  
1016 provide chronologic opportunities for untangling the mysterious history of lunar evolution.  
1017 Chronologic opportunities that exist from analyses of returned samples include U-Th-P, Rb-Sr,  
1018 Sm-Nd, Lu-Hf, and Ar-Ar.

1019 These data will address issues such as the age of the Moon, timing of crucial events in lunar  
1020 history, allow for recalibration of melt extraction model ages, crystallization ages of lithologies,  
1021 and impact flux during the early Solar system. It is evident samples returned from the Artemis  
1022 exploration zone will provide incredible insight into the history of the Moon and early Solar  
1023 system. There is no 'silver bullet' analytical approach for all sample types. It will take a highly

1024 coordinated effort between lithologies, chronometers, instruments, and institutions to fully  
1025 understand what can be learned from these precious samples.

## 1026 **Acknowledgments**

- 1027 • The author acknowledges the Center for Lunar Science and Exploration for providing  
1028 funding to support the completion of this manuscript.
- 1029 • Since beginning this manuscript, the first author has become employed by Jacobs at  
1030 NASA Johnson Space Center in addition to her doctoral studies at University of  
1031 Houston.

## 1032 **Open Research**

1033 The reflectance and compositional mosaics used in this study are derived from Lemelin et al.  
1034 (2022) and can be found in Zenodo:[10.5281/zenodo.5847000](https://zenodo.org/doi/10.5281/zenodo.5847000).

## 1035 **References**

- 1036 Abelson P. H. (1970) The Moon Issue. *Science* **167**, 447–447.
- 1037 Albee A. L., Chodos A. A., Dymek R. F., Gancarz A. J., Goldman D. S., Papanastassiou D. A.  
1038 and Wasserburg G. J. (1974) Dunite From the Lunar Highlands: Petrography,  
1039 Deformational History, Rb-Sr Age. In *Lunar and Planetary Science Conference* p. 3.
- 1040 Amelin Y. (2005) Meteorite Phosphates Show Constant <sup>176</sup>Lu Decay Rate Since 4557 Million  
1041 Years Ago. *Science* **310**, 839–841.
- 1042 Amelin Y. and Zaitsev A. N. (2002) Precise geochronology of phoscorites and carbonatites:: The  
1043 critical role of U-series disequilibrium in age interpretations. *Geochimica et*  
1044 *Cosmochimica Acta* **66**, 2399–2419.
- 1045 Anderson A. T., Crewe A. V., Goldsmith J. R., Moore P. B., Newton J. C., Olsen E. J., Smith J.  
1046 V. and Wyllie P. J. (1970) Petrologic History of Moon Suggested by Petrography,  
1047 Mineralogy, and Crystallography. *Science* **167**, 587–590.
- 1048 Arvidson R. E., Boyce J., Chapman C., Cintala M., Fulchignoni M., Moore H., Neukum G.,  
1049 Schultz P. H., Soderblom L., Strom R., Woronow A. and Young R. (1979) Standard  
1050 techniques for presentation and analysis of crater size-frequency data. *Icarus* **37**, 467–  
1051 474.
- 1052 Ballhaus C., Laurenz V., Münker C., Fonseca R. O. C., Albarède F., Rohrbach A., Lagos M.,  
1053 Schmidt M. W., Jochum K.-P., Stoll B., Weis U. and Helmy H. M. (2013) The U/Pb ratio  
1054 of the Earth’s mantle—A signature of late volatile addition. *Earth and Planetary Science*  
1055 *Letters* **362**, 237–245.
- 1056 Barboni Melanie, Boehnke P., Keller B., Kohl I. E., Schoene B., Young E. D. and McKeegan K.  
1057 D. (2017) Early formation of the Moon 4.51 billion years ago. *Sci. Adv.* **3**, e1602365.

- 1058 Barboni M, Boehnke P., Keller C., Kohl I., Schoene B., Young E. and McKeegan K. (2017) The  
 1059 Age of the Moon. In id. 1900. Lunar and Planetary Science XLVIII. Lunar and Planetary  
 1060 Institute, The Woodlands, Texas.
- 1061 Barnes J. J., Kring D. A., Tartèse R., Franchi I. A., Anand M. and Russell S. S. (2016) An  
 1062 asteroidal origin for water in the Moon. *Nat Commun* **7**, 11684.
- 1063 Beard B. L., Taylor L. A., Scherer E. E., Johnson C. M. and Snyder G. A. (1998) The Source  
 1064 Region and Melting Mineralogy of High-Titanium and Low-Titanium Lunar Basalts  
 1065 Deduced from Lu-Hf Isotope Data. *Geochimica et Cosmochimica Acta* **62**, 525–544.
- 1066 Beard S. P., Swindle T. D., Lapen T. J. and Kring D. A. (2022) Ar -Ar and U -Pb ages of  
 1067 Chelyabinsk and a re-evaluation of its impact chronology. *Meteorit & Planetary Scien*  
 1068 **57**, 2276–2288.
- 1069 Besserer J., Nimmo F., Wiczorek M. A., Weber R. C., Kiefer W. S., McGovern P. J., Andrews-  
 1070 Hanna J. C., Smith D. E. and Zuber M. T. (2014) GRAIL gravity constraints on the  
 1071 vertical and lateral density structure of the lunar crust. *Geophys. Res. Lett.* **41**, 5771–  
 1072 5777.
- 1073 Bickel V., Aaron J., Manconi A., Loew S. and Mall U. (2020) Impacts drive lunar rockfalls over  
 1074 billions of years. *Nature Communications* **11**.
- 1075 Bischoff A. and Stöffler D. (1984) Chemical and structural changes induced by thermal  
 1076 annealing of shocked feldspar inclusions in impact melt rocks from Lappajärvi Crater,  
 1077 Finland. *J. Geophys. Res.* **89**, B645.
- 1078 Bischoff A. and Stöffler D. (1992) Shock metamorphism as a fundamental process in the  
 1079 evolution of planetary bodies: Information from meteorites. *European Journal of*  
 1080 *Mineralogy* **4**, 707–755.
- 1081 Borg L., Connelly J., Boyet M. and Carlson R. (2011) The Age of Lunar Ferroan Anorthosite  
 1082 60025 with Implications for the Interpretation of Lunar Chronology and the Magma  
 1083 Ocean Model. In id. 1171. Lunar and Planetary Science XLII. Lunar and Planetary  
 1084 Institute, The Woodlands, Texas.
- 1085 Borg L. E., Brennecka G. A. and Kruijer T. S. (2022) The origin of volatile elements in the  
 1086 Earth–Moon system. *Proc. Natl. Acad. Sci. U.S.A.* **119**, e2115726119.
- 1087 Borg L. E. and Carlson R. W. (2023) The Evolving Chronology of Moon Formation. *Annu. Rev.*  
 1088 *Earth Planet. Sci.* **51**, annurev-earth-031621-060538.
- 1089 Borg L. E., Gaffney A. M., Kruijer T. S., Marks N. A., Sio C. K. and Wimpenny J. (2019)  
 1090 Isotopic evidence for a young lunar magma ocean. *Earth and Planetary Science Letters*  
 1091 **523**, 115706.
- 1092 Borg L. E., Gaffney A. M. and Shearer C. K. (2015) A review of lunar chronology revealing a  
 1093 preponderance of 4.34–4.37 Ga ages. *Meteorit Planet Sci* **50**, 715–732.

- 1094 Borg L. E., Gaffney A. M., Shearer C. K., DePaolo D. J., Hutcheon I. D., Owens T. L., Ramon  
 1095 E. and Brennecka G. (2009) Mechanisms for incompatible-element enrichment on the  
 1096 Moon deduced from the lunar basaltic meteorite Northwest Africa 032. *Geochimica et*  
 1097 *Cosmochimica Acta* **73**, 3963–3980.
- 1098 Borst A. M., Foing B. H., Davies G. R. and van Westrenen W. (2012) Surface mineralogy and  
 1099 stratigraphy of the lunar South Pole-Aitken basin determined from Clementine UV/VIS  
 1100 and NIR data. *Planetary and Space Science* **68**, 76–85.
- 1101 Bottke W. F., Walker R. J., Day J. M. D., Nesvorny D. and Elkins-Tanton L. (2010) Stochastic  
 1102 Late Accretion to Earth, the Moon, and Mars. *Science* **330**, 1527–1530.
- 1103 Boyce J. M., Schaber G. G. and Dial Jr A. L. (1977) Age of Luna 24 mare basalts based on crater  
 1104 studies. *Nature* **265**, 38–39.
- 1105 Boyet M. and Carlson R. W. (2007) A highly depleted moon or a non-magma ocean origin for  
 1106 the lunar crust? *Earth and Planetary Science Letters* **262**, 505–516.
- 1107 Brandon A. D., Lapen T. J., Debaille V., Beard B. L., Rankenburg K. and Neal C. (2009) Re-  
 1108 evaluating 142Nd/144Nd in lunar mare basalts with implications for the early evolution  
 1109 and bulk Sm/Nd of the Moon. *Geochimica et Cosmochimica Acta* **73**, 6421–6445.
- 1110 Brown H. M., Boyd A. K., Denevi B. W., Henriksen M. R., Manheim M. R., Robinson M. S.,  
 1111 Speyerer E. J. and Wagner R. V. (2022) Resource potential of lunar permanently  
 1112 shadowed regions. *Icarus* **377**, 114874.
- 1113 Burgess R., Fernandes V. A., Irving A. J. and Bunch T. E. (2007) Ar-Ar Ages of NWA 2977 and  
 1114 NWA 3160 – Lunar Meteorites Paired with NWA 773. In Lunar and Planetary Science  
 1115 XXXVIII. The Lunar and Planetary Science Institute, The Woodlands, Texas. p. Abstract  
 1116 1603.
- 1117 Bussey D. B. J., McGovern J. A., Spudis P. D., Neish C. D., Noda H., Ishihara Y. and Sørensen  
 1118 S.-A. (2010) Illumination conditions of the south pole of the Moon derived using Kaguya  
 1119 topography. *Icarus* **208**, 558–564.
- 1120 Cao H., Ling Z., Chen J., Fu X., Zou Y. and Joy K. (2021) Petrography, mineralogy, and  
 1121 geochemistry of a new lunar magnesian feldspathic meteorite Northwest Africa 11460.  
 1122 *Meteorit Planet Sci* **56**, 1857–1889.
- 1123 Carlson R. W., Borg L. E., Gaffney A. M. and Boyet M. (2014) Rb-Sr, Sm-Nd and Lu-Hf  
 1124 isotope systematics of the lunar Mg-suite: the age of the lunar crust and its relation to the  
 1125 time of Moon formation. *Phil. Trans. R. Soc. A* **372**, 20130246.
- 1126 Černok A., White L. F., Anand M., Tait K. T., Darling J. R., Whitehouse M., Miljković K.,  
 1127 Lemelin M., Reddy S. M., Fougèrouse D., Rickard W. D. A., Saxey D. W. and Ghent R.  
 1128 (2021) Lunar samples record an impact 4.2 billion years ago that may have formed the  
 1129 Serenitatis Basin. *Commun Earth Environ* **2**, 1–9.

- 1130 Charlier B. L. A., Ginibre C., Morgan D., Nowell G. M., Pearson D. G., Davidson J. P. and  
 1131 Ottley C. J. (2006) Methods for the microsampling and high-precision analysis of  
 1132 strontium and rubidium isotopes at single crystal scale for petrological and  
 1133 geochronological applications. *Chemical Geology* **232**, 114–133.
- 1134 Che X., Nemchin A., Liu D., Long T., Wang C., Norman M. D., Joy K. H., Tartese R., Head J.,  
 1135 Jolliff B., Snape J. F., Neal C. R., Whitehouse M. J., Crow C., Benedix G., Jourdan F.,  
 1136 Yang Z., Yang C., Liu J., Xie S., Bao Z., Fan R., Li D., Li Z. and Webb S. G. (2021) Age  
 1137 and composition of young basalts on the Moon, measured from samples returned by  
 1138 Chang’e-5. *Science* **374**, 887–890.
- 1139 Cheek L. C., Donaldson Hanna K. L., Pieters C. M., Head J. W. and Whitten J. L. (2013) The  
 1140 distribution and purity of anorthosite across the Orientale basin: New perspectives from  
 1141 Moon Mineralogy Mapper data: CRYSTALLINE ANORTHOSITE ACROSS  
 1142 ORIENTALE. *J. Geophys. Res. Planets* **118**, 1805–1820.
- 1143 Cherniak D. J. and Watson E. B. (2001) Pb diffusion in zircon. *Chemical Geology* **172**, 5–24.
- 1144 Chew D., Drost K., Marsh J. H. and Petrus J. A. (2021) LA-ICP-MS imaging in the geosciences  
 1145 and its applications to geochronology. *Chemical Geology* **559**, 119917.
- 1146 Coan D. (2020) Exploration EVA System Concept of Operations.
- 1147 Cohen B. A., Swindle T. D. and Kring D. A. (2005) Geochemistry and  $^{40}\text{Ar}$ - $^{39}\text{Ar}$   
 1148 geochronology of impact-melt clasts in feldspathic lunar meteorites: Implications for  
 1149 lunar bombardment history. *Meteoritics & Planetary Science* **40**, 755–777.
- 1150 Cohen B. A., Swindle T. D. and Kring D. A. (2000) Support for the Lunar Cataclysm Hypothesis  
 1151 from Lunar Meteorite Impact Melt Ages. *Science* **290**, 1754–1756.
- 1152 Čuk M., Gladman B. J. and Stewart S. T. (2010) Constraints on the source of lunar cataclysm  
 1153 impactors. *Icarus* **207**, 590–594.
- 1154 Culler T. S., Becker T. A., Muller R. A. and Renne P. R. (2000) Lunar Impact History from  $^{40}$   
 1155  $\text{Ar}/^{39}\text{Ar}$  Dating of Glass Spherules. *Science* **287**, 1785–1788.
- 1156 Curran N. M., Joy K. H., Snape J. F., Pernet-Fisher J. F., Gilmour J. D., Nemchin A. A.,  
 1157 Whitehouse M. J. and Burgess R. (2019) The early geological history of the Moon  
 1158 inferred from ancient lunar meteorite Miller Range 13317. *Meteorit & Planetary Scien*  
 1159 **54**, 1401–1430.
- 1160 Dalrymple G. B. and Ryder G. (1993)  $^{40}\text{Ar}/^{39}\text{Ar}$  age spectra of Apollo 15 impact melt rocks by  
 1161 laser step-heating and their bearing on the history of lunar basin formation. *J. Geophys.*  
 1162 *Res.* **98**, 13085–13095.
- 1163 Dalrymple G. B. and Ryder G. (1991)  $^{40}\text{Ar}/^{39}\text{Ar}$  ages of six Apollo 15 impact melt rocks by  
 1164 laser step heating. *Geophysical Research Letters* **18**, 1163–1166.

- 1165 Dalrymple G. B. and Ryder G. (1996) Argon-40/argon-39 age spectra of Apollo 17 highlands  
 1166 breccia samples by laser step heating and the age of the Serenitatis basin. *J. Geophys.*  
 1167 *Res.* **101**, 26069–26084.
- 1168 Dauphas N., Hopp T., Craig G., J. Zhang Z., C. Valdes M., R. Heck P., A. Charlier B. L., A. Bell  
 1169 E., Mark Harrison T., M. Davis A., Dussubieux L., R. Williams P., J. Krawczynski M.,  
 1170 Bouman C., S. Lloyd N., Tollstrup D. and B. Schwieters J. (2022) In situ 87 Rb– 87 Sr  
 1171 analyses of terrestrial and extraterrestrial samples by LA-MC-ICP-MS/MS with double  
 1172 Wien filter and collision cell technologies. *Journal of Analytical Atomic Spectrometry* **37**,  
 1173 2420–2441.
- 1174 Day J. M., Floss C., Taylor L. A., Anand M. and Patchen A. D. (2006) Evolved mare basalt  
 1175 magmatism, high Mg/Fe feldspathic crust, chondritic impactors, and the petrogenesis of  
 1176 Antarctic lunar breccia meteorites Meteorite Hills 01210 and Pecora Escarpment 02007.  
 1177 *Geochimica et Cosmochimica Acta* **70**, 5957–5989.
- 1178 Deutsch A. N., Head J. W. and Neumann G. A. (2020) Analyzing the ages of south polar craters  
 1179 on the Moon: Implications for the sources and evolution of surface water ice. *Icarus* **336**,  
 1180 113455.
- 1181 Deutsch A. and Scharer U. (1994) Dating terrestrial impact events. *Meteoritics* **29**, 301–322.
- 1182 Deutsch A. and Stöffler D. (1987) Rb-Sr-analyses of Apollo 16 melt rocks and a new age  
 1183 estimate for the Imbrium basin: Lunar basin chronology and the early heavy  
 1184 bombardment of the moon. *Geochimica et Cosmochimica Acta* **51**, 1951–1964.
- 1185 Donaldson Hanna K. L., Cheek L. C., Pieters C. M., Mustard J. F., Greenhagen B. T., Thomas I.  
 1186 R. and Bowles N. E. (2014) Global assessment of pure crystalline plagioclase across the  
 1187 Moon and implications for the evolution of the primary crust: Pure Plagioclase on the  
 1188 Moon. *J. Geophys. Res. Planets* **119**, 1516–1545.
- 1189 Dressler B. O. and Reimold W. U. (2001) Terrestrial impact melt rocks and glasses. *Earth-*  
 1190 *Science Reviews* **56**, 205–284.
- 1191 Duncan A. R., Mckay S. M., Stoesser J. W., Lindstrom M. M., Lindstrom D. J., Fruchter J. S. and  
 1192 Goles G. G. (1975) Lunar polymict breccia 14321: a compositional study of its principal  
 1193 components. *Geochimica et Cosmochimica Acta* **39**, 247–260.
- 1194 Dymek R. F., Albee A. L. and Chodos A. A. (1975) Comparative petrology of lunar cumulate  
 1195 rocks of possible primary origin: dunitite 72415, troctolite 76535, norite 78235, and  
 1196 anorthosite 62237. In Lunar Science Conference VI. New York, Pergamon Press, Inc.,  
 1197 Houston, Texas. pp. 301–341.
- 1198 Edmunson J., Borg L. E., Nyquist L. E. and Asmerom Y. (2009) A combined Sm–Nd, Rb–Sr,  
 1199 and U–Pb isotopic study of Mg-suite norite 78238: Further evidence for early  
 1200 differentiation of the Moon. *Geochimica et Cosmochimica Acta* **73**, 514–527.

- 1201 Elardo S. M., Draper D. S. and Shearer C. K. (2011) Lunar Magma Ocean crystallization  
 1202 revisited: Bulk composition, early cumulate mineralogy, and the source regions of the  
 1203 highlands Mg-suite. *Geochimica et Cosmochimica Acta* **75**, 3024–3045.
- 1204 Elardo S. M., McCubbin F. M. and Shearer C. K. (2012) Chromite symplectites in Mg-suite  
 1205 troctolite 76535 as evidence for infiltration metasomatism of a lunar layered intrusion.  
 1206 *Geochimica et Cosmochimica Acta* **87**, 154–177.
- 1207 Elkins-Tanton L. T., Burgess S. and Yin Q.-Z. (2011) The lunar magma ocean: Reconciling the  
 1208 solidification process with lunar petrology and geochronology. *Earth and Planetary  
 1209 Science Letters* **304**, 326–336.
- 1210 Elkins-Tanton L. T., Van Orman J. A., Hager B. H. and Grove T. L. (2002) Re-examination of  
 1211 the lunar magma ocean cumulate overturn hypothesis: melting or mixing is required.  
 1212 *Earth and Planetary Science Letters* **196**, 239–249.
- 1213 Eugster O., Geiss J. and Grogler N. (1983) Dating of early regolith exposure and the evolution of  
 1214 trapped  $^{40}\text{Ar}/^{36}\text{Ar}$  with time. *14th Lunar and Planetary Science Conference*, 177–178.
- 1215 Eugster O., Groegler N., Eberhardt P. and Geiss J. (1980) Double drive tube 74001/2-  
 1216 Composition of noble gases trapped 3.7 AE ago. In In: Lunar and Planetary Science  
 1217 Conference, 11th, Houston, TX, March 17-21, 1980, Proceedings. Volume 2.(A82-22296  
 1218 09-91) New York, Pergamon Press, 1980, p. 1565-1592. Swiss National Science  
 1219 Foundation. pp. 1565–1592.
- 1220 Eugster O. and Polnau E. (1997) Further data for the calibration of the antiquity indicator Ar-  
 1221  $^{40}\text{Ar}/\text{Ar}-36$  for lunar soil. In Conference Paper, 28th Annual Lunar and Planetary Science  
 1222 Conference, p. 341. p. 341.
- 1223 Eugster O., Terribilini D., Polnau E. and Kramers J. (2001) The antiquity indicator argon-  
 1224  $^{40}\text{Ar}/\text{argon}-36$  for lunar surface samples calibrated by uranium-235-xenon-136 dating.  
 1225 *Meteoritics & Planetary Science* **36**, 1097–1115.
- 1226 Fagan A. L., Joy K. H., Bogard D. D. and Kring D. A. (2014) Ages of Globally Distributed  
 1227 Lunar Paleoregoliths and Soils from 3.9 Ga to the Present. *Earth Moon Planets* **112**, 59–  
 1228 71.
- 1229 Fairweather J. H., Lagain A., Servis K., Benedix G. K., Kumar S. S. and Bland P. A. (2022)  
 1230 Automatic Mapping of Small Lunar Impact Craters Using LRO-NAC Images. *Earth and  
 1231 Space Science* **9**.
- 1232 Fernandes V. A., Fritz J., Weiss B. P., Garrick-Bethell I. and Shuster D. L. (2013) The  
 1233 bombardment history of the Moon as recorded by  $^{40}\text{Ar}-^{39}\text{Ar}$  chronology. *Meteorit  
 1234 Planet Sci* **48**, 241–269.
- 1235 Gaffney A. M. and Borg L. E. (2014) A young solidification age for the lunar magma ocean.  
 1236 *Geochimica et Cosmochimica Acta* **140**, 227–240.

- 1237 Gagnepain-Beyneix J., Lognonné P., Chenet H., Lombardi D. and Spohn T. (2006) A seismic  
 1238 model of the lunar mantle and constraints on temperature and mineralogy. *Physics of the*  
 1239 *Earth and Planetary Interiors* **159**, 140–166.
- 1240 Ganapathy R., Morgan J., Higuchi H., Anders E. and Anderson Jr A. (1974) Meteoritic and  
 1241 volatile elements in Apollo 16 rocks and in separated phases from 14306 Lunar Science  
 1242 V. *The Lunar Science Institute. Part*, 257–259.
- 1243 Garrick-Bethell I., Miljković K., Hiesinger H., van der Bogert C. H., Laneuville M., Shuster D.  
 1244 L. and Korycansky D. G. (2020) Troctolite 76535: A sample of the Moon’s South Pole-  
 1245 Aitken basin? *Icarus* **338**, 113430.
- 1246 Garrick-Bethell I. and Zuber M. T. (2009) Elliptical structure of the lunar South Pole-Aitken  
 1247 basin. *Icarus* **204**, 399–408.
- 1248 Gawronska A. J., Barrett N., Boazman S. J., Gilmour C. M., Halim S. H., Harish, McCanaan K.,  
 1249 Satyakumar A. V., Shah J., Meyer H. M. and Kring D. A. (2020) Geologic context and  
 1250 potential EVA targets at the lunar south pole. *Advances in Space Research* **66**, 1247–  
 1251 1264.
- 1252 Gopalan K., Kaushal S., Lee-Hu C. and Wetherill G. (1970) Rb-Sr and U, Th-Pb ages of lunar  
 1253 materials. *Geochimica et Cosmochimica Acta Supplement* **2**, 1195–1205.
- 1254 Grieve R. A. F., Stöffler D. and Deutsch A. (1991) The Sudbury structure: Controversial or  
 1255 misunderstood? *J. Geophys. Res.* **96**, 22753.
- 1256 Grieve R. A., McKay G. A., Smith H. D. and Weill D. F. (1975) Lunar polymict breccia 14321:  
 1257 a petrographic study. *Geochimica et Cosmochimica Acta* **39**, 229–245.
- 1258 Gros J., Takahashi H., Hertogen J., Morgan J. W. and Anders E. (1976) Composition of the  
 1259 projectiles that bombarded the lunar highlands. In In: Lunar Science Conference, 7th,  
 1260 Houston, Tex., March 15-19, 1976, Proceedings. Volume 2.(A77-34651 15-91) New  
 1261 York, Pergamon Press, Inc., 1976, p. 2403-2425. pp. 2403–2425.
- 1262 Gross J., Hilton A., Prissel T. C., Setera J. B., Korotev R. L. and Calzada-Diaz A. (2020)  
 1263 Geochemistry and Petrogenesis of Northwest Africa 10401: A New Type of the Mg-Suite  
 1264 Rocks. *JGR Planets* **125**.
- 1265 Gross J., Treiman A. H. and Mercer C. N. (2014) Lunar feldspathic meteorites: Constraints on  
 1266 the geology of the lunar highlands, and the origin of the lunar crust. *Earth and Planetary*  
 1267 *Science Letters* **388**, 318–328.
- 1268 Halim S., Barrett N., Boazman S., Gawronska A., Gilmour C., Harish, McCanaan K.,  
 1269 Satyakumar A., Shah J. and Kring D. (2021) Numerical modeling of the formation of  
 1270 Shackleton crater at the lunar south pole. *Icarus* **354**, 113992.
- 1271 Hapke B. (1981) Bidirectional reflectance spectroscopy: 1. Theory. *J. Geophys. Res.* **86**, 3039–  
 1272 3054.

- 1273 Hapke B. (2001) Space weathering from Mercury to the asteroid belt. *J. Geophys. Res.* **106**,  
 1274 10039–10073.
- 1275 Haruyama J., Matsunaga T., Ohtake M., Morota T., Honda C., Yokota Y., Torii M., Ogawa Y.,  
 1276 and LISM Working Group (2008) Global lunar-surface mapping experiment using the  
 1277 Lunar Imager/Spectrometer on SELENE. *Earth, Planets and Space* **60**, 243–255.
- 1278 Haskin L. A. (1998) The Imbrium impact event and the thorium distribution at the lunar  
 1279 highlands surface. *J. Geophys. Res.* **103**, 1679–1689.
- 1280 Haskin L. A., Korotev R. L., Rockow K. M. and Jolliff B. L. (1998) The case for an Imbrium  
 1281 origin of the Apollo thorium-rich impact-melt breccias. *Meteoritics & Planetary Science*  
 1282 **33**, 959–975.
- 1283 Hawke B. R. (2003) Distribution and modes of occurrence of lunar anorthosite. *J. Geophys. Res.*  
 1284 **108**, 5050.
- 1285 Head J. W., Murchie S., Mustard J. F., Pieters C. M., Neukum G., McEwen A., Greeley R.,  
 1286 Nagel E. and Belton M. J. S. (1993) Lunar impact basins: New data for the western limb  
 1287 and far side (Orientale and South Pole-Aitken Basins) from the first Galileo flyby. *J.*  
 1288 *Geophys. Res.* **98**, 17149.
- 1289 Head J. W. and Wilson L. (1992) Lunar mare volcanism: Stratigraphy, eruption conditions, and  
 1290 the evolution of secondary crusts. *Geochimica et Cosmochimica Acta* **56**, 2155–2175.
- 1291 Hess P. C. (1994) Petrogenesis of lunar troctolites. *J. Geophys. Res.* **99**, 19083.
- 1292 Hess P. C. and Parmentier E. M. (1995) A model for the thermal and chemical evolution of the  
 1293 Moon's interior: implications for the onset of mare volcanism. *Earth and Planetary*  
 1294 *Science Letters* **134**, 501–514.
- 1295 Hiesinger H. (2006) New Views of Lunar Geoscience: An Introduction and Overview. *Reviews*  
 1296 *in Mineralogy and Geochemistry* **60**, 1–81.
- 1297 Hiesinger H., van der Bogert C. H., Pasckert J. H., Funcke L., Giacomini L., Ostrach L. R. and  
 1298 Robinson M. S. (2012) How old are young lunar craters? *Journal of Geophysical*  
 1299 *Research: Planets* **117**.
- 1300 Higuchi H. and Morgan J. W. (1975) Ancient meteoritic component in Apollo 17 boulders. In  
 1301 Lunar and Planetary Science Conference Proceedings. pp. 1625–1651.
- 1302 Horz F., Grieve R., Heiken G., Spudis P. and Binder A. (1991) Chapter 4: Lunar Surface  
 1303 Processes. In *The Lunar Sourcebook* Cambridge University Press/Lunar and Planetary  
 1304 Institute. pp. 61–120.
- 1305 Howard K. A., Wilhelms D. E. and Scott D. H. (1974) Lunar basin formation and highland  
 1306 stratigraphy. *Rev. Geophys.* **12**, 309.

- 1307 Huang (黄俊) J., Xiao (肖智勇) Z., Xiao (肖龙) L., Horgan B., Hu (胡晓依) X., Lucey P., Xiao  
 1308 (肖潇) X., Zhao (赵思源) S., Qian (钱煜奇) Y., Zhang (张昊) H., Li (李春来) C., Xu (徐  
 1309 睿) R., He (何志平) Z., Yang (杨建峰) J., Xue (薛彬) B., He (何琦) Q., Zhong (钟杰) J.,  
 1310 Lin (林宏宇) H., Huang (黄长宁) C. and Xie (谢剑锋) J. (2020) Diverse rock types  
 1311 detected in the lunar South Pole–Aitken Basin by the Chang’E-4 lunar mission. *Geology*  
 1312 **48**, 723–727.
- 1313 Hui H., Neal C. R., Shih C.-Y. and Nyquist L. E. (2013) Petrogenetic association of the oldest  
 1314 lunar basalts: Combined Rb–Sr isotopic and trace element constraints. *Earth and*  
 1315 *Planetary Science Letters* **373**, 150–159.
- 1316 Hult M., Vidmar T., Rosengård U., Marissens G., Lutter G. and Sahin N. (2014) Half-life  
 1317 measurements of lutetium-176 using underground HPGe-detectors. *Applied Radiation*  
 1318 *and Isotopes* **87**, 112–117.
- 1319 Huneke J. C. (1978) 40Ar-39Ar Microanalysis of single 74220 glass balls and 72435 breccia  
 1320 clasts. *Proceedings of the Lunar and Planetary Science Conference* **9**, 2345–2362.
- 1321 Hurley P. and Pinson, Jr. W. (1970) Whole-rock Rb-Sr isotopic age relationships in Apollo 11  
 1322 lunar samples. *Geochimica et Cosmochimica Acta Supplement* **2**, 1195–1205.
- 1323 Hurwitz D. M. and Kring D. A. (2014) Differentiation of the South Pole–Aitken basin impact  
 1324 melt sheet: Implications for lunar exploration. *J. Geophys. Res. Planets* **119**, 1110–1133.
- 1325 Ibanez-Mejia M., Gehrels G. E., Ruiz J., Vervoort J. D., Eddy M. P. and Li C. (2014) Small-  
 1326 volume baddeleyite (ZrO<sub>2</sub>) U–Pb geochronology and Lu–Hf isotope geochemistry by  
 1327 LA-ICP-MS. Techniques and applications. *Chemical Geology* **384**, 149–167.
- 1328 Jaffey A. H., Flynn K. F., Glendenin L. E., Bentley W. C. and Essling A. M. (1971) Precision  
 1329 Measurement of Half-Lives and Specific Activities of U 235 and U 238. *Phys. Rev. C* **4**,  
 1330 1889–1906.
- 1331 James O. (1996) Siderophile elements in lunar impact melts define nature of the impactors. In  
 1332 *Lunar and Planetary Science*, volume 27, page 603.
- 1333 James O. B. (2002) Distinctive Meteoritic Components in Lunar ‘‘Cataclysm’’ Impact-Melt  
 1334 Breccias. In *Lunar and Planetary Science Conference*. p. 1210.
- 1335 Johnston S., Brandon A., McLeod C., Rankenburg K., Becker H. and Copeland P. (2022) Nd  
 1336 isotope variation between the Earth–Moon system and enstatite chondrites. *Nature* **611**,  
 1337 501–506.
- 1338 Jolliff B. L., Gillis J. J., Haskin L. A., Korotev R. L. and Wieczorek M. A. (2000) Major lunar  
 1339 crustal terranes: Surface expressions and crust-mantle origins. *J. Geophys. Res.* **105**,  
 1340 4197–4216.

- 1341 Jolliff B. L., Korotev R. L. and Haskin L. A. (1993) An iridium-rich iron micrometeorite with  
 1342 silicate inclusions from the Moon. In Lunar and Planetary Inst., Twenty-Fourth Lunar  
 1343 and Planetary Science Conference. Part 2: GM.
- 1344 Jourdan F. (2012) The  $^{40}\text{Ar}/^{39}\text{Ar}$  dating technique applied to planetary sciences and terrestrial  
 1345 impacts. *Australian Journal of Earth Sciences* **59**, 199–224.
- 1346 Joy K. H., Crawford I. A., Anand M., Greenwood R. C., Franchi I. A. and Russell S. S. (2008)  
 1347 The petrology and geochemistry of Miller Range 05035: A new lunar gabbroic meteorite.  
 1348 *Geochimica et Cosmochimica Acta* **72**, 3822–3844.
- 1349 Joy K. H., Crawford I. A., Curran N. M., Zolensky M., Fagan A. F. and Kring D. A. (2016) The  
 1350 Moon: An Archive of Small Body Migration in the Solar System. *Earth Moon Planets*  
 1351 **118**, 133–158.
- 1352 Joy K. H., Kring D. A., Bogard D. D., McKay D. S. and Zolensky M. E. (2011) Re-examination  
 1353 of the formation ages of the Apollo 16 regolith breccias. *Geochimica et Cosmochimica*  
 1354 *Acta* **75**, 7208–7225.
- 1355 Joy K. H., Tartèse R., Messenger S., Zolensky M. E., Marrocchi Y., Frank D. R. and Kring D. A.  
 1356 (2020) The isotopic composition of volatiles in the unique Bench Crater carbonaceous  
 1357 chondrite impactor found in the Apollo 12 regolith. *Earth and Planetary Science Letters*  
 1358 **540**, 116265.
- 1359 Kenkmann T. and Artemieva N. (2021) The terrestrial impact crater record: A statistical analysis  
 1360 of morphologies, structures, ages, lithologies, and more. *Meteorit Planet Sci* **56**, 1024–  
 1361 1070.
- 1362 Kereszturi A., Tomka R., Gläser P. A., Pal B. D., Steinmann V. and Warren T. (2022)  
 1363 Characteristics of de Gerlache crater, site of girdlands and slope exposed ice in a lunar  
 1364 polar depression. *Icarus* **388**, 115231.
- 1365 Kettrup B., Deutsch A. and Masaitis V. L. (2003) Homogeneous impact melts produced by a  
 1366 heterogeneous target? *Geochimica et Cosmochimica Acta* **67**, 733–750.
- 1367 Korotev R. L., Gillis J. J., Haskin L. A. and Jolliff B. L. (2002) On the Age of the Nectaris  
 1368 Basin. In *The Moon Beyond 2002: Next Steps in Lunar Science and Exploration*. p. 31.
- 1369 Kraetli G., Schmidt M. W. and Liebske C. (2022) Fractional crystallization of a basal lunar  
 1370 magma ocean: A dense melt-bearing garnetite layer above the core? *Icarus* **371**, 114699.
- 1371 Kramer G. Y., Kring D. A., Nahm A. L. and Pieters C. M. (2013) Spectral and photogeologic  
 1372 mapping of Schrödinger Basin and implications for post-South Pole-Aitken impact deep  
 1373 subsurface stratigraphy. *Icarus* **223**, 131–148.
- 1374 Krasilnikov S. S., Ivanov M. A., Head J. W. and Krasilnikov A. S. (2023) Geologic history of  
 1375 the south circumpolar region (SCR) of the Moon. *Icarus* **394**, 115422.

- 1376 Kring D. A. (2008) Deciphering the Chronology and Implications of Impact Cratering on the  
 1377 Moon: A High Science Priority for Lunar Exploration. In *Lunar and Planetary Science*  
 1378 XXXIX. The Woodlands, TX.
- 1379 Kring D. A. (2006) Exploring Lunar Impact Craters and Their Implications for the Origin and  
 1380 Early Evolution of Life on Earth.
- 1381 Kring D. A. (2005) Hypervelocity collisions into continental crust composed of sediments and an  
 1382 underlying crystalline basement: comparing the Ries (~24 km) and Chicxulub (~180  
 1383 km) impact craters. *Geochemistry* **65**, 1–46.
- 1384 Kring D. A. (2019) Lunar South Pole Geology: Preparing for a Seventh Lunar Landing. In  
 1385 NASA Exploration Science Forum.
- 1386 Kring D. A. (2009) Targeting Complex Craters and Multi-Ring Basins to Determine the Tempo  
 1387 of Impact Bombardment while Simultaneously Probing the Lunar Interior. In *Lunar*  
 1388 *Reconnaissance Orbiter Science Targeting Meeting*.
- 1389 Kring D. A. (2007) Using the Moon to Determine the Magnitude of the Inner Solar System  
 1390 Cataclysm and Post-Cataclysm Impact Flux. In *NAC Lunar Meeting*.
- 1391 Kring D. A., Bickel V. T., Van Der Bogert C. H., Fagan A. L., Gaddis L. R., Hiesinger H.,  
 1392 Hurtado J. M., Joy K. H., Lemelin M., Looper C. A., Osinski G. R., Pösges G., Siegler  
 1393 M., Tikoo S. M. and Zacny K. (2023) Elevation Changes and Slope that May Affect EVA  
 1394 Workload Near Potential Artemis Landing Sites. In *2023 IEEE Aerospace Conference*  
 1395 *2023 IEEE Aerospace Conference*. IEEE, Big Sky, MT, USA. pp. 1–17.
- 1396 Kring D. A., Claeys P., Gulick S. P. S., Morgan J. V. and Collins G. S. (2017) Chicxulub and the  
 1397 Exploration of Large Peak-Ring Impact Craters through Scientific Drilling. *GSAT*, 4–8.
- 1398 Kring D. A. and Cohen B. A. (2002) Cataclysmic bombardment throughout the inner solar  
 1399 system 3.9–4.0 Ga. *J. Geophys. Res.* **107**.
- 1400 Kring D. A., Gruener J. E. and Eppler D. B. (2020) Artemis III EVA Opportunities on Malapert  
 1401 and Leibnitz B Massifs. *Science Definition Team for Artemis*.
- 1402 Kring D. A., Kramer G. Y., Bussey D. B. J., Hurley D. M., Stickle A. M. and van der Bogert C.  
 1403 H. (2021) Prominent volcanic source of volatiles in the south polar region of the Moon.  
 1404 *Advances in Space Research* **68**, 4691–4701.
- 1405 Kring D. A., Kramer G. Y., Collins G. S., Potter R. W. K. and Chandnani M. (2016) Peak-ring  
 1406 structure and kinematics from a multi-disciplinary study of the Schrödinger impact basin.  
 1407 *Nat Commun* **7**, 13161.
- 1408 Kring D. A., Lemelin M., van der Bogert C. H., Bickel V., Hiesinger H., Hurtado J. M., Petro N.,  
 1409 Siegler M. A., Looper C. A., Huning T., Osinski G. R. and Gaddis L. (2022) Geological  
 1410 EVA Science along a South Pole-Aitken (SPA) Basin Massif Ridge Cross-Cut by  
 1411 Shackleton Crater. In *Lunar and Planetary Science LIII*. The Woodlands, Texas.

- 1412 Kring D. A., Swindle T. D., Strom R. G., Ito T. and Yoshida F. (2005) Exploring Impact  
 1413 Cratering on the Moon and its Implications for the Biologic Evolution of, and Habitable  
 1414 Conditions on, the Earth. In *Space Resources Roundtable VII*. Golden, Colorado.
- 1415 Kruijjer T. S. and Kleine T. (2017) Tungsten isotopes and the origin of the Moon. *Earth and*  
 1416 *Planetary Science Letters* **475**, 15–24.
- 1417 Kumari N., Bretzfelder J. M., Ganesh I., Lang A. and Kring D. A. (2022) Surface Conditions and  
 1418 Resource Accessibility at Potential Artemis Landing Sites 007 and 011. *Planet. Sci. J.* **3**,  
 1419 224.
- 1420 Lagain A., Kreslavsky M., Baratoux D., Liu Y., Devillepoix H., Bland P., Benedix G. K., Doucet  
 1421 L. S. and Servis K. (2022) Has the impact flux of small and large asteroids varied through  
 1422 time on Mars, the Earth and the Moon? *Earth and Planetary Science Letters* **579**,  
 1423 117362.
- 1424 Lally J. S., Christie J. M., Nord Jr. G. L. and Heuer A. H. (1976) Deformation, recovery and  
 1425 recrystallization of lunar dunite 72417. In *Lunar and Planetary Science VII* New York,  
 1426 Pergamon Press, Inc., Houston, Texas. pp. 1845–1863.
- 1427 Lapen T. J., Richter M., Brandon A. D., Debaille V., Beard B. L., Shafer J. T. and Peslier A. H.  
 1428 (2010) A Younger Age for ALH84001 and Its Geochemical Link to Shergottite Sources  
 1429 in Mars. *Science* **328**, 347–351.
- 1430 Le Feuvre M. and Wieczorek M. A. (2011) Nonuniform cratering of the Moon and a revised  
 1431 crater chronology of the inner Solar System. *Icarus* **214**, 1–20.
- 1432 Lemelin M., Lucey P. G. and Camon A. (2022) Compositional Maps of the Lunar Polar Regions  
 1433 Derived from the Kaguya Spectral Profiler and the Lunar Orbiter Laser Altimeter Data.  
 1434 *Planet. Sci. J.* **3**, 63.
- 1435 Lemelin M., Lucey P. G., Crites S. T. and Jha K. (2017) Mineralogy and Iron Content of the  
 1436 Lunar Polar Regions using the Kaguya Spectral Profiler and the Lunar Orbiter Laser  
 1437 Altimeter. In *New Views of the Moon 2 Europe*.
- 1438 Lemelin M., Lucey P. G., Miljković K., Gaddis L. R., Hare T. and Ohtake M. (2019) The  
 1439 compositions of the lunar crust and upper mantle: Spectral analysis of the inner rings of  
 1440 lunar impact basins. *Planetary and Space Science* **165**, 230–243.
- 1441 Lemelin M., Lucey P. G., Song E. and Taylor G. J. (2015) Lunar central peak mineralogy and  
 1442 iron content using the Kaguya Multiband Imager: Reassessment of the compositional  
 1443 structure of the lunar crust: LUNAR CENTRAL PEAK MINERALOGY AND IRON. *J.*  
 1444 *Geophys. Res. Planets* **120**, 869–887.
- 1445 Levinson A. A. (1970) Proceedings of the Apollo 11 Lunar Science Conference (issued as  
 1446 *Geochimica et Cosmochimica Acta*, supplement no. 1, vol. 34, 1970). *Geochimica et*  
 1447 *Cosmochimica Acta* **34**, 1367–1372.

- 1448 Li Q.-L., Zhou Q., Liu Y., Xiao Z., Lin Y., Li J.-H., Ma H.-X., Tang G.-Q., Guo S., Tang X.,  
 1449 Yuan J.-Y., Li J., Wu F.-Y., Ouyang Z., Li C. and Li X.-H. (2021) Two-billion-year-old  
 1450 volcanism on the Moon from Chang'e-5 basalts. *Nature* **600**, 54–58.
- 1451 Li S. and Milliken R. E. (2017) Water on the surface of the Moon as seen by the Moon  
 1452 Mineralogy Mapper: Distribution, abundance, and origins. *Sci. Adv.* **3**, e1701471.
- 1453 Lin Honglei, He Z., Yang W., Lin Y., Xu R., Zhang C., Zhu M.-H., Chang R., Zhang J., Li C.,  
 1454 Lin Hongyu, Liu Y., Gou S., Wei Y., Hu S., Xue C., Yang J., Zhong J., Fu X., Wan W.  
 1455 and Zou Y. (2020) Olivine-norite rock detected by the lunar rover Yutu-2 likely  
 1456 crystallized from the SPA impact melt pool. *National Science Review* **7**, 913–920.
- 1457 Lock S. J., Stewart S. T., Petaev M. I., Leinhardt Z., Mace M. T., Jacobsen S. B. and Cuk M.  
 1458 (2018) The Origin of the Moon Within a Terrestrial Synestia. *J. Geophys. Res. Planets*  
 1459 **123**, 910–951.
- 1460 Lovering J. F., Wark D. A., Gleadow A. J. W. and Britten R. (1974) Lunar monazite: A late-  
 1461 stage (mesostasis) phase in mare basalt. *Earth and Planetary Science Letters* **21**, 164–  
 1462 168.
- 1463 Lucey P. G., Taylor G. J., Hawke B. R. and Spudis P. D. (1998) FeO and TiO<sub>2</sub> concentrations in  
 1464 the South Pole-Aitken basin: Implications for mantle composition and basin formation. *J.*  
 1465 *Geophys. Res.* **103**, 3701–3708.
- 1466 Lucey P., Korotev R., Gillis J., Taylor L., Lawrence D., Campbell B., Elphic R., Feldman B.,  
 1467 Hood L., Hunten D., Mendillo M., Noble S., Papike J., Reedy R., Lawson S., Prettyman  
 1468 T., Gasnault O. and Maurice S. (2006) Understanding the Lunar Surface and Space-Moon  
 1469 Interactions. In *Reviews in Mineralogy and Geochemistry* Mineralogical Society of  
 1470 America. pp. 83–219.
- 1471 Marks N. E., Borg L. E., Shearer C. K. and Cassata W. S. (2019) Geochronology of an Apollo 16  
 1472 Clast Provides Evidence for a Basin-Forming Impact 4.3 Billion Years Ago. *JGR Planets*  
 1473 **124**, 2465–2481.
- 1474 Mazarico E., Neumann G. A., Smith D. E., Zuber M. T. and Torrence M. H. (2011) Illumination  
 1475 conditions of the lunar polar regions using LOLA topography. *Icarus* **211**, 1066–1081.
- 1476 Mazrouei S., Ghent R. R., Bottke W. F., Parker A. H. and Gernon T. M. (2019) Earth and Moon  
 1477 impact flux increased at the end of the Paleozoic. *Science* **363**, 253–257.
- 1478 McCallum I. S., Domeneghetti M. C., Schwartz J. M., Mullen E. K., Zema M., Cámara F.,  
 1479 McCammon C. and Ganguly J. (2006) Cooling history of lunar Mg-suite gabbro-norite  
 1480 76255, troctolite 76535 and Stillwater pyroxenite SC-936: The record in exsolution and  
 1481 ordering in pyroxenes. *Geochimica et Cosmochimica Acta* **70**, 6068–6078.
- 1482 McCubbin F. M. and Barnes J. J. (2020) The chlorine-isotopic composition of lunar KREEP  
 1483 from magnesian-suite troctolite 76535. *American Mineralogist* **105**, 1270–1274.

- 1484 McDougall I., Harrison T. M., McDougall P. of G. I. and Harrison P. of G. D. of E. and S. S. T.  
 1485 M. (1999) *Geochronology and Thermochronology by the  $^{40}\text{Ar}/^{39}\text{Ar}$  Method.*, Oxford  
 1486 University Press.
- 1487 McKay D. S., Bogard D. D., Morris R. V., Korotev R. L., Johnson P. and Wentworth S. J. (1986)  
 1488 Apollo 16 regolith breccias: Characterization and evidence for early formation in the  
 1489 mega-regolith. *J. Geophys. Res.* **91**, 277–303.
- 1490 McKay D. S., Heiken G., Basu A., Blanford G., Simon S., Reedy R., French B. M. and Papike J.  
 1491 (1991) Chapter 7: The Lunar Regolith. In *The Lunar Sourcebook* Cambridge University  
 1492 Press/Lunar and Planetary Institute. pp. 285–356.
- 1493 McLeod C. L., Brandon A. D. and Armytage R. M. G. (2014) Constraints on the formation age  
 1494 and evolution of the Moon from  $^{142}\text{Nd}$ – $^{143}\text{Nd}$  systematics of Apollo 12 basalts. *Earth*  
 1495 *and Planetary Science Letters* **396**, 179–189.
- 1496 McLeod C. L., Brandon A. D., Fernandes V. A., Peslier A. H., Fritz J., Lapen T., Shafer J. T.,  
 1497 Butcher A. R. and Irving A. J. (2016) Constraints on formation and evolution of the lunar  
 1498 crust from feldspathic granulitic breccias NWA 3163 and 4881. *Geochimica et*  
 1499 *Cosmochimica Acta* **187**, 350–374.
- 1500 McSween Jr H. Y. (1976) A new type of chondritic meteorite found in lunar soil. *Earth and*  
 1501 *Planetary Science Letters* **31**, 193–199.
- 1502 Mercer C. M. and Hodges K. V. (2016) ArAR — A software tool to promote the robust  
 1503 comparison of K–Ar and  $^{40}\text{Ar}/^{39}\text{Ar}$  dates published using different decay, isotopic, and  
 1504 monitor-age parameters. *Chemical Geology* **440**, 148–163.
- 1505 Mercer C. M., Hodges K. V., Jolliff B. L., Van Soest M. C., Wartho J. and Weirich J. R. (2019)  
 1506 Exploring the variability of argon loss in Apollo 17 impact melt rock 77135 using high-  
 1507 spatial resolution  $^{40}\text{Ar}/^{39}\text{Ar}$  geochronology. *Meteorit & Planetary Sci* **54**, 721–739.
- 1508 Mercer C. M., Young K. E., Weirich J. R., Hodges K. V., Jolliff B. L., Wartho J.-A. and Van  
 1509 Soest M. C. (2015) Refining lunar impact chronology through high spatial resolution  $^{40}$   
 1510  $\text{Ar}/^{39}\text{Ar}$  dating of impact melts. *Sci. Adv.* **1**, e1400050.
- 1511 Merle R. E., Nemchin A. A., Grange M. L., Whitehouse M. J. and Pidgeon R. T. (2014) High  
 1512 resolution U-Pb ages of Ca-phosphates in Apollo 14 breccias: Implications for the age of  
 1513 the Imbrium impact. *Meteorit Planet Sci* **49**, 2241–2251.
- 1514 Meyer H. M., Denevi B. W., Boyd A. K. and Robinson M. S. (2016) The distribution and origin  
 1515 of lunar light plains around Orientale basin. *Icarus* **273**, 135–145.
- 1516 Michaut C. and Pinel V. (2018) Magma Ascent and Eruption Triggered by Cratering on the  
 1517 Moon: MAGMA ASCENT BELOW IMPACT CRATERS. *Geophys. Res. Lett.* **45**,  
 1518 6408–6416.

- 1519 Miljković K., Wieczorek M. A., Laneuville M., Nemchin A., Bland P. A. and Zuber M. T.  
 1520 (2021) Large impact cratering during lunar magma ocean solidification. *Nat Commun* **12**,  
 1521 5433.
- 1522 Moore H. J., Hodges C. A. and Scott D. H. (1974) Multiringed basins- illustrated by Orientale  
 1523 and associated features. In *Proceedings of the Lunar and Planetary Science, V*  
 1524 Supplement 5, *Geochimica et Cosmochimica Acta*. Pergamon Press Inc., Houston, Texas.  
 1525 pp. 71–100.
- 1526 Morbidelli A., Marchi S., Bottke W. F. and Kring D. A. (2012) A sawtooth-like timeline for the  
 1527 first billion years of lunar bombardment. *Earth and Planetary Science Letters* **355–356**,  
 1528 144–151.
- 1529 Morgan J. W., Krahenbuhl U., Ganapathy R. and Anders E. (1972a) Trace elements in Apollo 15  
 1530 samples: implications for meteorite influx and volatile depletion on the moon.  
 1531 *Proceedings of the Third Lunar Science Conference* **2**, 1361–1376.
- 1532 Morgan J. W., Laul J. C., Krahenbuhl U., Ganapathy R. and Anders E. (1972b) Major impacts on  
 1533 the Moon: characterization from trace elements in Apollo 12 and 14 samples. *Proceedings*  
 1534 *of the Third Lunar Science Conference* **3**, 1377.
- 1535 Moriarty Daniel P., Dygert N., Valencia S. N., Watkins R. N. and Petro N. E. (2021) The search  
 1536 for lunar mantle rocks exposed on the surface of the Moon. *Nat Commun* **12**, 4659.
- 1537 Moriarty D. P. and Pieters C. M. (2018) The Character of South Pole-Aitken Basin: Patterns of  
 1538 Surface and Subsurface Composition. *J. Geophys. Res. Planets* **123**, 729–747.
- 1539 Moriarty D. P., Watkins R. N., Valencia S. N., Kendall J. D., Evans A. J., Dygert N. and Petro N.  
 1540 E. (2021) Evidence for a Stratified Upper Mantle Preserved Within the South Pole-  
 1541 Aitken Basin. *J Geophys Res Planets* **126**.
- 1542 Mukhametshin Ch. R., Semenov A. and Shpekin M. (2018) Experience of modeling relief of  
 1543 impact lunar crater Aitken based on high-resolution orbital images. *Journal of Physics:*  
 1544 *Conference Series* **1015**.
- 1545 Müller W. F. and Hornemann U. (1969) Shock-induced planar deformation structures in  
 1546 experimentally shock-loaded olivines and in olivines from chondritic meteorites. *Earth*  
 1547 *and Planetary Science Letters* **7**, 251–264.
- 1548 Nagaoka H., Takeda H., Karouji Y., Ohtake M., Yamaguchi A., Yoneda S. and Hasebe N.  
 1549 (2014) Implications for the origins of pure anorthosites found in the feldspathic lunar  
 1550 meteorites, Dhofar 489 group. *Earth, Planets and Space* **66**, 115.
- 1551 Nagurney A. B., Treiman A. H. and Spudis P. D. (2016) Petrology, Bulk Composition, and  
 1552 Provenance of Meteorite Northwest Africa 5000 (NWA 5000). In 47th Lunar and  
 1553 Planetary Science Conference. The Woodlands, TX.

- 1554 Nakamura R., Matsunaga T., Ogawa Y., Yamamoto S., Hiroi T., Saiki K., Hirata N., Arai T.,  
 1555 Kitazato K., Takeda H., Sugihara T., Kodama S., Ohtake M., Haruyama J. and Yokota Y.  
 1556 (2009) Ultramafic impact melt sheet beneath the South Pole–Aitken basin on the Moon.  
 1557 *Geophys. Res. Lett.* **36**, L22202.
- 1558 NASA (2022) NASA Identifies Candidate Regions for Landing Next Americans on Moon.  
 1559 *NASA*.
- 1560 NASA (2021) NASA Prompts Companies for Artemis Lunar Terrain Vehicle Solutions. *Press*  
 1561 *Release*.
- 1562 NASA (2023) NASA Pursues Lunar Terrain Vehicle Services for Artemis Missions. *Press*  
 1563 *Release*.
- 1564 NASA (2020a) NASA’s lunar exploration program overview. *NASA’s lunar exploration*  
 1565 *program overview*.
- 1566 NASA (2020b) *NASA’s Plan for Sustained Lunar Exploration and Development.*, National  
 1567 Aeronautics and Space Administration.
- 1568 Nelson W. S., Hammer J. E., Shea T., Hellebrand E. and Jeffrey Taylor G. (2021) Chemical  
 1569 heterogeneities reveal early rapid cooling of Apollo Troctolite 76535. *Nat Commun* **12**,  
 1570 7054.
- 1571 Nemchin A., Timms N., Pidgeon R., Geisler T., Reddy S. and Meyer C. (2009) Timing of  
 1572 crystallization of the lunar magma ocean constrained by the oldest zircon. *Nature Geosci*  
 1573 **2**, 133–136.
- 1574 Neukum G. (1984) *Meteorite bombardment and dating of planetary surfaces, Translation of:*  
 1575 *Meteoritenbombardement und Datierung planetarer Oberflächen, Tenure Thesis,*  
 1576 *Ludwig-Maximilians University, Munich, Germany.*, NASA, NASA Headquarters  
 1577 Washington, DC United States.
- 1578 Neukum G., Ivanov B. A. and Hartmann W. K. (2001) Cratering Records in the Inner Solar  
 1579 System in Relation to the Lunar Reference System. In *Chronology and Evolution of Mars*  
 1580 (eds. R. Kallenbach, J. Geiss, and William K. Hartmann). Space Sciences Series of ISSI.  
 1581 Springer Netherlands, Dordrecht. pp. 55–86.
- 1582 Neukum G., König B. and Arkani-Hamed J. (1975) A study of lunar impact crater size-  
 1583 distributions. *The Moon* **12**, 201–229.
- 1584 Niihara T., Beard S. P., Swindle T. D., Schaffer L. A., Miyamoto H. and Kring D. A. (2019)  
 1585 Evidence for multiple 4.0–3.7 Ga impact events within the Apollo 16 collection. *Meteorit*  
 1586 *Planet Sci* **54**, 675–698.
- 1587 Niihara T., Kaiden H., Misawa K. and Sekine T. (2009) U-Pb Isotopic Systematics of  
 1588 Experimentally Shocked Baddeleyite. In id. 1562. 40th Lunar and Planetary Science  
 1589 Conference. Lunar and Planetary Institute, The Woodlands, Texas.

- 1590 Norman M. D., Bennett V. C. and Ryder G. (2002) Targeting the impactors: siderophile element  
 1591 signatures of lunar impact melts from Serenitatis. *Earth and Planetary Science Letters*  
 1592 **202**, 217–228.
- 1593 Norman M. D., Borg L. E., Nyquist L. E. and Bogard D. D. (2003) Chronology, geochemistry,  
 1594 and petrology of a ferroan noritic anorthosite clast from Descartes breccia 67215: Clues  
 1595 to the age, origin, structure, and impact history of the lunar crust. *Meteoritics &*  
 1596 *Planetary Science* **38**, 645–661.
- 1597 Norman M. D., Duncan R. A. and Huard J. J. (2006) Identifying impact events within the lunar  
 1598 cataclysm from  $40\text{Ar}$ – $39\text{Ar}$  ages and compositions of Apollo 16 impact melt rocks.  
 1599 *Geochimica et Cosmochimica Acta* **70**, 6032–6049.
- 1600 Norman M. D., Jourdan F. and Hui S. S. M. (2019) Impact History and Regolith Evolution on  
 1601 the Moon: Geochemistry and Ages of Glasses from the Apollo 16 Site. *JGR Planets* **124**,  
 1602 3167–3180.
- 1603 NRC (2007) *The Scientific Context for Exploration of the Moon.*,
- 1604 Nyquist L., Bogard D., Yamaguchi A., Shih C.-Y., Karouji Y., Ebihara M., Reese Y., Garrison  
 1605 D., McKay G. and Takeda H. (2006) Feldspathic clasts in Yamato-86032: Remnants of  
 1606 the lunar crust with implications for its formation and impact history. *Geochimica et*  
 1607 *Cosmochimica Acta* **70**, 5990–6015.
- 1608 Nyquist L. E., Bogard D. D., Shih C.-Y., Greshake A., Stöffler D. and Eugster O. (2001) Ages  
 1609 and Geologic Histories of Martian Meteorites. In *Chronology and Evolution of Mars*  
 1610 (eds. R. Kallenbach, J. Geiss, and W. K. Hartmann). Space Sciences Series of ISSI.  
 1611 Springer Netherlands, Dordrecht. pp. 105–164.
- 1612 Nyquist L. E. and Shih C. Y. (1992) The isotopic record of lunar volcanism. *Geochimica et*  
 1613 *Cosmochimica Acta* **56**, 2213–2234.
- 1614 Nyquist L. E., Wiesmann H., Bansal B., Shih C.-Y., Keith J. E. and Harper C. L. (1995)  $146\text{Sm}$ -  
 1615  $142\text{Nd}$  formation interval for the lunar mantle. *Geochimica et Cosmochimica Acta* **59**,  
 1616 2817–2837.
- 1617 Ohtake M., Matsunaga T., Haruyama J., Yokota Y., Morota T., Honda C., Ogawa Y., Torii M.,  
 1618 Miyamoto H., Arai T., Hirata N., Iwasaki A., Nakamura R., Hiroi T., Sugihara T., Takeda  
 1619 H., Otake H., Pieters C. M., Saiki K., Kitazato K., Abe M., Asada N., Demura H.,  
 1620 Yamaguchi Y., Sasaki S., Kodama S., Terazono J., Shirao M., Yamaji A., Minami S.,  
 1621 Akiyama H. and Josset J.-L. (2009) The global distribution of pure anorthosite on the  
 1622 Moon. *Nature* **461**, 236–240.
- 1623 Ostertag R. (1983) Shock experiments on feldspar crystals. *J. Geophys. Res.* **88**, B364.
- 1624 Papanastassiou D. A., Wasserburg G. J. and Burnett D. S. (1970) Rb-Sr ages of lunar rocks from  
 1625 the sea of tranquillity. *Earth and Planetary Science Letters* **8**, 1–19.

- 1626 Papike J. J., Burger P. V., Bell A. S. and Shearer C. K. (2018) Mn-Fe Systematics in Martian  
 1627 Olivine: Effect of Mantle Source, Oxygen Fugacity, and Temperature of Crystallization.  
 1628 In *Lunar and Planetary Science XLIX*. The Woodlands, Texas.
- 1629 Papike J., Ryder G. and Shearer C. (2006) Lunar Samples. In *Planetary Materials Reviews in*  
 1630 *Mineralogy*. Mineralogical Society of America. pp. 5–103 to 5–161.
- 1631 Patchett P. J. and Tatsumoto M. (1981) A routine high-precision method for Lu-Hf isotope  
 1632 geochemistry and chronology. *Contr. Mineral. and Petrol.* **75**, 263–267.
- 1633 Patchett P. J. and Tatsumoto M. (1980) Lu–Hf total-rock isochron for the eucrite meteorites.  
 1634 *Nature* **288**, 571–574.
- 1635 Patterson R. V., Frizzell K. R., Kodikara G. R. L., Kopp M., Luchsinger K. M., Madera A.,  
 1636 Meier M. L., Paladino T. G., Tai Udovicic C. J., Wroblewski F. B. and Kring D. A.  
 1637 (2022) In situ resource utilization investigations of potential Artemis landing site 105,  
 1638 lunar south pole. In *Lunar and Planetary Science LIII*. The Woodlands, Texas.
- 1639 Petro N. E. and Pieters C. M. (2008) The lunar-wide effects of basin ejecta distribution on the  
 1640 early megaregolith. *Meteoritics & Planetary Science* **43**, 1517–1529.
- 1641 Phinney W. (2015) *Science Training History of the Apollo Astronauts.*, NASA.
- 1642 Pieters C. M., Head J. W., Gaddis L., Jolliff B. and Duke M. (2001) Rock types of South Pole-  
 1643 Aitken basin and extent of basaltic volcanism. *J. Geophys. Res.* **106**, 28001–28022.
- 1644 Pieters C. M., Staid M. I., Fischer E. M., Tompkins S. and He G. (1994) A Sharper View of  
 1645 Impact Craters from Clementine Data. *Science* **266**, 1844–1848.
- 1646 Potter R. W. K., Collins G. S., Kiefer W. S., McGovern P. J. and Kring D. A. (2012)  
 1647 Constraining the size of the South Pole-Aitken basin impact. *Icarus* **220**, 730–743.
- 1648 Prissel T. C. and Prissel K. B. (2021) A lunar sample renaissance. *Nat Commun* **12**, 7053.
- 1649 Puchtel I. S., Walker R. J., James O. B. and Kring D. A. (2008) Osmium isotope and highly  
 1650 siderophile element systematics of lunar impact melt breccias: implications for the late  
 1651 accretion history of the Moon and Earth. *Geochimica et Cosmochimica Acta* **72**, 3022–  
 1652 3042.
- 1653 Rankenburg K., Brandon A. D. and Norman M. D. (2007) A Rb–Sr and Sm–Nd isotope  
 1654 geochronology and trace element study of lunar meteorite LaPaz Icefield 02205.  
 1655 *Geochimica et Cosmochimica Acta* **71**, 2120–2135.
- 1656 Rankenburg K., Brandon A. and Neal C. (2006) Constraints on the formation of the Moon from  
 1657 high-precision and Nd-isotopic measurements of lunar basalts. In *Lunar and Planetary*  
 1658 *Science Conference*. Lunar and Planetary Institute, The Woodlands, Texas.

- 1659 Rapp J. F. and Draper D. S. (2018) Fractional crystallization of the lunar magma ocean:  
 1660 Updating the dominant paradigm. *Meteorit & Planetary Scienc* **53**, 1432–1455.
- 1661 Rasmussen B., Fletcher I. R. and Muhling J. R. (2008) Pb/Pb geochronology, petrography and  
 1662 chemistry of Zr-rich accessory minerals (zirconolite, tranquillityite and baddeleyite) in  
 1663 mare basalt 10047. *Geochimica et Cosmochimica Acta* **72**, 5799–5818.
- 1664 Reimold W. U. and Stöffler D. (1978) Experimental shock metamorphism of dunite. In Lunar  
 1665 and Planetary Science Conference IV. The Woodlands, Texas. pp. 2805–2824.
- 1666 Renne P. R., Balco G., Ludwig K. R., Mundil R. and Min K. (2011) Response to the comment by  
 1667 W.H. Schwarz et al. on “Joint determination of 40K decay constants and 40Ar\*/40K for  
 1668 the Fish Canyon sanidine standard, and improved accuracy for 40Ar/39Ar  
 1669 geochronology” by P.R. Renne et al. (2010). *Geochimica et Cosmochimica Acta* **75**,  
 1670 5097–5100.
- 1671 Rubin A. E. (1997) The Hadley Rille enstatite chondrite and its agglutinate-like rim: Impact  
 1672 melting during accretion to the Moon. *Meteoritics & Planetary Science* **32**, 135–141.
- 1673 Schaal R. B., Hörz F., Thompson T. D. and Bauer J. F. (1979) Shock metamorphism of  
 1674 granulated lunar basalt. *Lunar and Planetary Science Conference X*, 2547–2571.
- 1675 Schaen A. J., Jicha B. R., Hodges K. V., Vermeesch P., Stelten M. E., Mercer C. M., Phillips D.,  
 1676 Rivera T. A., Jourdan F., Matchan E. L., Hemming S. R., Morgan L. E., Kelley S. P.,  
 1677 Cassata W. S., Heizler M. T., Vasconcelos P. M., Benowitz J. A., Koppers A. A. P., Mark  
 1678 D. F., Niespolo E. M., Sprain C. J., Hames W. E., Kuiper K. F., Turrin B. D., Renne P.  
 1679 R., Ross J., Nomade S., Guillou H., Webb L. E., Cohen B. A., Calvert A. T., Joyce N.,  
 1680 Ganerød M., Wijbrans J., Ishizuka O., He H., Ramirez A., Pfänder J. A., Lopez-Martínez  
 1681 M., Qiu H. and Singer B. S. (2020) Interpreting and reporting <sup>40</sup>Ar/<sup>39</sup>Ar geochronologic  
 1682 data. *GSA Bulletin*.
- 1683 Scherer E., Münker C. and Mezger K. (2001) Calibration of the Lutetium-Hafnium Clock.  
 1684 *Science* **293**, 683–687.
- 1685 Schoene B. (2014) U-Th-Pb Geochronology. In *Treatise on Geochemistry* Elsevier. pp. 341–377.
- 1686 Schoene B., Crowley J. L., Condon D. J., Schmitz M. D. and Bowring S. A. (2006) Reassessing  
 1687 the uranium decay constants for geochronology using ID-TIMS U–Pb data. *Geochimica*  
 1688 *et Cosmochimica Acta* **70**, 426–445.
- 1689 Schultz P. H. and Spudis P. D. (1983) Beginning and end of lunar mare volcanism. *Nature* **302**,  
 1690 233–236.
- 1691 Shaulis B. J., Righter M., Lapen T. J., Jolliff B. L. and Irving A. J. (2017) 3.1 Ga crystallization  
 1692 age for magnesian and ferroan gabbro lithologies in the Northwest Africa 773 clan of  
 1693 lunar meteorites. *Geochimica et Cosmochimica Acta* **213**, 435–456.

- 1694 Shearer C., Hess P., Wieczorek M., Pritchard M., Parmentier E., Borg L., Longhi J., Elkins-  
 1695 Tanton L., Neal C., Antonenko I., Canup R., Halliday A., Grove T., Hager B., Lee D. and  
 1696 Wiechert U. (2006) Thermal and Magmatic Evolution of the Moon. In *New Views on the*  
 1697 *Moon* Mineralogical Society of America. pp. 365–518.
- 1698 Shearer C. K., Elardo S. M., Petro N. E., Borg L. E. and McCubbin F. M. (2015) Origin of the  
 1699 lunar highlands Mg-suite: An integrated petrology, geochemistry, chronology, and  
 1700 remote sensing perspective. *American Mineralogist* **100**, 294–325.
- 1701 Shearer C. K. and Papike J. J. (2005) Early crustal building processes on the moon: Models for  
 1702 the petrogenesis of the magnesian suite. *Geochimica et Cosmochimica Acta* **69**, 3445–  
 1703 3461.
- 1704 Shih C.-Y., Nyquist L. E., Dasch E. J., Bogard D. D., Bansal B. M. and Wiesmann H. (1993)  
 1705 Ages of pristine noritic clasts from lunar breccias 15445 and 15455. *Geochimica et*  
 1706 *Cosmochimica Acta* **57**, 915–931.
- 1707 Shirley M. and Balaban E. (2022) An Overview of Mission Planning for the VIPER Rover.
- 1708 Silver L. T. (1970) Uranium-Thorium-Lead Isotope Relations in Lunar Materials. *Science* **167**,  
 1709 468–471.
- 1710 Snape J. F., Curran N. M., Whitehouse M. J., Nemchin A. A., Joy K. H., Hopkinson T., Anand  
 1711 M., Bellucci J. J. and Kenny G. G. (2018) Ancient volcanism on the Moon: Insights from  
 1712 Pb isotopes in the MIL 13317 and Kalahari 009 lunar meteorites. *Earth and Planetary*  
 1713 *Science Letters* **502**, 84–95.
- 1714 Söderlund U., Patchett P. J., Vervoort J. D. and Isachsen C. E. (2004) The  $^{176}\text{Lu}$  decay constant  
 1715 determined by Lu–Hf and U–Pb isotope systematics of Precambrian mafic intrusions.  
 1716 *Earth and Planetary Science Letters* **219**, 311–324.
- 1717 Spangler R. R., Warasila R. and Delano J. W. (1984)  $^{39}\text{Ar}$ - $^{40}\text{Ar}$  ages for the Apollo 15 green  
 1718 and yellow volcanic glasses. *J. Geophys. Res.* **89**, B487.
- 1719 Speyerer E. J. and Robinson M. (2013) Persistently illuminated regions at the lunar poles: Ideal  
 1720 sites for future exploration. *ICARUS* **222**, 122–136.
- 1721 Sprung P., Kleine T. and Scherer E. E. (2013) Isotopic evidence for chondritic Lu/Hf and Sm/Nd  
 1722 of the Moon. *Earth and Planetary Science Letters* **380**, 77–87.
- 1723 Spudis P. D., Bussey B., Plescia J., Josset J.-L. and Beauvivre S. (2008) Geology of Shackleton  
 1724 Crater and the south pole of the Moon. *Geophysical Research Letters* **35**.
- 1725 Spudis P. D. and Davis P. A. (1986) A chemical and petrological model of the lunar crust and  
 1726 implications for lunar crustal origin. *J. Geophys. Res.* **91**, E84.

- 1727 Spudis P. D., Hawke B. R. and Lucey P. G. (1988) Materials and formation of the Imbrium  
 1728 Basin. In *A89-10851 01-91 Proceedings of the Lunar and Planetary Science XVIII*.  
 1729 Cambridge University Press/Lunar and Planetary Institute, Houston, Texas. pp. 155–168.
- 1730 Srivastava Y., Basu Sarbadhikari A., Day J. M. D., Yamaguchi A. and Takenouchi A. (2022) A  
 1731 changing thermal regime revealed from shallow to deep basalt source melting in the  
 1732 Moon. *Nat Commun* **13**, 7594.
- 1733 Staudacher T., Jessberger E., Dominik B., Kirsten T. and Schaefferh O. (1982) Ar-40-Ar-39 ages  
 1734 of rocks and glasses from the Noerdlinger Ries Crater and the temperature history of  
 1735 impact breccias. *Journal of Geophysics* **51**, 1–11.
- 1736 Steele I. M. and Smith J. V. (1971) Mineralogy of Apollo 15415 “Genesis Rock” : Source of  
 1737 Anorthosite on Moon. *Nature* **234**, 138–140.
- 1738 Steiger R. H. and Jäger E. (1977) Subcommittee on geochronology: Convention on the use of  
 1739 decay constants in geo- and cosmochronology. *Earth and Planetary Science Letters* **36**,  
 1740 359–362.
- 1741 Stephan T. and Jessberger E. K. (1992) Isotope systematics and shock-wave metamorphism: III.  
 1742 K-Ar in experimentally and naturally shocked rocks; the Haughton impact structure,  
 1743 Canada. *Geochimica et Cosmochimica Acta* **56**, 1591–1605.
- 1744 Stöffler D. (1974) Deformation and transformation of rock forming minerals by natural and  
 1745 experimental shock processes. *Fortschr Mineral* **II**, 256–289.
- 1746 Stöffler D., Bischoff A., Borchardt R., Burgehele A., Deutsch A., Jessberger E. K., Ostertag R.,  
 1747 Palme H., Spettel B., Reimold W. U., Wacker K. and Wänke H. (1985) Composition and  
 1748 evolution of the lunar crust in the Descartes Highlands, Apollo 16. *J. Geophys. Res.* **90**,  
 1749 C449.
- 1750 Stöffler D. and Hornemann U. (1972) Quartz and feldspar glasses produced by natural and  
 1751 experimental shock. *Meteoritics* **7**, 371–394.
- 1752 Stöffler D., Knoll H. D. and Maerz U. (1979) Genetic Classification and Nomenclature of Lunar  
 1753 Highland Rocks Based on the Texture and Geological Setting of Terrestrial Impact  
 1754 Breccias. In *Lunar and Planetary Science X*. Houston, Texas.
- 1755 Stöffler D., Knoll H. D., Marvin U. B., Simonds C. H. and Warren P. H. (1980) *Recommended*  
 1756 *Classification and Nomenclature of Lunar Highland Rocks- a Committee Report.*, Lunar  
 1757 and Planetary Institute.
- 1758 Stöffler D. and Ryder G. (2001) Stratigraphy and Isotope Ages of Lunar Geologic Units:  
 1759 Chronological Standard for the Inner Solar System. In *Chronology and Evolution of Mars*  
 1760 (eds. R. Kallenbach, J. Geiss, and W. K. Hartmann). Space Sciences Series of ISSI.  
 1761 Springer Netherlands, Dordrecht. pp. 9–54.

- 1762 Stöffler D., Ryder G., Ivanov B. A., Artemieva N. A., Cintala M. J. and Grieve R. A. F. (2006)  
 1763 Cratering History and Lunar Chronology. In *New Views of the Moon Reviews in*  
 1764 *Mineralogy and Geochemistry*. Mineralogical Society of America. pp. 519–596.
- 1765 Swindle T. D., Isachsen C. E., Weirich J. R. and Kring D. A. (2009) <sup>40</sup>Ar-<sup>39</sup>Ar ages of H-  
 1766 chondrite impact melt breccias. *Meteoritics & Planetary Science* **44**, 747–762.
- 1767 Tai Udovicic C. J., Frizzell K. R., Kodikara G. R. L., Kopp M., Luchsinger K. M., Madera A.,  
 1768 Meier M. L., Paladino T. G., Patterson R. V., Wroblewski F. B. and Kring D. A. (2022)  
 1769 Modeling the Effects of Basin Impacts and Ballistic Sedimentation on Ice in Lunar Cold  
 1770 Traps. In 53rd Lunar and Planetary Science Conference. The Woodlands, TX.
- 1771 Tatsumoto M. and Rosholt J. N. (1970) Age of the Moon: An Isotopic Study of Uranium-  
 1772 Thorium-Lead Systematics of Lunar Samples. *Science* **167**, 461–463.
- 1773 Taylor D. J., McKeegan K. D. and Harrison T. M. (2009) Lu–Hf zircon evidence for rapid lunar  
 1774 differentiation. *Earth and Planetary Science Letters* **279**, 157–164.
- 1775 Tera F., Papanastassiou D. A. and Wasserburg G. J. (1974) Isotopic evidence for a terminal lunar  
 1776 cataclysm. *Earth and Planetary Science Letters* **22**, 1–21.
- 1777 Touboul M., Kleine T., Bourdon B., Palme H. and Wieler R. (2007) Late formation and  
 1778 prolonged differentiation of the Moon inferred from W isotopes in lunar metals. *Nature*  
 1779 **450**, 1206–1209.
- 1780 Turner G. (1972) <sup>40</sup>Ar-<sup>39</sup>Ar age and cosmic ray irradiation history of the Apollo 15 anorthosite,  
 1781 15415. *Earth and Planetary Science Letters* **14**, 169–175.
- 1782 Turner G. (1970) Argon-40/ Argon-39 Dating of Lunar Rock Samples. *Science* **167**, 466–468.
- 1783 Turner G. and Cadogan P. H. (1975) The history of lunar bombardment inferred from <sup>40</sup>Ar-<sup>39</sup>Ar  
 1784 dating of highland rocks. *Lunar and Planetary Science Conference Proceedings* **2**, 1509–  
 1785 1538.
- 1786 Turner G., Cadogan P. H. and Yonge C. J. (1973) Argon selenochronology. *Lunar and Planetary*  
 1787 *Science Conference Proceedings* **4**, 1889.
- 1788 Tye A. R., Fassett C. I., Head J. W., Mazarico E., Basilevsky A. T., Neumann G. A., Smith D. E.  
 1789 and Zuber M. T. (2015) The age of lunar south circumpolar craters Haworth, Shoemaker,  
 1790 Faustini, and Shackleton: Implications for regional geology, surface processes, and  
 1791 volatile sequestration. *Icarus* **255**, 70–77.
- 1792 Uemoto K., Ohtake M., Haruyama J., Matsunaga T., Yokota Y., Morota T., Nakamura R.,  
 1793 Yamamoto S. and Iwata T. (2010) Purest anorthosite distribution in the lunar South Pole-  
 1794 Aitken Basin derived from SELENE Multiband Imager. In 41st Lunar and Planetary  
 1795 Science Conference. The Woodlands, TX.

- 1796 Unruh D. M., Stille P., Patchett P. J. and Tatsumoto M. (1984) Lu-Hf and Sm-Nd evolution in  
1797 lunar mare basalts. *J. Geophys. Res.* **89**, B459.
- 1798 Vaughan W. M. and Head J. W. (2014) Impact melt differentiation in the South Pole-Aitken  
1799 basin: Some observations and speculations. *Planetary and Space Science* **91**, 101–106.
- 1800 Villa I. M., De Bièvre P., Holden N. E. and Renne P. R. (2015) IUPAC-IUGS recommendation  
1801 on the half life of 87Rb. *Geochimica et Cosmochimica Acta* **164**, 382–385.
- 1802 Villa I. M., Holden N. E., Possolo A., Ickert R. B., Hibbert D. B. and Renne P. R. (2020)  
1803 IUPAC-IUGS recommendation on the half-lives of 147Sm and 146Sm. *Geochimica et*  
1804 *Cosmochimica Acta* **285**, 70–77.
- 1805 Villa I. M., Holden N. E., Possolo A., Ickert R. B., Hibbert D. B., Renne P. R., Bonardi M. L.  
1806 and Bièvre P. D. (2022) IUGS–IUPAC recommendations and status reports on the half-  
1807 lives of 87Rb, 146Sm, 147Sm, 234U, 235U, and 238U (IUPAC Technical Report). *Pure*  
1808 *and Applied Chemistry* **94**, 1085–1092.
- 1809 Wang S.-J. (2022) First Location And Characterization Of Lunar Highland Clasts In Chang'E-5  
1810 Breccias Using TIMA-SEM-EPMA. *At.Spectrosc.* **43**, 351–362.
- 1811 Warren P. H. and Korotev R. L. (2022) Ground truth constraints and remote sensing of lunar  
1812 highland crust composition. *Meteorit & Planetary Scien* **57**, 527–557.
- 1813 Weirich J. R., Wittmann A., Isachsen C. E., Rumble D., Swindle T. D. and Kring D. A. (2010)  
1814 The Ar-Ar age and petrology of Miller Range 05029: Evidence for a large impact in the  
1815 very early solar system: Ar-Ar age and petrology of MIL 05029. *Meteoritics & Planetary*  
1816 *Science* **45**, 1868–1888.
- 1817 White L. F., Tait K. T., Kamo S. L., Moser D. E. and Darling J. R. (2020) Highly accurate dating  
1818 of micrometre-scale baddeleyite domains through combined focused ion beam extraction  
1819 and U–Pb thermal ionization mass spectrometry (FIB-TIMS). *Geochronology* **2**, 177–  
1820 186.
- 1821 Wieczorek M. A. and Zuber M. T. (2001) The composition and origin of the lunar crust:  
1822 Constraints from central peaks and crustal thickness modeling. *Geophys. Res. Lett.* **28**,  
1823 4023–4026.
- 1824 Wilhelms D. E., McCauley J. F. and Trask N. J. (1987) *The geologic history of the Moon.*,
- 1825 Wilshire H. G., Schaber G. G., Silver L. T., Phinney W. C. and Jackson E. D. (1972) Geologic  
1826 Setting and Petrology of Apollo 15 Anorthosite (15415). *Geol Soc America Bull* **83**,  
1827 1083.
- 1828 Wilson L. and Head J. W. (1981) Ascent and eruption of basaltic magma on the Earth and Moon.  
1829 *J. Geophys. Res.* **86**, 2971–3001.

- 1830 Wittmann A., Friedrich J. M., Troiano J., Macke R. J., Britt D. T., Swindle T. D., Weirich J. R.,  
 1831 Rumble D., Lasue J. and Kring D. A. (2011) H/L chondrite LaPaz Icefield 031047 – A  
 1832 feather of Icarus? *Geochimica et Cosmochimica Acta* **75**, 6140–6159.
- 1833 Wood J. A. (1970) Petrology of the lunar soil and geophysical implications. *J. Geophys. Res.* **75**,  
 1834 6497–6513.
- 1835 Wood J. A., Dickey J. S., Marvin U. B. and Powell B. N. (1970) Lunar Anorthosites. *Science*  
 1836 **167**, 602–604.
- 1837 Wu B., Wang Y., Lin T. J., Hu H. and Werner S. C. (2019) Impact cratering in and around the  
 1838 Orientale Basin: Results from recent high-resolution remote sensing datasets. *Icarus* **333**,  
 1839 343–355.
- 1840 Xie M., Liu T. and Xu A. (2020) Ballistic Sedimentation of Impact Crater Ejecta: Implications  
 1841 for the Provenance of Lunar Samples and the Resurfacing Effect of Ejecta on the Lunar  
 1842 Surface. *Journal of Geophysical Research: Planets* **125**, e2019JE006113.
- 1843 Xu Xiaoqing, Hui H., Chen W., Huang S., Neal C. R. and Xu Xisheng (2020) Formation of lunar  
 1844 highlands anorthosites. *Earth and Planetary Science Letters* **536**, 116138.
- 1845 Yamamoto S., Nakamura R., Matsunaga T., Ogawa Y., Ishihara Y., Morota T., Hirata N., Ohtake  
 1846 M., Hiroi T., Yokota Y. and Haruyama J. (2012) Massive layer of pure anorthosite on the  
 1847 Moon: Pure anorthosite on the Moon. *Geophys. Res. Lett.* **39**, n/a-n/a.
- 1848 Yamamoto S., Nakamura R., Matsunaga T., Ogawa Y., Ishihara Y., Morota T., Hirata N., Ohtake  
 1849 M., Hiroi T., Yokota Y. and Haruyama J. (2010) Possible mantle origin of olivine around  
 1850 lunar impact basins detected by SELENE. *Nature Geosci* **3**, 533–536.
- 1851 Yokota Y., Matsunaga T., Ohtake M., Haruyama J., Nakamura R., Yamamoto S., Ogawa Y.,  
 1852 Morota T., Honda C., Saiki K., Nagasawa K., Kitazato K., Sasaki S., Iwasaki A., Demura  
 1853 H., Hirata N., Hiroi T., Honda R., Iijima Y. and Mizutani H. (2011) Lunar photometric  
 1854 properties at wavelengths 0.5–1.6  $\mu\text{m}$  acquired by SELENE Spectral Profiler and their  
 1855 dependency on local albedo and latitudinal zones. *Icarus* **215**, 639–660.
- 1856 Yue Z., Shi K., Di K., Lin Y. and Gou S. (2022) Progresses and prospects of impact crater  
 1857 studies. *Sci. China Earth Sci.*
- 1858 Zellner N. E. B. and Delano J. W. (2015)  $^{40}\text{Ar}/^{39}\text{Ar}$  ages of lunar impact glasses: Relationships  
 1859 among Ar diffusivity, chemical composition, shape, and size. *Geochimica et*  
 1860 *Cosmochimica Acta* **161**, 203–218.
- 1861 Zellner N. E. B., Delano J. W., Swindle T. D., Barra F., Olsen E. and Whittet D. C. B. (2009)  
 1862 Apollo 17 regolith, 71501,262: A record of impact events and mare volcanism in lunar  
 1863 glasses. *Meteoritics & Planetary Science* **44**, 839–851.

- 1864 Zhang B., Lin Y., Moser D. E., Warren P. H., Hao J., Barker I. R., Shieh S. R. and Bouvier A.  
1865 (2021) Timing of lunar Mg-suite magmatism constrained by SIMS U-Pb dating of Apollo  
1866 norite 78238. *Earth and Planetary Science Letters* **569**, 117046.
- 1867 Zhang J., Yang W., Hu S., Lin Y., Fang G., Li C., Peng W., Zhu S., He Z., Zhou B., Lin H.,  
1868 Yang J., Liu E., Xu Y., Wang J., Yao Z., Zou Y., Yan J. and Ouyang Z. (2015) Volcanic  
1869 history of the Imbrium basin: A close-up view from the lunar rover Yutu. *Proc. Natl.*  
1870 *Acad. Sci. U.S.A.* **112**, 5342–5347.
- 1871 Zhang W. (2022) In Situ Rb-Sr Dating Of Lunar Meteorites Using Laser Ablation MC-ICP-MS.  
1872 *At.Spectrosc.* **43**.
- 1873 Zhu M.-H., Artemieva N., Morbidelli A., Yin Q.-Z., Becker H. and Wünnemann K. (2019)  
1874 Reconstructing the late-accretion history of the Moon. *Nature* **571**, 226–229.
- 1875 Zolensky M. E. (1997) Structural water in the Bench Crater chondrite returned from the Moon.  
1876 *Meteoritics & Planetary Science* **32**, 15–18.
- 1877 Zolensky M. E., Weisburg M. K. and Buchanan P. C. (1996) Mineralogy of carbonaceous  
1878 chondrite clasts in HED achondrites and the Moon. *Meteoritics & Planetary Science* **31**,  
1879 537.
- 1880 Zuber M. T., Head J. W., Smith D. E., Neumann G. A., Mazarico E., Torrence M. H., Aharonson  
1881 O., Tye A. R., Fassett C. I., Rosenburg M. A. and Melosh H. J. (2012) Constraints on the  
1882 volatile distribution within Shackleton crater at the lunar south pole. *Nature* **486**, 378–  
1883 381.
- 1884